

CRWMS/M&O

Design Analysis Cover Sheet

Complete only applicable items.

①

QA: L

Page: 1 Of: 59

2. DESIGN ANALYSIS TITLE Design Basis Cladding Analysis			
3. DOCUMENT IDENTIFIER (Including Rev. No.) BBA000000-01717-0200-00054 REV 01			4. TOTAL PAGES 59
5. TOTAL ATTACHMENTS 8		6. ATTACHMENT NUMBERS - NO. OF PAGES IN EACH I-5, II-5, III-4, IV-5, V-5, VI-5, VII-13, VIII-9	
	Printed Name	Signature	Date
7. Originator	J. K. McCoy	<i>J. K. McCoy</i>	3-5-98
8. Checker	Z. Ceylan	<i>Zekir Ceylan</i>	3/5/98
9. Lead Design Engineer	David Stahl	<i>David Stahl</i>	3/5/98
10. Department Manager	David Stahl	<i>David Stahl</i>	3/5/98
11. REMARKS TBV-228 and TBV-231 apply to this analysis. In the body of the analysis, changes are noted by vertical lines in the margin. Attachments I through IV have been heavily revised, and Attachments V through VIII are new, so no change marks are provided in the Attachments.			

INFORMATION ONLY

INFORMATION ONLY

Design Analysis Revision Record

Complete only applicable items.

①

2. DESIGN ANALYSIS TITLE Design Basis Cladding Analysis	
3. DOCUMENT IDENTIFIER (Including Rev. No.) BBA000000-01717-0200-00054 REV 01	
4. Revision No.	5. Description of Revision
00	Issued approved
01	Issued approved. Analysis was revised to extend previous treatment and make a quantitative prediction of the fraction of fuel failed by mechanical loading. New data on block size distribution were applied. Sections 4.1.8 through 4.1.10 and Attachments V through VIII were added. Section 4.3.2 was renumbered. Revisions were made in the Table of Contents, Sections 1, 2, 4, 4.1, 4.1.4 through 4.1.6, 4.2, 4.4, 5, 6, 7.3, 7.8.1, 7.8.2, 8, and 9, and Attachments I through IV.

Table of Contents

Item	Page
1. PURPOSE	4
2. QUALITY ASSURANCE	4
3. METHOD	4
4. DESIGN INPUTS	4
4.1 Design Parameters	5
4.2 Criteria	17
4.3 Assumptions	18
4.4 Codes and Standards	20
5. REFERENCES	20
6. USE OF COMPUTER SOFTWARE	23
7. DESIGN ANALYSIS	26
7.1 Introduction	26
7.2 Quantity of stainless steel clad fuel	27
7.3 Environment and mechanisms	30
7.4 Creep rupture	31
7.5 Dry cladding oxidation	40
7.6 Dry fuel oxidation	43
7.7 Aqueous corrosion	44
7.8 External mechanical loading	45
8. CONCLUSIONS	57
9. ATTACHMENTS	58

1. PURPOSE

The objective of this analysis is to determine, for various mechanisms, which spent nuclear fuel cladding designs are most susceptible to failure in a repository. The document considers commercial pressurized water reactor and boiling water reactor fuels. The purpose of this analysis is to provide input for calculations of cladding degradation.

2. QUALITY ASSURANCE

The Quality Assurance (QA) program applies to this analysis. The work reported in this document is part of the waste package design analyses that will eventually support the License Application Design phase. This activity, when appropriately confirmed, can affect the proper functioning of the Mined Geologic Disposal System (MGDS) waste package. The QAP-2-3 (*Classification of Permanent Items*) evaluation entitled *Classification of the Preliminary MGDS Repository Design* (Ref. 5.2, TBV-228) has identified the waste package as an MGDS item important to safety, waste isolation, and physical protection of materials. The Waste Package Operations responsible manager has evaluated this activity in accordance with QAP-2-0, *Conduct of Activities*. The QAP-2-0 activity evaluation, *Analyze Material and Performance Information and Data in Support of Waste Pack/Engineered Barrier Segment Development* (Ref. 5.32), has determined that work performed for this analysis is subject to *Quality Assurance Requirements and Description* (Ref. 5.26) requirements. As specified in NLP-3-18, *Documentation of QA Controls on Drawings, Specifications, Design Analyses, and Technical Documents*, this activity is subject to QA controls.

3. METHOD

Information on spent fuel inventories and on fuel assembly geometry and materials were collected from a variety of sources. Models of fuel cladding degradation were also collected, and the models were analyzed to determine which types of fuel are most susceptible to degradation by that mechanism. Results are tabulated for the most susceptible types and the most common types of fuel assemblies.

All U.S. commercial nuclear reactor fuel discharged to date has either stainless steel or zirconium alloy cladding. The total quantity of stainless steel clad fuel is determined, but there is no analysis of its degradation. Modeling of stainless steel cladding degradation is not justified at this time because there are only small amounts of stainless steel clad fuel, and thus this material is not expected to have a large effect on system performance.

4. DESIGN INPUTS

All design inputs which are identified in this analysis are for the preliminary stage of the design process; some or all of these design inputs will require subsequent confirmation (or superseding inputs) as the waste package design proceeds. Consequently, the use of any data from this analysis for input into documents supporting construction, fabrication, or procurement is required

| to be controlled and tracked as TBV or TBD in accordance with NLP-3-15, *To Be Verified (TBV)*
| *and To Be Determined (TBD) Monitoring System*, or other appropriate procedures.

4.1 Design Parameters

| Based on the rationale that the conclusions derived by this analysis are for preliminary design
| and will not be used as input into documents supporting construction, fabrication, or procure-
| ment, a notation of TBV or TBD will not be carried to the conclusions of this analysis.

4.1.1 Cladding materials and quantities of discharged fuel

Except as noted in Section 4.1.3, numbers of discharged fuel assemblies were taken from Ref. 5.3, Table B5. The Energy Information Administration (EIA) assembly codes, numbers of discharged assemblies, and cladding materials, are repeated in Table 4.1.1-1. The numbers of assemblies in Ref. 5.3 are more recent than those given in the *LWR* [light-water reactor] *Fuel Assemblies PC* [personal computer] *Database (FADB)* (see Section 6). Among the pressurized water reactor assemblies there are 87 that are of "undetermined" type. As is explained in Ref. 5.3, p. 241, Note 10, these are temporarily discharged assemblies. Utilities are not required to report complete data until the assemblies are permanently discharged, so the characteristics of these assemblies are unknown.

In addition to the numbers of discharged assemblies in Table 4.1.1-1, the following information on quantities of spent nuclear fuel is used:

- total amount of uranium in discharged pressurized water reactor fuel: 19102.0 metric tons (Ref. 5.3, p. 28)
- total amount of uranium in discharged boiling water reactor fuel: 10901.3 metric tons (Ref. 5.3, p. 27)

The total amount of uranium in discharged light water reactor fuel is therefore 30003.3 metric tons.

Table 4.1.1-1. Design parameters from Ref. 5.3.

Pressurized Water Reactor Fuels			Boiling Water Reactor Fuels		
EIA			EIA		
Assembly	Clad	Number	Assembly	Clad	Number
Code	Material	Discharged	Code	Material	Discharged
B1515B2	ZR	0	G2307G2A	ZR	1672
B1515B3	ZR	1	G2307G2B	ZR	5047
B1515B4	ZR	4134	G2307G3	ZR	394
B1515B4Z	ZR	89	G2308G4	ZR	3876
B1515B5	ZR	58	G2308G5	ZR	879
B1515B5Z	ZR	29	G2308GP	ZR	2832
B1515B6	ZR	130	G2308GB	ZR	1376
B1515B7	ZR	96	G2308G8A	ZR	312
B1515B8	ZR	229	G2308G8B	ZR	360
B1515B9	ZR	21	G2308G9	ZR	0
B1515B10	ZR	0	G2308G10	ZR	188
B1515B	ZR	0	G2309G11	ZR	0
B1515BZ	ZR	640	G2310G12	ZR	0
B1515BEB	ZR	0	G2309G13	ZR	0
B1515BGD	ZR	4	G2307A	ZR	260
B1515W	ZR	4	G2308A	ZR	1409
B1717B	ZR	4	G2308AP	ZR	32
C1414C	ZR	3368	G2309A	ZR	176
C1414A	ZR	761	G2309A5	ZR	0
C1414W	ZR	436	G2309A9X	ZR	0
C1616CSD	ZR	2340	G2309AIX	ZR	0
C8016C	ZR	1132	G4607G2	ZR	1142
W1414W	ZR	622	G4607G3A	ZR	3752
W1414WL	ZR	1410	G4607G3B	ZR	1184
W1414WO	ZR	965	G4608G4A	ZR	1785
W1414A	ZR	806	G4608G4B	ZR	1787
W1414ATR	ZR	288	G4608G5	ZR	4380
W1414B	ZR	2	G4608GP	ZR	11625
W1515W	ZR	1580	G4608GB	ZR	8575
W1515WL	ZR	3481	G4608G8	ZR	1886
W1515WO	ZR	1533	G4608G9	ZR	242
W1515WV5	ZR	0	G4608G10	ZR	5
W1515A	ZR	884	G4609G11	ZR	40
W1515APL	ZR	12	G4610G12	ZR	0
W1515B	ZR	0	G4609G13	ZR	0
W1717WL	ZR	9525	G4608A	ZR	1336
W1717WO	ZR	2969	G4608AP	ZR	404
W1717WV5	ZR	1296	G4609A	ZR	1108
W1717WV + ZIRLO		35	G4609A5	ZR	36
W1717WVH	ZR	587	G4609A9X	ZR	0
W1717WVJ	ZIRLO	0	G4609AIX	ZR	4

Table 4.1.1-1. Design parameters from Ref. 5.3 (continued).

Pressurized Water Reactor Fuels			Boiling Water Reactor Fuels		
EIA			EIA		
Assembly	Clad	Number	Assembly	Clad	Number
Code	Material	Discharged	Code	Material	Discharged
W1717A	ZR	332	G4609AX +	ZR	0
W1717AB	ZR	0	G4610A	ZR	0
W1717B	ZR	130	G4608W	ZR	4
WST17W	ZR	421	G4610C	ZR	0
XFC14C	ZR	378	XBR12G	SS	0
XFC14A	ZR	192	XBR11G	ZR	6
XFC14W	ZR	0	XBR07G	ZR	4
XHN15W	SS	309	XBR08G	ZR	2
XHN15MS	SS	2	XBR09G	ZR	143
XHN15MZ	ZR	2	XBR09A	ZR	4
XHN15HS	SS	1	XBR11A	ZR	254
XHN15HZ	ZR	2	XBR11N	ZR	8
XHN15B	SS	576	XDR06G	ZR	1
XHN15BZ	ZR	0	XDR07G	SS	0
XIP14B	SS	0	XDR06G3B	ZR	163
XIP14W	SS	160	XDR06G3F	ZR	96
XPA15C	ZR	273	XDR06G5	ZR	106
XPA15A	ZR	520	XDR07GS	ZR	1
XSL16C	ZR	544	XDR08G	ZR	1
XSO14W	SS	665	XDR06U	ZR	458
XSO14WZ	ZR	0	XDR06A	ZR	66
XYR18W	SS	76	XHB07G	SS	0
XYR16U	ZR	73	XHB07G2	ZR	88
XYR16A	ZR	228	XHB06G	ZR	176
XYR16C	ZR	156	XHB06A	ZR	126
(undetermined)		87	XLC10L	SS	155
TOTAL		44598	XLC10A	SS	178
			TOTAL		60144
EIA = Energy Information Administration					
SS = stainless steel					
ZR = Zircaloy (zirconium alloy)					
ZIRLO = Zirlo (zirconium alloy)					

Table 4.1.2-1. Design parameters from the FADB.

EIA Assembly Code	Init. Use Year	Last Disch. Year	Rod Pitch, in.	Mass of U, kg	Rod Diam., in.	Rod Length, in.		Active Length, in.		Clad Material	Clad Thickness, in.		Plenum Length, in.
						min/nom	max	min/nom	max		min/nom	max	
B1515B	1974	1989	0.568	463.2	0.43	153.68		141.8	144	Zircaloy-4	0.0265		11.72
B1515B2	1973	1980	0.568	466.7	0.43			144		Zircaloy-4	0.0265		
B1515B3	1973	1985	0.568	463.5	0.43			141.75	144	Zircaloy-4	0.0265		
B1515B4	1976	1989	0.568	464.5	0.43	153.68		141.8	143.5	Zircaloy-4	0.0265		11.72
B1515B4Z	1981	1989	0.568	463.2	0.43			141.8		Zircaloy-4	0.0265		
B1515B5	1982	1989	0.568	463.5	0.43			141.8	143.2	Zircaloy-4	0.265		
B1515B5Z	1985	1989	0.568	463.4	0.43			141.8		Zircaloy-4	0.265		
B1515B6	1988	1989	0.568	463	0.43			141.8		Zircaloy-4	0.265		
B1515B7	1988	1989	0.568	463	0.43			141.8		Zircaloy-4	0.265		
B1515B8	1989	1989	0.568	463	0.43			141.8		Zircaloy-4	0.0265		
B1515BEB	1981	1988	0.568	436.1						Zircaloy-4			
B1515BGD	1983	1989	0.568	430				143.5		Zircaloy-4			
B1515W				460						Zircaloy-4			
B1717B	1976	1981	0.502	456.7	0.379	152.688		143		Zircaloy-4	0.024		9.52
XBR11A	1973	1989	0.577	128.3	0.449	78.601		70		Zircaloy-2	0.034		4.301
XBR11G	1972	1973	0.577	124.2	0.449			70		Zircaloy-2	0.034		
XBR11N	1972	1977	0.577	129						Zircaloy-2			
XBR12G			0.533		0.388			70		St. Steel 304	0.019		
XBR07G		1968	0.921	131.4	0.7			65	66.3	Zircaloy-2	0.04		
XBR08G		1969	0.807	112.3	0.57	66	67.3			Zircaloy-2	0.035		
XBR09A	1972	1977	0.707	127	0.5625			68		Zircaloy-2			
XBR09G	1971	1980	0.707	137.2	0.5625			70		Zircaloy-2	0.04		
C1414A	1981	1989	0.58	369.5	0.44	146.484		134.08		Zircaloy-4	0.031		
C1414C	1973	1989	0.58	382.2	0.44	147		137		Zircaloy-4	0.028		8.375
C1414W	1980	1989	0.58	406.8	0.44	146.44		136.7		Zircaloy-4	0.026		
C1616CSD	1978	1989	0.506	415.9	0.382	161		150		Zircaloy-4	0.025		9.527
C8016C	1985	1989	0.506	413.3	0.382	161		150		Zircaloy-4	0.025		9.527
XDR06A	1977	1978	0.694	95.2	0.5645	116.65		108.25		Zircaloy-2	0.036	0.046	
XDR06G	1959	1969	0.71	111.4						Zircaloy-2			
XDR06G3B	1964	1977	0.71	101.8	0.555	114		109		Zircaloy-2	0.035		
XDR06G3F	1965	1977	0.71	102	0.5625	114		108.25		Zircaloy-2	0.035		
XDR06G5	1967	1978	0.71	105.9	0.5625	114.22		108.25		Zircaloy-2	0.035		5.27
XDR06U	1968	1978	0.71	102						Zircaloy-2			
XDR07G													
XDR07GS	1964	1969											
XDR08G										Zircaloy-4			
XFC14A	1980	1988	0.58	352.8						Zircaloy-4			
XFC14C	1973	1987	0.58	365.6	0.44	137		128		Zircaloy-4	0.028		7.01
XFC14W			8.1							Zircaloy-4			
G2307A	1972	1983	0.738	182.3	0.57	158.15		144		Zircaloy-2	0.036	0.046	

Table 4.1.2-1. Design parameters from the FADB (continued).

EIA Assembly Code	Init. Use Year	Last Disch. Year	Rod Pitch, in.	Mass of U, kg	Rod Diam., in.	Rod Length, in.		Active Length, in.		Clad Material	Clad Thickness, in.		Plenum Length, in.
						min/nom	max	min/nom	max		min/nom	max	
G2307G2A	1969	1979	0.738	194.9	0.57	160		144		Zircaloy-2	0.0355		11.25
G2307G2B	1969	1981	0.738	192.8	0.563	160		144		Zircaloy-2	0.032		11.24
G2307G3	1972	1983	0.738	187.5	0.563	160		144		Zircaloy-2	0.037		11
G2308A	1975	1989	0.641	174.5	0.484	158.665		145.24		Zircaloy-2	0.36		10.02
G2308AP			0.641	174.5	0.484	160		145.24		Zircaloy-2	0.36		
G2308GB	1979	1989	0.64	177.5	0.483			145.24		Zircaloy-2	0.032		9.48
G2308G10			0.64	171						Zircaloy-2			
G2308G4	1973	1987	0.64	184.1	0.493	160		144		Zircaloy-2	0.034		11.24
G2308G5	1978	1989	0.64	177.1	0.483	160		145.24		Zircaloy-2	0.032		9.48
G2308G8			0.64	171	0.483	160		145.24		Zircaloy-2			
G2308G9			0.64	171						Zircaloy-2			
G2308GP	1979	1989	0.64	177	0.483			145.24		Zircaloy-2	0.032		9.48
G2309A			0.572	167.7	0.424	159.07		145.24		Zircaloy-2	0.03		9.58
G2309A5			0.572	162						Zircaloy-2			
G2309A9X			0.572	162						Zircaloy-2			
G2309AIX			0.572	171						Zircaloy-2			
G2309G11										Zircaloy-2			
G4610S	1989	1989	0.488	176.3	0.3787			150		Zircaloy-2	0.0248		
G4607G2	1972	1979	0.738	194.7	0.563			144		Zircaloy-2	0.032		16
G4607G3A	1973	1985	0.738	187.4	0.563			144		Zircaloy-2	0.037		16
G4607G3B	1974	1982	0.738	189.9	0.563			146		Zircaloy-2	0.037		14
G4608A	1985	1989	0.641	176.3	0.484	163.424		150		Zircaloy-2	0.036		10.024
G4608AP			0.641	176.3						Zircaloy-2			
G4608GB	1983	1989	0.64	184.7	0.483			150		Zircaloy-2	0.032		9.48
G4608G10			0.64	179						Zircaloy-2			
G4608G4A	1974	1985	0.64	184	0.493			144		Zircaloy-2	0.034		16
G4608G4B	1976	1985	0.64	186.7	0.493			146		Zircaloy-2	0.034		14
G4608G5	1978	1989	0.64	183	0.483			150		Zircaloy-2	0.032		9.48
G4608G8			0.64	179						Zircaloy-2			
G4608G9			0.64	179						Zircaloy-2			
G4608GP	1976	1989	0.64	183.2	0.483			150		Zircaloy-2	0.032		9.48
G4608W			0.609	174	0.458	160.6		150		Zircaloy-2	0.029		10
G4609A			0.572	173	0.424	163.84		150		Zircaloy-2	0.03		9.578
G4609A5			0.572	167						Zircaloy-2			
G4609A9X	1989	1989	0.569	167.7	0.431			150		Zircaloy-2	0.029		
G4609AIX			0.569	176.8	0.431			150		Zircaloy-2	0.025		
G4609G11										Zircaloy-2			
XHN15B	1973	1989	0.563	411.9	0.422	126.68		120.5		St.Steel 304	0.0165		4.81
XHN15BZ			0.563	412						Zircaloy-4			
XHN15IS	1971	1975	0.563	406.2						St.Steel 304			

Table 4.1.2-1. Design parameters from the FADB (continued).

EIA Assembly Code	Init. Use Year	Last Disch. Year	Rod Pitch, in.	Mass of U, kg	Rod Diam., in.	Rod Length, in.		Active Length, in.		Clad Material	Clad Thickness, in.		Plenum Length, in.
						min/nom	max	min/nom	max		min/nom	max	
XHN15IZ	1971	1973	0.563	362.9						Zircaloy-4			
XHN15MS	1970	1973	0.563	406						St.Steel 304			
XHN15MZ	1970	1973	0.563	370.8						Zircaloy-4			
XHN15W	1967	1977	0.563	415.6	0.422	126.52	126.72	120	122	St.Steel 304	0.0165		
XHB06A	1974	1984	0.74	69.7						Zircaloy-2			
XHB06G	1970	1984	0.74	76.4	0.563			77.5		Zircaloy-2	0.032		5.2
XHB07G			0.631		0.486	83.2		79		Zircaloy-2	0.033		3.5
XHB07G2	1970	1973	0.631	76.3						Zircaloy-2			
XIP14W	1967	1974	0.441	191.2	0.3415	105.13		100.26		St.Steel 304	0.0285		
XIP14B			0.3805		0.3124	16.5		90		St.Steel 304	0.02		
XLC10L	1967	1982	0.565	120.2	0.396	88.08		83		St.Steel 348H	0.02		3.93
XLC10A	1977	1987	0.557	108.7	0.394	89.98		83		St.Steel 348H	0.022		3.89
XPA15A	1975	1988	0.55	391.1	0.417	139.423		131.8		Zircaloy-4	0.03		
XPA15C	1972	1981	0.55	412.4	0.418	140		132		Zircaloy-4	0.026		
XSO14W	1969	1988	0.556	366.3	0.422	126.13	126.68	120		St.Steel 304	0.0165		
WST17W	1988	1989	0.496	542	0.374	176.642				Zircaloy-4	0.0225		
XSL16C	1983	1989	0.506	377	0.382	146.499		136.7		Zircaloy-4	0.025		8.158
W1414A	1974	1989	0.556	376.7	0.424	149.1		142		Zircaloy-4	0.03		5.9
W1414ATR	1981	1988	0.556	360.6	0.417	152		144		Zircaloy-4	0.0295		7.28
W1414B	1974	1977	0.556	383.2						Zircaloy-4			
W1414WL	1970	1989	0.556	399.1	0.422	148.55	152.4	141.2	145.2	Zircaloy-4	0.0225		
W1414WO	1981	1989	0.556	357.9	0.4	148.61	151.85	135.2	144	Zircaloy-4	0.0243		7.158
W1414W	1971	1986	0.556	393.8	0.422	148.55	152.4	141.2	145.2	Zircaloy-4	0.0225		6.99
W1515A	1975	1988	0.563	428.6	0.424	152.065		144		Zircaloy-4	0.03		6.8
W1515AP	1987	1989	0.563	300						Zircaloy-4			
W1515B			0.563							Zircaloy-4			
W1515WL	1970	1989	0.563	454.8	0.422	148.59	151.88	142	144	Zircaloy-4	0.0242		8.2
W1515WO	1982	1989	0.563	460	0.422	151.85		144		Zircaloy-4	0.0242		8.2
W1515W	1972	1988	0.563	453.9	0.422	148.59	151.88	142	144	Zircaloy-4	0.0242		8.2
W1717A	1982	1988	0.496	401.5	0.36	152		144		Zircaloy-4	0.025		7.26
W1717B	1989	1989	0.496	425		0.374				Zircaloy-4	0.024		
W1717WL	1974	1989	0.496	460.2	0.374	151.56	151.635	144		Zircaloy-4	0.0225		6.3
W1717WO	1979	1989	0.496	424.9	0.36	151.56	151.635	144		Zircaloy-4	0.0225		6.9
W1717WV +			0.496	425						ZIRLO			
W1717WV5	1984	1988	0.496	425.7	0.36	152.3		144		Zircaloy-4	0.0225		7.405
W1717WVH			0.496	425						Zircaloy-4			
XYR16A	1975	1987	0.472	233.5	0.365	95.34		91		Zircaloy-4	0.024		
XYR16C	1985	1988	0.472	229.1		95		91		Zircaloy-4	0.026		1.55
XYR16U	1972	1977		238.6						Zircaloy-4			
XYR18W	1968	1975	0.422	273.4	0.34			91.86		St.Steel 348H			

Title: Design Basis Cladding Analysis

Document Identifier: BBA000000-01717-0200-00054 REV 01

Page 11 of 59

Table 4.1.2-1. Design parameters from the FADB (continued).

EIA Assembly Code	Init. Use Year	Last Disch. Year	Rod Pitch, in.	Mass of U, kg	Rod Diam., in.	Rod Length, in.		Active Length, in.		Clad Material	Clad Thickness, in.		Plenum Length, in.
						min/nom	max	min/nom	max		min/nom	max	
Init. = initial Disch. = discharge Mass of U = uranium per assembly Diam. = diameter min/nom = minimum value if a maximum is listed; nominal value otherwise max = maximum													

4.1.2 Information on fuel assembly design

Information on fuel assembly design was taken from the FADB and is repeated in Table 4.1.2-1. The data in the FADB are only for discharges through December 31, 1989, so discharge dates of 1989 in Table 4.1.2-1 mean "1989 or later". Information on amounts of uranium per assembly in the tables taken from the FADB is preferred to that given in Ref. 5.3, Table B5 because the FADB gives more precise values.

Not all of the values in Tables 4.1.1-1 and 4.1.2-1 appear in Section 7 of the analysis. These data may be of two types. First, there are data that are used but not tabulated. For example, numbers of assemblies discharged are given in Table 4.1.1-1 for all assembly types, but if the assembly type is not notable, the number does not appear in the tables in Section 7. Second, there are data that are included for completeness but not used. For example, information on last discharge year is included in Table 4.1.2-1 for many assembly types, but only that for stainless steel clad assemblies is used.

The data in the FADB are reported at different levels of precision. For example, a G4608G4B assembly is said to have an active length of "146" inches, but a G2308G5 assembly is said to have an active length of "145.24" inches. In standard engineering design practice, the former value implies a tolerance of ± 0.5 inches, while the latter implies a tolerance of ± 0.005 inches. It seems implausible that two assembly types from the same manufacturer should have tolerances that differ by a factor of 100. It was concluded that the values in the FADB are merely nominal values, and so no effort has been made to preserve trailing zeros in Table 4.1.2-1. For example, the FADB reports an active length for a G4608G5 assembly as "150.0" inches, but Table 4.1.2-1 reports it as "150" inches.

Although the data in Table 4.1.2-1 are from approved software, the following values are considered notable:

- For assembly types B1515B5, B1515B5Z, B1515B6, B1515B7, G2308A, and G2308AP, the cladding thickness is greater than half of the rod diameter; therefore, these assemblies are not considered in the design analysis.
- For assembly type XFC14W, the rod pitch is unusually large. Correction of the rod pitch would not affect the analysis. This value might have been used in calculations for external mechanical loading, but it is not used because information on spacer grid locations is not available.
- For assembly type W1717B, the rod length is unusually small. Correction of the rod length would not affect the analysis. This value might have been used in calculations of the effect of changes in gas volume, but it is not used because active and plenum lengths are not available.

4.1.3 Spent fuel inventory at Haddam Neck

Information on the spent fuel inventory at Haddam Neck was obtained through a telephone conversation with staff at the reactor site; that information was captured in Ref. 5.5. The following numbers of assemblies were used:

- 80 stainless-clad assemblies at General Electric in Morris
- 3 stainless-clad assemblies at Battelle-Columbus
- 858 stainless-clad assemblies on site
- 108 Zircaloy-clad assemblies with stainless steel structural components on site
- 53 Zircaloy-clad assemblies with Zircaloy structural components on site
- 4 stainless-clad assemblies, with some rods removed, on site
- 1 storage container with failed fuel rods taken from assemblies.

4.1.4 In-reactor corrosion of cladding

The following information on the depth of in-reactor corrosion is used:

- | - corrosion depth of 35 to 52 μm for rod-averaged burnup of 56 GWd/MTU (gigawatt-day per metric ton uranium), Fort Calhoun fuel (Ref. 5.16, pp. 3, 31, 47)
- | - corrosion depth of 36 to 57 μm , 45.3 μm average, for local burnup of 55 GWd/MTU, Oconee 1 fuel (Ref. 5.14, p. 3-25)
- corrosion depth of 65 μm for a burnup of 50 GWd/MTU, fuel irradiated in European reactors (Ref. 5.17, Figure 1).

Since in-reactor corrosion is related to burnup, the number of high-burnup assemblies is of interest in discussions of corrosion. Ref. 5.3 reports the total number of pressurized water reactor assemblies of various burnups discharged through 1994. The number with burnups of 45 GWd/MTU or more is $1513 + 102 + 11 = 1626$ (Ref. 5.3, p. 26).

4.1.5 Densities, molar masses, and gravity

The following information on densities and molar masses is used:

- | - molar mass of zirconium (Zr): 91.224 g/mol (Ref. 5.20, inside front cover)
- | - density of zirconium: 6490 kg/m³ (Ref. 5.21, p. B-165)
- | - molar mass of oxygen (O): 15.9994 g/mol (Ref. 5.20, inside front cover)
- | - density of ZrO₂ (baddeleyite): 5890 kg/m³ (Ref. 5.21, p. B-166)
- | - bulk density of TSw2 tuff: 2270 kg/m³ (Ref. 5.28, p. 42, Figure 30).

4.1.6 Mechanical properties of Zircaloy

The following mechanical properties of Zircaloy are used:

- | - yield stress (typical fuel): 780 MPa (Ref. 5.36, p. 82, Table 21, line 1)
- | - ultimate tensile stress (typical fuel): 925 MPa (Ref. 5.36, p. 82, Table 21, line 1)
- | - uniform elongation (strain) (typical fuel): 3.5% (Ref. 5.36, p. 82, Table 21, line 1)

- | – uniform elongation (high-burnup fuel, local burnup of 59.0 GWd/MTU): 0.15% (Ref. 5.16, p. 71, Table 19, line 1)
- | – elastic modulus: 99.284 GPa (Ref. 5.30, p. 830). (The value for pure zirconium is appropriate for Zircaloy, which is zirconium alloyed with a small amount of tin (1.20% to 1.70%) and even smaller amounts (< 0.25% each) of other elements (Ref. 5.22, Table 2).)

The mechanical properties are used in a calculation that applies at times long after emplacement. At such long times there will be little decay heat, so the use of room-temperature data is justified.

4.1.7 Distance between spacer grids

The locations of spacer grids or the distances between them are shown in some of the drawings in Ref. 5.24. All drawings in this report for pressurized water reactor fuel assemblies were inspected to determine the locations of spacer grids, and the information available is summarized in Table 4.1.7-1. The column "Page" gives the page number of the drawing. Since Ref. 5.24 predates the FADB, the nomenclature for assembly types differs between the two sources. The notes following the table explain how the Energy Information Administration (EIA) assembly code was uniquely identified from information in Ref. 5.24. The column "Maximum distance, in." gives the maximum center-to-center distance from one spacer grid to an adjacent spacer grid, with the value given in inches. Distances and dimensions on the drawings were taken to be in inches. If no distance is given in the table, the drawing did not give sufficient information to determine the spacing. The columns "Measurement 1, in." and "Measurement 2, in." give the values of measurements on the drawings from which the spacing was determined by difference. The measurements are given in the same form (fractional or decimal) and to the same precision as on the drawings. If the columns "Measurement 1, in." and "Measurement 2, in." are blank, the drawing did not specify the locations of the spacer grids or the spacing was given directly. The maximum distance between spacer grids is given in the same form as the measurements and to the same precision as the measurements (or the precision of the less precise measurement if the precisions differ).

Of the assembly types listed in Table 4.1.7-1 for which spacer grid distances could be determined, assembly types XHN15B, XSO14W, and XHN15W were not considered in Section 7.8 because the cladding for these assemblies is stainless steel. Type XYR16C was not considered because the FADB does not list a rod diameter for this fuel type.

Table 4.1.7-1. Maximum distance between spacer grids as shown in Ref. 5.24. See text above and notes following table for explanation. If distances between grids were shown on the drawing, the maximum distance is tabulated. If distances from an arbitrary reference location were shown, Measurement 1 and Measurement 2 are tabulated.

Page	EIA Assembly Code	Maximum distance, in.	Measurement 1, in.	Measurement 2, in.
2A-35	B1515B4	21 1/8	48 7/8	27 3/4
2A-41	XHN15B	21.08	66.22	45.14
2A-53	B1717B	22	132 3/4	110 3/4
2A-59*	C1414C	18 55/64		
2A-65	XFC14C	16 13/16		
2A-71	XPA15C	15 1/2		
2A-77	C1616CSD			
2A-83	XSL16C			
2A-89	C1616CSD	14 13/16		
2A-95	C8016C			
2A-101	XYR16C	18.300	38.210	19.910
2A-167	W1414A	22.00	131.78	109.78
2A-173	C1414A	18.859	53.781	34.922
2A-179	W1414ATR	26.190	52.335	26.145
2A-191	W1515A	26.190	52.215	26.025
2A-197	XPA15A	15.500	30.847	15.347
2A-203	XYR16A	18.300	40.195	21.895
2A-209	W1717A	24.43	25.98	1.55
2A-299	W1414WO	26.19	57.19	31.00
2A-305	W1414W	26.19	56.81	30.62
2A-311	XSO14W	21.08	45.14	24.06
2A-317	C1414W			
2A-323	W1515W	26.19	56.81	30.62
2A-329	W1515WO	26.19	57.19	31.00
2A-335	XHN15W	21.08	45.14	24.06
2A-347	W1717WL	24.43	30.62	6.190
2A-353	W1717WO	24.89	31.08	6.190
2A-359	W1717WV5			
2A-365	WST17W	22.1	51.4	29.3

* Corrected page number. Figure was actually bound before page 2A-55.

Notes on Table 4.1.7-1:

In the notes below, "table" without modifiers refers to the data table in Ref. 5.24 that accompanies the drawing under discussion.

B1515B4: Drawing reads "Mark - B4", table specifies Babcock & Wilcox as manufacturer.

XHN15B: Drawing reads "Conn Yankee" (= Haddam Neck, according to Ref. 5.7), table specifies Babcock & Wilcox as manufacturer and stainless steel as cladding material.

B1717B: Drawing reads "Mark - C", table specifies Babcock & Wilcox as manufacturer.

C1414C: Drawing lists Combustion Engineering 14 × 14 plants (Ref. 5.3, p. 114), table specifies Combustion Engineering as manufacturer.

XFC14C: Table specifies Combustion Engineering as manufacturer and Fort Calhoun as plant.

XPA15C: Table specifies Combustion Engineering as manufacturer, drawing lists Palisades as plant.

C1616CSD: Drawing lists Combustion Engineering 16 × 16 plants (Ref. 5.3, p. 114).

XSL16C: Drawing lists St. Lucie 2 as plant.

C1616CSD: Drawing lists Combustion Engineering 16 × 16 plants (Ref. 5.3, p. 114).

C8016C: Drawing lists Combustion Engineering 16 × 16 System 80 plants (Ref. 5.3, p. 114).

XYR16C: Drawing lists Yankee Rowe as plant, table specifies Combustion Engineering as manufacturer.

W1414A: Table specifies Westinghouse 14 × 14 as assembly class, ANF as manufacturer, 1271.2 lbs as total weight. This matches the FADB value for W1414A.

C1414A: Table specifies Combustion Engineering 14 × 14 as assembly class, ANF as manufacturer.

W1414ATR: Table comments list a Westinghouse 14 × 14 plant (Ref. 5.3, p. 114), table specifies ANF Top Rod as assembly type.

W1515A: Table specifies Westinghouse 15 × 15 as assembly class, ANF as manufacturer, 1432.8 lbs as total assembly weight. This matches the FADB value for W1515A.

XPA15A: Table specifies ANF as manufacturer, Combustion Engineering 15 × 15 reactor. Palisades is the only Combustion Engineering 15 × 15 reactor (Ref. 5.4, pp. 40-42; Ref. 5.3, Table B4).

XYR16A: Table comments list Yankee Rowe as plant, table specifies ANF as manufacturer.

W1717A: Table specifies Westinghouse 17 × 17 as assembly class, ANF as manufacturer.

W1414WO: Table specifies Westinghouse 14 × 14 OFA (optimized fuel assembly) as assembly type.

W1414W: Table specifies Westinghouse 14 × 14 Standard as assembly type.

XSO14W: Table specifies Westinghouse as manufacturer, 14 × 14 as array size, Type 304 stainless steel as cladding material. Only San Onofre 1 used such fuel.

C1414W: Table specifies Westinghouse as manufacturer, 14 × 14 as array size. Table gives overall length of 157.238 in., which matches value in the FADB for C1414W.

W1515W: Table specifies Westinghouse 15 × 15 Standard as assembly type.

W1515WO: Table specifies Westinghouse 15 × 15 OFA as assembly type.

XHN15W: Table specifies Westinghouse as manufacturer, 15 × 15 as array size, Type 304 stainless steel as cladding material. Only Haddam Neck used such fuel.

W1717WL: Table specifies Westinghouse 17 × 17 as assembly class, 1482.0 lbs as total assembly weight.

W1717WO: Table specifies Westinghouse 17 × 17 OFA as assembly type.

W1717WV5: Table specifies Westinghouse 17 × 17 Vant (= Vantage) 5 as assembly type.

WST17W: Table comments specify South Texas Reactors.

4.1.8 Volume of rubble blocks

Volumes of rubble blocks for TSw2 tuff are consistent with those in Ref. 5.28, pages VI-10 through VI-23. Because of the volume of data, these parameters are given in Attachment VII. As is discussed in Section 9, Attachment VII contains a listing of the file `esfblock.txt`. Each line of the file contains two numbers: a cumulative frequency of occurrence (expressed as a number from 0 to 1) and a block volume in cubic meters. To avoid errors, the data in Attachment VII were obtained from the electronic data file used to prepare Ref. 5.28 rather than from a printed copy. Accordingly, the numbers in Attachment VII are expressed to higher precision. Some digits in Attachment VII may not be significant. The data from Ref. 5.28 were supplemented with an additional data point: a cumulative frequency of occurrence of 0 for blocks with volume no larger than 0 m³. This point simply expresses the fact that all blocks must have a positive volume.

Ref. 5.28 contains TBV-231. However, this item does not apply to the rock density or block volumes, so it is not carried to this document.

4.1.9 Characteristics of disposal container

The following dimensions of a 21-PWR (pressurized water reactor) disposal container are used:

- inside diameter of corrosion resistant (inner) barrier: 1423.4 mm (Ref. 5.29)
- width of basket side guide assembly: 733 mm (Ref. 5.37)

The following characteristics of the arrangement of fuel assemblies in a 21-PWR disposal container is used:

- capacity: 21 fuel assemblies (Ref. 5.38)
- number of columns of assemblies: 5 (Ref. 5.38)

4.1.10 Burnup distribution of PWR fuel

The following information on the burnup distribution of PWR fuel discharged through 1986 is used:

- total number of assemblies discharged: 19968 (Ref. 5.3, Table 6)
- total number of assemblies discharged with burnups of 40 GWd/MTU or more: 200 (Ref. 5.3, Table 6)

The numbers above are obtained by adding numbers tabulated in the data source.

4.2 Criteria

Based on the rationale that the conclusions derived by this analysis are for preliminary design and will not be used as input into documents supporting construction, fabrication, or procurement, a notation of TBV or TBD will not be carried to the conclusions of this analysis.

Since fuel cladding is not specifically designed for waste isolation, only a few requirements are imposed on it in the *Engineered Barrier Design Requirements Document* (EB-DRD) (Ref. 5.27). Based on the rationale that the conclusions derived by this analysis are for preliminary design that will not be used as input to documents supporting construction, fabrication, or procurement, the TBD designations in Ref. 5.27 will not be carried to the conclusions of this analysis. In the quotations below, "TBD" denotes "to be determined". The following criteria are considered in the analysis.

"Engineered Barrier Segment structures, systems, and components important to safety shall be designed so that the effects of anticipated natural phenomena and environmental conditions will not interfere with necessary safety functions."

[EB-DRD 3.2.6.1.A]

The preceding requirement is considered to the extent that the response of different types of fuel cladding to various anticipated natural phenomena and environmental conditions is analyzed.

"The Engineered Barrier Segment shall maintain performance under rock-induced loading (TBD)."

[EB-DRD 3.7.F]

The preceding requirement is considered to the extent that the energy required to break fuel rods in an exposed assembly is analyzed.

"Packages for [spent nuclear fuel] and [high-level waste] shall be designed so that the in situ chemical, physical, and nuclear properties of the waste package and its interactions with the emplacement environment do not compromise the function of the waste packages or the performance of the underground facility or the geologic setting."

[EB-DRD 3.7.1.A]

The preceding requirement is considered to the extent that mechanical (i.e., physical) interactions between the waste form and the environment are discussed.

"The design of waste packages shall include, but not be limited to, consideration of the following factors: solubility, oxidation/reduction reactions, corrosion, hydriding, gas generation, thermal effects, mechanical strength, mechanical stress, radiolysis, radiation damage, radionuclide retardation, leaching, fire and explosion hazards, thermal loads, and synergistic interactions."

[EB-DRD 3.7.1.B]

The preceding requirement is considered to the extent that corrosion, thermal effects, mechanical strength, and mechanical stress are considered in the discussion of cladding degradation mechanisms.

4.3 Assumptions

4.3.1 Controlled design assumptions

The following assumptions from the *Controlled Design Assumptions Document* (Ref. 5.25) were used in the development of this document:

Key 008: Rod consolidation will not be performed at the Mined Geologic Disposal System (MGDS).

The assumption above is used in Section 7.8 in that the as-built geometry of the fuel assemblies, rather than a consolidated geometry, is used in calculations for rock loading

Key 073: The addition of filler material to spent nuclear fuel (SNF) arriving in disposable containers is not required.

The assumption above is used in Section 7.8 in that calculations of rock loading do not include filler material and its effect in transferring loads through a fuel assembly.

Key 011: Waste packages will be emplaced in-drift in a horizontal mode.

The assumption above is used in Section 7.8 in that rock loading is assumed to occur on the side of a fuel assembly rather than on the end.

DCWP 001: Limit the fuel cladding temperature to less than 350 degrees C.

The assumption above is used in Section 7.4 in that temperature will determine the applicability of models for creep rupture of cladding.

The bases for the assumptions above are given in Ref. 5.25. Based on the rationale that the conclusions derived by this analysis are for preliminary design that will not be used as input to documents supporting construction, fabrication, or procurement, any TBVs carried by Ref. 5.25 will not be carried to the conclusions of this analysis.

4.3.2 Density of fuel rods after compaction

When a rubble block impacts on a fuel assembly, it compresses the array of fuel rods, increasing the density of the fuel rod array until it reaches 0.9 times the density corresponding to a tightly packed hexagonal array of rods.

The basis for this assumption is that irregularities in the initial arrangement of rods will prevent them from reaching full density. A small (10%) decrease in density was chosen on the basis of engineering judgment. This assumption is used in Section 7.8.

4.4 Codes and Standards

One reference published by the American Society for Testing and Materials (Ref. 5.22) is used as a source of information in the analysis.

5. REFERENCES

- 5.1 *Total System Performance Assessment - 1995: An Evaluation of the Potential Yucca Mountain Repository* (Civilian Radioactive Waste Management System (CRWMS) Management and Operating Contractor (M&O), B00000000-01717-2200-00136 REV 01)
- 5.2 *Classification of the Preliminary MGDS Repository Design* (CRWMS M&O, B00000000-01717-0200-00134 REV 00)
- 5.3 *Spent Nuclear Fuel Discharges from U.S. Reactors 1994* (Department of Energy (DOE) Energy Information Administration, SR/CNEAF/96-01, February 1996)
- 5.4 "World List of Nuclear Power Plants", *Nuclear News*, March 1996, pp. 29-44.
- 5.5 CRWMS M&O Interoffice Correspondence LV.WP.JKM.01/97-018, "Spent nuclear fuel from Haddam Neck", from J. K. McCoy to File, January 30, 1997.
- 5.6 "Connecticut Yankee votes for premature shutdown", *Nuclear News*, January 1997, p. 19.
- 5.7 "Economic review points to permanent shutdown", *Nuclear News*, November 1996, p. 21.
- 5.8 *Control of Degradation of Spent LWR Fuel During Dry Storage in an Inert Atmosphere* (Pacific Northwest Laboratory, PNL-6364, October 1987)
- 5.9 *Safety Evaluation Report Related to the Topical Safety Analysis Report for Castor V/21 Dry Spent Fuel Storage Cask Submitted by General Nuclear Systems, Inc.* (U.S. Nuclear Regulatory Commission Office of Nuclear Material Safety and Safeguards, September 1985)
- 5.10 *Zircaloy Cladding Performance Under Spent Fuel Disposal Conditions* (Brookhaven National Laboratory, BNL 52235, April 1990)
- 5.11 *Temperature Limit Determination for the Inert Dry Storage of Spent Nuclear Fuel* (Electric Power Research Institute, EPRI TR-103949, May 1994)
- 5.12 *Waste Package Materials Selection Analysis* (CRWMS M&O, BBA000000-01717-0200-00020 REV 01)

- 5.13 *Spent Fuel Cladding Integrity During Dry Storage* (Lawrence Livermore National Laboratory, UCID-21181, September 1987)
- 5.14 "Waterside Corrosion of PWR Fuel Rods Through Burnups of 50,000 MWd/MTU" in *Light Water Reactor Fuel Performance* (DOE/NE/34130-1, vol. 1), pp. 3-17 to 3-35.
- 5.15 Warren C. Young, *Roark's Formulas for Stress and Strain*, 6th ed. (McGraw-Hill, New York, NY, 1989)
- 5.16 *Hot Cell Examination of Extended Burnup Fuel from Fort Calhoun* (Combustion Engineering, DOE/ET/34030-11, September 1986)
- 5.17 J. P. Mardon et al., "Update on the Development of Advanced Zirconium Alloys for PWR Fuel Rod Claddings", in *Proceedings of the 1997 International Topical Meeting on LWR Fuel Performance* (American Nuclear Society, La Grange Park, IL, 1997), pp. 405-412.
- 5.18 M. Mayuzumi and T. Onchi, "Creep Deformation and Rupture Properties of Unirradiated Zircaloy-4 Nuclear Fuel Cladding Tube at Temperatures of 727 to 857 K", *Journal of Nuclear Materials*, vol. 175, pp. 135-142, 1990.
- 5.19 R. E. Einziger, "Preliminary Spent LWR Fuel Oxidation Source Term Model", in *High Level Radioactive Waste Management: Proceedings of the Fifth International Conference* (American Nuclear Society, La Grange Park, IL, and American Society of Civil Engineers, New York, NY, 1994), pp. 554-559.
- 5.20 *CRC Handbook of Chemistry and Physics*, 74th ed., David R. Lide, editor (CRC Press, Boca Raton, FL, 1993)
- 5.21 *CRC Handbook of Chemistry and Physics*, 61st ed., Robert C. Weast, editor (CRC Press, Boca Raton, FL, 1980)
- 5.22 *Standard Specification for Wrought Zirconium Alloy Seamless Tubes for Nuclear Reactor Fuel Cladding* (American Society for Testing and Materials, Philadelphia, PA, ASTM B 811-90)
- 5.23 *Dry Oxidation and Fracture of LWR Spent Fuels* (U.S. Nuclear Regulatory Commission, Office of Nuclear Material Safety and Safeguards, NUREG-1565, November 1996)
- 5.24 *Characteristics of Spent Fuel, High-Level Waste, and other Radioactive Wastes Which May Require Long-Term Isolation* (DOE Office of Civilian Radioactive Waste Management (OCRWM), DOE/RW-0184, December 1987)

- 5.25 *Controlled Design Assumptions Document* (CRWMS M&O, B00000000-01717-4600-00032 REV 04, ICN 3)
- 5.26 *Quality Assurance Requirements and Description* (DOE OCRWM, DOE/RW-0333P, Rev. 7)
- 5.27 *Engineered Barrier Design Requirements Document* (DOE Yucca Mountain Site Characterization Project Office, YMP/CM-0024 Rev. 0, ICN 1)
- 5.28 *Confirmation of Empirical Design Methodologies* (CRWMS M&O, BABEE0000-01717-5705-00002 REV 00)
- 5.29 *21-PWR Waste Package Corrosion Resistant Shell* (CRWMS M&O, BBAA00000-01717-2700-16004 REV 00)
- 5.30 *Metals Handbook, 9th ed., vol. 2, Properties and Selection: Nonferrous Alloys and Pure Metals* (American Society for Metals, Metals Park, OH, 1979)
- 5.31 *CRC Standard Mathematical Tables, 19th ed., Samuel M. Selby, editor* (Chemical Rubber Co., Cleveland, OH, 1971)
- 5.32 QAP-2-0 Activity Evaluation WP-03, *Analyze Material and Performance Information and Data in Support of Waste Pack/Engineered Barrier Segment Development* (CRWMS M&O, August 3, 1997)
- 5.33 *Recommended Temperature Limits for Dry Storage of Spent Light Water Reactor Zircaloy-Clad Fuel Rods in Inert Gas* (Pacific Northwest Laboratory, PNL-6189, May 1987)
- 5.34 *Potential Corrosion and Degradation Mechanisms of Zircaloy Cladding on Spent Nuclear Fuel in a Tuff Repository* (Lawrence Livermore National Laboratory, UCID-20172, September 1984)
- 5.35 M. P. Puls, "The Influence of Hydride Size and Matrix Strength on Fracture Initiation at Hydrides in Zirconium Alloys", *Metallurgical Transactions A*, vol. 19A, pp. 1507-1522, 1988.
- 5.36 *Evaluating Strength and Ductility of Irradiated Zircaloy, Task 5* (Battelle Columbus Laboratories, NUREG/CR-1729, BMI-2066, vol. 1, May 1981)
- 5.37 *21-PWR Waste Package Basket Side Guide Assembly* (CRWMS M&O, BBAA00000-01717-2700-16006 REV 00)

5.38 21-PWR Waste Package Disposal Container Assembly (CRWMS M&O, BBAA00000-01717-2700-15998 REV 00)

6. USE OF COMPUTER SOFTWARE

Two qualified programs from the Characteristics Data Base were used as sources of information: the *LWR Fuel Assemblies PC Database* (Computer Software Configuration Item A00000000-02268-1200-20004 V 1.1) (FADB) and the *LWR Quantities PC Database* (Computer Software Configuration Item 20003 V 1.3) (QTYDB). This software (1) was appropriate for the application made in the analysis, (2) was used only within its range of validation, and (3) was obtained from Software Configuration Management in accordance with appropriate procedures. This software was executed on an IBM-compatible personal computer.

Industry standard software used in this analysis is Mathcad PLUS version 6.0 and Excel version 97. This software was also executed on an IBM-compatible personal computer. Mathcad PLUS and Excel are not controlled computer software, have not been qualified under the QAP-SI series of M&O procedures, and will not be qualified under the M&O procedures.

Attachments I, II, IV, V, and VI contain software routines used with Mathcad PLUS, and Attachments III and VIII contain software routines used with Excel. The software routine information described in QAP-SI-0, Attachment VI is given below. The software routines were appropriate for the application, were qualified in accordance with QAP-SI-0, and were used only within the range of qualification.

Computer Software Configuration Item identifiers have not been assigned to the routines. The attachment numbers and/or the filenames shown in the heading lines serve as names for the routines. The version is identified by the date and time of modification. Descriptions and equations of mathematical models, algorithms, and numerical solution techniques are described in comments in the routines or in the analysis itself, as applicable. Descriptions of the routines and their execution environments are given in Section 9. Test cases and test results (including input and output files) are not provided because the form of the routines is such that the routines lend themselves to easy verification by visual inspection.

Attachment I has been verified for the following ranges of the input parameters:

- maximum distance between spacer grids greater than zero (variable name = $msmt_{j,0}$)
- cladding thickness greater than zero and less than or equal to half the outside diameter of the cladding (variable name = $msmt_{j,1}$)
- outside diameter of the cladding greater than zero (variable name = $msmt_{j,2}$)
- rod pitch greater than the outside diameter of the cladding (variable name = $msmt_{j,3}$)
- number of rods along one side of an assembly that is greater than zero (variable name = $msmt_{j,4}$)
- elastic modulus greater than zero (variable name = E)
- yield strength greater than zero (variable name = σ_y)
- ultimate strength greater than the yield strength (variable name = σ_u)

- uniform elongation greater than zero (used in defining variable named ϵ_u)
- fractional offset of the neutral axis from the axis of the cladding that is greater than or equal to zero and less than or equal to one (variable name = δ)
- bulk density of tuff at in situ saturation greater than zero (variable name = ρ)

Attachment II has been verified for the following ranges of the input parameters:

- distance between spacer grids greater than zero (variable name = L)
- cladding wall thickness greater than zero and less than or equal to half the outside diameter of the cladding (variable name = t)
- cladding radius greater than zero (variable name = R)
- elastic modulus greater than zero (variable name = E)
- yield strength greater than zero (variable name = σ_y)
- ultimate strength greater than the yield strength (variable name = σ_u)
- uniform elongation greater than zero (used in defining variable named ϵ_u)
- fractional offset of the neutral axis from the axis of the cladding that is greater than or equal to zero and less than or equal to one (variable name = δ)
- intermediate strain greater than the yield strain and less than or equal to the elastic plus plastic uniform elongation (variable name = ϵ_m)

Attachment III has been verified for the following ranges of the input parameters:

- force greater than zero (cells in range A6:A20)
- displacement greater than zero (cells in range B6:B20)
- fitting exponent greater than zero (cell A27)

Attachment IV has been verified for the following ranges of the input parameters:

- maximum distance between spacer grids greater than zero (variable name = $msmt_{j,0}$)
- cladding thickness greater than zero and less than or equal to half the outside diameter of the cladding (variable name = $msmt_{j,1}$)
- outside diameter of the cladding greater than zero (variable name = $msmt_{j,2}$)
- rod pitch greater than the outside diameter of the cladding (variable name = $msmt_{j,3}$)
- number of rods along one side of an assembly that is greater than zero (variable name = $msmt_{j,4}$)
- number of assemblies discharged greater than or equal to zero (variable name = $msmt_{j,5}$)
- length of fuel rods greater than or equal to zero (variable name = $msmt_{j,6}$)
- type of assembly greater than or equal to zero and less than or equal to 19 (variable name = type)
- effectiveness of rods in achieving dense packing that is less than or equal to one and sufficiently large that the final density is greater than the original density ($\rho_f > \rho_o$) (variable name = pack)
- displacement at yield greater than zero (used in defining variable named Dy)
- displacement at failure for typical fuel that is greater than displacement at yield (used in defining variable named Du)
- displacement at failure for high-burnup fuel that is greater than displacement at yield (used in defining variable named Duhb)

- | - force at yield greater than zero (used in defining variable named Fy)
- | - force at failure for typical fuel that is greater than force at yield (used in defining variable named Fu)
- | - force at failure for high-burnup fuel that is greater than force at yield (used in defining variable named Fuhb)
- | - fitting exponent greater than zero (used in defining function named D(F))

Attachment V has been verified for the following ranges of the input parameters:

- | - density of rock blocks greater than zero (variable name = density)
- | - fall height greater than or equal to zero (variable name = fallht)
- | - number of assemblies in one stack greater than zero (variable name = nstack)
- | - focusing parameter greater than zero and less than or equal to one (variable name = focus)
- | - angle between punch blade and rods greater than or equal to zero and less than or equal to 90° (variable name = angle)
- | - high-burnup fuel switch of zero or one (variable name = hb)
- | - rod pitch greater than zero (variable name = rp)
- | - number of rods per side greater than zero (variable name = nrod)
- | - energy to start breaking rods greater than zero (variable name = Estart)
- | - energy to break one additional rod greater than zero (variable name = Eaddl)
- | - displacement to start breaking rods greater than zero (variable name = zstart)
- | - effective rod pitch greater than zero (variable name = rp_{eff})
- | - number of assemblies discharged greater than or equal to zero (variable name = ndisch)
- | - length of fuel rods greater than zero (variable name = rodlen)
- | - cumulative probability for block of given volume greater than or equal to zero and less than or equal to one (variable name = cumprobm_x)
- | - corresponding block volume for cumulative probability that is greater than or equal to zero (variable name = blkvolm_x)

Attachment VI has been verified for the following ranges of the input parameters:

- | - density of rock blocks greater than zero (variable name = density)
- | - fall height greater than or equal to zero (variable name = fallht)
- | - number of assemblies in one stack greater than zero (variable name = nstack)
- | - focusing parameter greater than zero and less than or equal to one (variable name = focus)
- | - high-burnup fuel switch of zero or one (variable name = hb)
- | - rod pitch greater than zero (variable name = rp)
- | - number of rods per side greater than zero (variable name = nrod)
- | - energy to start breaking rods greater than zero (variable name = Estart)
- | - energy to break one additional rod greater than zero (variable name = Eaddl)
- | - displacement to start breaking rods greater than zero (variable name = zstart)
- | - effective rod pitch greater than zero (variable name = rp_{eff})
- | - number of assemblies discharged greater than or equal to zero (variable name = ndisch)
- | - length of fuel rods greater than zero (variable name = rodlen)
- | - cumulative probability for block of given volume greater than or equal to zero and less than or equal to one (variable name = cumprobm_x)

– corresponding block volume for cumulative probability that is greater than or equal to zero (variable name = blkvolmx)

Attachment VIII has been verified for the following ranges of the input parameters:

- number of breaks per rod greater than or equal to zero (cells with numeric values in range A5:B84)
- fraction of rods broken greater than or equal to zero (cells with numeric values in range D5:E84)
- fraction of fuel exposed greater than or equal to zero (cells with numeric values in range G5:H84)

For accuracy of the treatment of the cladding as a simple, thin-walled tubular beam, additional limitations on Attachments I and IV are that the grid-to-grid distance should be large in comparison to the rod diameter, and the rod diameter should be large in comparison to the cladding wall thickness. No additional limitations apply to Attachments II, III, V, VI, or VIII. The input parameters used with software routines documented in Attachments I, II, III, IV, V, VI, and VIII were all within the ranges of verification listed above.

Appropriate references are cited in comments in the routines. A directory listing of executable and data files is not provided; instead, the source code and data files are printed in the analysis and its attachments.

Attachment I requires the input file that is documented in Table 7.8.1-1. Output from Attachment I is documented in Table 7.8.2-1 as described in Section 9.

Attachment II uses no input files. Output from Attachment II is documented in Attachment III.

Attachment IV requires the input file that is documented in Table 7.8.1-1. Output from Attachment IV is documented in Table 7.8.2-2.

Attachments V and VI require two input files; one of these is documented in Attachment VII, the other is documented in Table 7.8.2-2. Output from Attachments V and VI is documented in Attachment VIII.

Attachments III and VIII document their own input and output.

7. DESIGN ANALYSIS

7.1 Introduction

A recent total system performance assessment (Ref. 5.1, p. 8-9) considered the effect of cladding on release from the engineered barrier system. Reductions in the release rate for various radionuclides were noted when it was assumed that cladding provided protection of spent nuclear fuel from ground water. However, the approach was strictly empirical in that the fraction of the

fuel surface area available for dissolution was simply assumed. In light of the reduced release rate, an effort was undertaken to compile information that would help in constructing more defensible models for the next total system performance assessment. This analysis reports on that effort.

A description of the spent nuclear fuel that will be placed in a high-level radioactive waste repository necessarily includes estimation and prediction. However, there is substantial documentation in the open literature for both nuclear fuel designs and quantities of spent fuel. Information in this documentation can be used to characterize a design-basis cladding.

Commercial light-water reactor spent fuel in the U.S. may be divided into two classes: that with stainless steel cladding and that with zirconium alloy cladding. In developing a design-basis cladding for spent nuclear fuel, it is important to determine what quantity of fuel falls into each class, because the composition differences between stainless steel and zirconium alloy cladding are expected to produce large differences in corrosion performance after waste package breach. Section 7.2 of this analysis quantifies the amount of stainless steel clad fuel. The remainder of the analysis, Sections 7.3 through 7.8, considers only fuel with a zirconium alloy cladding.

Section 7.3 briefly discusses the different environments that are expected in a repository, and the degradation mechanisms that will be operative in different environments. Sections 7.4 through 7.8 then discuss the individual degradation mechanisms in turn: creep rupture, dry cladding oxidation, dry fuel oxidation, aqueous corrosion, and external mechanical loading. For each mechanism, the fuel that is most susceptible to degradation is identified.

In the discussion below, assembly types and classes are denoted by the appropriate EIA assembly type codes and assembly classes as listed in Ref. 5.3, Table B4. In the tables in this analysis, the total amount of uranium for the assemblies of a given assembly type is the amount of uranium per assembly times the number of assemblies discharged, expressed in metric tons and rounded to the nearest metric ton.

It is noted that the FADB and Ref. 5.3 have different conventions for counting assemblies. This is evident from inspection of data for fuel with EIA assembly code XBR12G. The FADB reports discharges of 66 assemblies of this type, but Ref. 5.3, Table B5 reports none. The comments in the FADB explain the difference. The FADB number includes assemblies that were subsequently reprocessed, whereas the number in Ref. 5.3, Table B5 does not. Per Ref. 5.3, p. 240, Note 6, "A number of assemblies were discharged and reprocessed prior to 1972. Data on these reprocessed assemblies are not included in this report, except for 962 reprocessed assemblies reflected in Table 9 as shipments." The convention of Ref. 5.3 is appropriate for analyses that pertain to a repository. Data from Table 9 of Ref. 5.3 are not used in this analysis.

7.2 Quantity of stainless steel clad fuel

The information in these databases was examined carefully to determine how much stainless-clad fuel has been discharged but not reprocessed. The calculated value is 723 metric tons of

uranium, or 2.4% of the total uranium discharged through 1994. This fuel is in 2179 assemblies, or 2.1% of the total number assemblies discharged through 1994. (See Section 4.1.1 for total amount of uranium and number of assemblies.) The remainder of this section lists the various types of fuel and discusses how the mass of uranium was determined for each.

An accurate value of the amount of stainless steel clad fuel can be obtained from available data. According to Table 4.1.1-1, stainless cladding was used in only eight reactors: Big Rock Point, Dresden 1, Haddam Neck, Humboldt Bay, Indian Point 1, LaCrosse, San Onofre 1, and Yankee Rowe. Six of these, Dresden 1, Humboldt Bay, Indian Point 1, LaCrosse, San Onofre 1, and Yankee Rowe were closed in 1978, 1976, 1974, 1987, 1992, and 1991, respectively (Ref. 5.4, p. 43). Since Section 4.1.1 includes information on discharges through 1994, all fuel from these reactors is listed in Table 4.1.1-1. Only one type of stainless-clad fuel was used at Big Rock Point, and the FADB notes that this was the initial core. All the other fuel at Big Rock Point has had zirconium alloy cladding, so no additional stainless-clad fuel is expected from this reactor. As is discussed below, Haddam Neck was recently shut down. Some of the recent discharges from Haddam Neck do not appear in Section 4.1.1, but assembly counts were obtained from the staff at the reactor site.

All of the 87 assemblies of "undetermined" type listed in Table 4.1.1-1 have zirconium alloy cladding. This is made clear in Ref. 5.3, p. 241, Note 10, which lists the reactors from which these assemblies were temporarily discharged. None of the reactors listed there is among the eight in which stainless steel clad fuel was irradiated.

In the discussions below, masses of uranium per assembly are as specified in Table 4.1.2-1.

Big Rock Point: Assemblies of type XBR12G, which had Type 304 stainless steel cladding, were irradiated in this reactor. However, Table 4.1.1-1 lists no assemblies of type XBR12G, so all of these assemblies were reprocessed.

Dresden 1: Assemblies of type XDR07G were irradiated in this reactor. According to Section 4.1.1, these assemblies had stainless steel cladding. However, Table 4.1.1-1 lists no assemblies of type XDR07G, so all of these assemblies were reprocessed.

Haddam Neck: Four types of stainless-clad fuel were irradiated at Haddam Neck. Table 4.1.1-1 states that the cladding for all four types of fuel was Type 304 stainless steel. The most important of these is type XHN15B. For this type of fuel, the average uranium loading is 411.9 kg (Table 4.1.2-1). Table 4.1.1-1 states that a total of 576 assemblies of this type were discharged, so the total mass of uranium for this assembly type is $411.9 \text{ kg/assembly} \times 576$ assemblies. However, there appears to be additional spent fuel of this type. See the last paragraph of the discussion of Haddam Neck fuel.

Table 4.1.1-1 states that one assembly of type XHN15HS was irradiated. Table 4.1.2-1 does not mention type XHN15HS but does describe type XHN15IS. Examination of the assembly

descriptions in Ref. 5.3, Table B4 and the FADB suggests that these two codes refer to the same fuel. Table 4.1.2-1 gives the mass of uranium in this assembly as 406.2 kg.

Table 4.1.1-1 states that two assemblies of type XHN15MS were irradiated. Table 4.1.2-1 gives the mass of uranium in these assemblies as 406.0 kg each.

Table 4.1.1-1 states that 309 assemblies of type XHN15W were irradiated. Table 4.1.2-1 gives the mass of uranium in these assemblies as 415.6 kg each.

As was noted above, Table 4.1.1-1 records discharges of 576 assemblies of type XHN15B. However, the QTYDB notes that fuel of this type was being discharged through 1993, so more recent information on fuel discharges was sought. Mr. J. R. Worsham of Framatome Cogema Fuels in Lynchburg, Virginia, provided information on the total inventory of Haddam Neck fuel, which is listed in Section 4.1.3.

No additional Haddam Neck fuel will be irradiated because this reactor has been permanently shut down (Ref. 5.6; Ref. 5.7). The data from Table 4.1.1-1 account for 888 assemblies with stainless cladding, and the data from Section 4.1.3 indicate a total of 945 stainless-clad assemblies, so it is clear that an additional 57 stainless-clad assemblies were discharged after 1994. Inspection of Table 4.1.2-1 shows that all stainless-clad fuel discharged from Haddam Neck after 1977 was of type XHN15B, so the additional discharges were taken to be of this type and clad with Type 304 stainless steel. The mass of uranium per assembly is specified as 411.9 kg in Table 4.1.2-1, so the total inventory of XHN15B stainless-clad fuel is $411.9 \text{ kg/assembly} \times (576 + 57)$ assemblies.

Humboldt Bay: Table 4.1.1-1 states that assemblies of type XHB07G were clad with stainless steel. However, it does not list any assemblies of this type, so all assemblies of this type were reprocessed.

Indian Point 1: Two types of fuel were irradiated at Indian Point 1. Table 4.1.2-1 states that the cladding for both types of fuel was Type 304 stainless steel. Table 4.1.1-1 lists zero assemblies of type XIP14B, so all assemblies of this type were reprocessed. The table also lists 160 fuel assemblies of type XIP14W. The mass of uranium for type XIP14W is 191.2 kg per assembly.

LaCrosse: Two types of fuel were irradiated at LaCrosse. Table 4.1.2-1 states that the cladding for both types of fuel was Type 348H stainless steel. Table 4.1.1-1 lists 155 assemblies of type XLC10L and 178 assemblies of the type XLC10A. According to Table 4.1.2-1, the mass of uranium for these assembly types is 120.2 kg per assembly and 108.7 kg/assembly, respectively, so the total amount of uranium is $120.2 \text{ kg/assembly} \times 155 \text{ assemblies} + 108.7 \text{ kg/assembly} \times 178 \text{ assemblies}$.

San Onofre 1: Table 4.1.1-1 lists one type of stainless-clad fuel, XSO14W. According to Table 4.1.2-1, this fuel had a cladding of Type 304 stainless steel. Table 4.1.1-1 notes 665 assemblies of this type. For this type of fuel, the uranium content is 366.3 kg per assembly.

Yankee Rowe: One of the types of fuel irradiated at Yankee Rowe was XYR18W, which, according to Table 4.1.2-1, had a clad of Type 348H stainless steel. All other fuel irradiated at Yankee Rowe had zirconium alloy cladding. Table 4.1.1-1 notes 76 assemblies of this type. The uranium content for this type of fuel was 273.4 kg/assembly.

Table 7.2-1 summarizes the quantities of stainless-clad fuel. From the number of assemblies discharged and the amount of uranium per assembly given in the table, the fuel with Type 304 stainless steel cladding contained 665 metric tons of uranium and the fuel with Type 348H stainless steel cladding contained 59 metric tons of uranium. Together these fuels contained 723 metric tons of uranium. (All three masses are rounded to the nearest metric ton.) There are 2179 assemblies with stainless steel cladding, which represent 2.1% of the total number discharged through 1994 (see Section 4.1.1).

Table 7.2-1. Amounts of spent nuclear fuel with stainless steel cladding.

EIA Assembly Code	Cladding material	Number discharged	Uranium per assembly, kg	Total uranium, metric tons
XHN15B	304 stainless steel	633*	411.9	261
XHN15HS (= XHN15IS)	304 stainless steel	1	406.2	0
XHN15MS	304 stainless steel	2	406.0	1
XHN15W	304 stainless steel	309	415.6	128
XIP14W	304 stainless steel	160	191.2	31
XLC10L	348H stainless steel	155	120.2	19
XLC10A	348H stainless steel	178	108.7	19
XSO14W	304 stainless steel	665	366.3	244
XYR18W	348H stainless steel	76	273.4	21
TOTAL	(not applicable)	2179	(not applicable)	723

* This number is taken from the text above rather than from Table 4.1.1-1.

7.3 Environment and mechanisms

Various authors have reviewed the degradation mechanisms of spent nuclear fuel (Ref. 5.8, Section 3; Ref. 5.9, p. 12; Ref. 5.10, Section 5; Ref. 5.11, Sections 3 and 5). Many of the investigations to date, however, have been restricted to degradation of fuel in dry storage, that is, in a hot, dry atmosphere of an inert gas such as helium. Repository environments may be more complex. It has been recommended that disposal containers for spent nuclear fuel be filled with

helium (Ref. 5.12, p. 111), so at short times the environment in a disposal container can be expected to be similar to that in a dry storage cask. The disposal container, however, is subject to various degradation mechanisms and may eventually be breached. In a breached disposal container, the spent nuclear fuel could be exposed to humid air or possibly liquid water. If the disposal container is degraded to the point that it loses its mechanical integrity and the emplacement drift has collapsed, the spent nuclear fuel could be subject to mechanical loads as well as a potentially corrosive environment.

In view of the variety of environments, different failure mechanisms may be important at different times. The mechanisms considered below are creep rupture, dry cladding oxidation, dry fuel oxidation, aqueous corrosion, and external mechanical loading. These mechanisms are treated in turn in the sections below.

7.4 Creep rupture

Several authors have considered the degradation of spent fuel in the inert environment of a dry storage container. Since this environment is similar to that of the interior of an unbreached waste package, the results for inerted dry storage may be applied directly to this stage of disposal. The authors of PNL-6364 concluded that creep rupture is the "Primary degradation mechanism" for cladding in inerted dry storage (Ref. 5.8, p. 3.17). Nuclear Regulatory Commission staff similarly concluded that diffusion-controlled cavity growth, a specific mechanism for creep rupture, was "the only mechanism of damage for dry storage ... that could cause degradation and gross rupture of the cladding" (Ref. 5.9, p. 12). Upon review of that work the authors of BNL 52235 concluded that "Creep rupture is potentially the most relevant failure mode" (Ref. 5.10, p. v). Although this statement sounds weak, it receives some reinforcement from statements that "for the overwhelming majority of fuel rods, DHC [delayed hydride cracking] is not likely to be an important mode of failure" and fuel-side stress corrosion cracking "is not believed to be an important mode of failure during storage and isolation" (Ref. 5.10, p. iv). EPRI TR-103949 is more decisive and states "there exists a general consensus that the temperature limits which can be tolerated during IDS [inerted dry storage] are determined primarily by the creep properties of the cladding. SCC [stress corrosion cracking] and DHC [delayed hydride cracking] have been discounted by all researchers as requiring much higher activation stresses than are achievable during IDS [inerted dry storage]" (Ref. 5.11, p. 30).

7.4.1 Degradation models

There are two chief models for creep rupture. One of these is the diffusion-controlled cavity growth model, which is theoretical and based on a micromechanical model for damage. The other is an empirical equation, "the Peehs model", for creep rate, which is used with a similarly empirical limit for the maximum amount of creep strain that can be tolerated.

In the diffusion-controlled cavity growth model, the cavities are nucleated, in a regular array, on the grain boundaries of the material. As the result of an applied tensile stress, vacancies are produced in the grain boundaries, and the vacancies diffuse to the cavities, causing cavity

growth. Failure is taken to occur when the cavities grow to such a size that they cover a certain fraction of the grain boundary area.

The diffusion-controlled cavity growth model has been applied in several reports, and some of the applications appear to be incorrect (Ref. 5.11, pp. 71-72). A derivation of the equations for cavity growth rate is given in UCID-21181 (Ref. 5.13). This derivation has sufficient detail for verification.

Various criticisms have been leveled at the diffusion-controlled cavity growth model. Perhaps the most significant of these is that the model requires the presence of a large number of cavities, but Ref. 5.11, p. 13 states that "Voids and cavities have been observed only *rarely* in irradiated Zircalloys and essentially only in Zircaloy-2 ... In fact, zirconium and zirconium-based alloys, as a whole, appear to be generally resistant to radiation-induced void and cavity formation", and six references with five principal authors are cited to support this position. In contrast, observations of cavities are supported by the work of only one principal author (Ref. 5.11, p. 43), and it has been argued that the observed cavities were actually artifacts of sample preparation (Ref. 5.11, p. 121). (The previous discussion does not extend to voids and cracks formed near failures, which are reported in Ref 5.35.)

For conditions of constant temperature and constant stress, the Peehs model takes the form (Ref. 5.11, p. 73)

$$\epsilon = A[B/T - \ln(\sigma/C) / \ln(t + 1) - 1]^{-m} \quad (1)$$

where ϵ is the strain in percent, σ is the stress in MPa, T is the temperature in K, and t is the time in hours. This equation was developed for an internally pressurized tube of unirradiated Zircaloy-4 cladding, and the stress and strain refer to the circumferential (hoop) components. For this material and these conditions, the constants are $A = 1.89 \times 10^{-3}$, $B = 610$, $C = 450$, and $m = 2.58$. The equation is said to be applicable to temperatures from 300°C to 450°C, stresses from 50 MPa to 300 MPa, and strains up to 10% (Ref. 5.11, p. 80). An alternative form of the equation uses t in place of $t + 1$ (Ref. 5.10, p. A-11). For the long times that are typical in creep experiments and dry storage, the difference between $\ln(t)$ and $\ln(t + 1)$ is small. The equation has been generalized to conditions of variable temperature and stress, with the result

$$\frac{d\epsilon}{dt} = \frac{-mA[(A/\epsilon)^{1/m}]^{-(m+1)} \Phi^2 (\sigma/C)^{1/\Phi}}{\ln(\sigma/C)} \quad (2)$$

where $\Phi = (A/\epsilon)^{1/m} - B/T + 1$ and the other constants and variables are as discussed above (Ref. 5.10, p. A-11). The generalization has not been verified by the author of the present analysis. With this model, failure of the cladding is taken to occur when the circumferential strain reaches 1%. This strain limit is apparently based on measurements of ductility (Ref. 5.11, p. 26). The use of a 1% strain criterion is supported by measurements on high-burnup (54.9 gigawatt-day per metric ton uranium (GWd/MTU) local burnup) fuel rods, for which a uniform elongation of $3.2\% \times (1 - 0.59) = 1.3\%$ was measured (Ref. 5.14, p. 3-26). It is noted that the Peehs model "has a built-in conservatism in that irradiated cladding creeps at a slower rate than the unirradiated cladding which forms the basis of the correlation" (Ref. 5.11, p. 80).

The Peehs model also has some limitations. As is noted in Ref. 5.11, p. 30, "the reference empirical correlation is tuned to Zircaloy tubing for KWU [Kraftwerk Union Aktiengesellschaft] PWR [pressurized water reactor] fuel and may not be directly applicable to clad tubing from other sources. The original study ... employed tubing from two manufacturers and it was found that the model coefficients differed, although not substantially, with each manufacturer. Further analysis may be needed to determine the variability of those coefficients and their applicability to clad tubing from US manufacturers." In addition, since the Peehs model is empirical, it is presumably based on fairly short-term data and would require substantial extrapolation to cover the period of high temperatures in a repository.

A feature of the Peehs model is that it allows predictions not only of the failure time but also of the current circumferential strain. As a result, a single, self-consistent treatment of both the strain to failure and the current changes in pressure as a result of creep strain can be developed.

7.4.2 Application of model

Predictions of the creep rupture behavior of fuel cladding require data for temperature and stress as functions of time. Predictions of cladding temperatures as a function of time will depend on the waste package and underground facility designs and are outside the scope of this analysis.

Several aspects of the cladding will affect the circumferential creep stress. The effects discussed here include those of cladding diameter and wall thickness, corrosion during irradiation, and changes in gas volume. The effect of thermal expansion of the gas is not discussed but can be treated by applying the ideal gas law.

7.4.2.1 Effect of cladding diameter and wall thickness

The circumferential stress in the cladding can be calculated from the gas pressure inside the fuel rod and the geometry of the rod. It has been argued (Ref. 5.11, p. 3) that the stress in the cladding should be calculated with the formula for a thick-walled cylinder because the ratio of the wall thickness to the inside radius is greater than 0.1. The maximum circumferential stress σ occurs at the inner surface and is

$$\sigma = P(R^2 + R_i^2) / (R^2 - R_i^2) \quad (3)$$

where R and R_i are the outside and inside radii of the cladding, respectively, and P is the internal gas pressure (Ref. 5.15, p. 638). Note that the circumferential stress is the product of the internal gas pressure and a stress multiplication factor $(R^2 + R_i^2) / (R^2 - R_i^2)$. The assembly types with the largest stress multiplication factor are clearly those that will be the most sensitive to internal pressurization. Tables 7.4.2.1-1 and 7.4.2.1-2 summarize the assembly types with the largest stress multiplication factors for internal pressure. The threshold for inclusion of an assembly type in these tables is arbitrary. The tables also include data for assembly types W1717WL and G4608GP, which are the most common spent fuel assembly types for pressurized water reactors and boiling water reactors, respectively. These data are given in shaded cells.

Table 7.4.2.1-1. Pressurized water reactor fuel assembly types with the largest stress multiplication factors for internal pressure.

EIA Assembly Code	Outside diameter, in.	Clad thickness, in.	Stress mult. factor	Number discharged	Uranium per assembly, kg	Total uranium, metric tons
W1414WL	0.422	0.0225	8.9	1410	399.1	563
W1414W	0.422	0.0225	8.9	622	393.8	245
W1515W	0.422	0.0242	8.2	1580	453.9	717
W1515WL	0.422	0.0242	8.2	3481	454.8	1583
W1515WO	0.422	0.0242	8.2	1533	460.0	705
W1717WL	0.374	0.0225	7.8	9525	460.2	4383

mult. = multiplication

Table 7.4.2.1-2. Boiling water reactor fuel assembly types with the largest stress multiplication factors for internal pressure.

EIA Assembly Code	Outside diameter, in.	Clad thickness, in.	Stress mult. factor	Number discharged	Uranium per assembly, kg	Total uranium, metric tons
XHB06G	0.563	0.032	8.3	176	76.4	13
G2307G2B	0.563	0.032	8.3	5047	192.8	973
G4607G2	0.563	0.032	8.3	1142	194.7	222
XBR07G	0.700	0.040	8.3	4	131.4	1
G4609AJX	0.431	0.025	8.2	4	176.8	1
XBR08G	0.570	0.035	7.7	2	112.3	0
XDR06G3F	0.5625	0.035	7.6	96	102.0	10
XDR06G5	0.5625	0.035	7.6	106	105.9	11
G2307G2A	0.570	0.0355	7.6	1672	194.9	326
XDR06G3B	0.555	0.035	7.5	163	101.8	17
G4608GP	0.483	0.032	7.1	11625	183.2	2130

mult. = multiplication

In Tables 7.4.2.1-1 and 7.4.2.1-2, the outside diameter, clad thickness, and amount of uranium per assembly are as reported in Table 4.1.2-1. Numbers of assemblies discharged are as given in Table 4.1.1-1. The stress multiplication factors are rounded to the nearest multiple of 0.1.

There are assembly types for which the rod outside diameter and cladding thickness are not both available, so there may be assembly types with stress concentration factors for internal stress that are larger than those listed above. However, in each assembly class except Haddam Neck there is at least one assembly type for which these data are available. The coverage of assembly types is therefore fairly inclusive, and the effect of assembly types for which data are not available is expected to be small.

For a few assembly types, the FADB specifies a range of cladding thicknesses. Even if the smallest thickness in the range is used, these fuels have smaller stress multiplication factors than those appearing in Tables 7.4.2.1-1 and 7.4.2.1-2.

Several adjustments are necessary in calculating the stress in the cladding. These include thermal expansion of the gas, a loss of cladding thickness from corrosion during irradiation, and an increase in gas volume as a result of creep strain.

7.4.2.2 Effect of corrosion during irradiation

Various measurements of oxide thickness have been made. In one study, oxides were measured on Fort Calhoun fuel that was irradiated to a rod-averaged burnup of 56 GWd/MTU. The thickness of the waterside cladding oxide layer varied between 35 and 52 μm (see Section 4.1.4). In independent work, metallographic measurements were taken on a sample of Oconee 1 fuel with a local burnup of approximately 55 GWd/MTU. On this sample, oxide thicknesses averaged 45.3 μm and ranged from 36 to 57 μm (see Section 4.1.4). By historical standards, these are very high burnups. In discharges through 1994, only 1626 out of 44598 pressurized water reactor assemblies had burnups of 45 GWd/MTU or higher (Section 4.1.4). It is expected that an oxide thickness of 57 μm , the largest of the thicknesses reported above, is an appropriate conservative value. As is discussed in Section 7.5.1, the oxide is about 1.49 times as thick as the metal from which it is formed, so this oxide thickness corresponds to a metal loss of about 38 μm . It should be noted, however, that the oxide thickness may depend on operating conditions. In Ref. 5.17, Figure 1 (see Section 4.1.4), the curve for Zircaloy 4 appears to indicate that a burnup of only 50 GWd/MTU corresponds to an oxide thickness of about 65 μm . However, the work reported there is apparently primarily for European reactors (Ref. 5.17, Table 4), which may have different operating conditions or reactor water chemistries. The corrosion rate during irradiation will also depend on the exact composition of the cladding, as is discussed in Section 7.7.1.

In general, the wall thickness of the cladding for spent fuel, $R - R_c$, will be slightly smaller than that for fresh fuel because of corrosion during irradiation. The stress multiplication factors for internal pressure given in the tables above reflect the as-manufactured fuel geometry, and reduction of wall thicknesses will increase the stress multiplication factor more for some assembly types than for others. However, the change in wall thickness is small, so there will not be a large change in the relative resistance of different assembly types to internal gas pressure.

7.4.2.3 Effect of changes in gas volume

Creep of the fuel cladding will increase gas volume of the fuel rod and thus decrease the internal pressure. Changes in gas volume are discussed in this section.

The circumferential stress is given by Eq. 3 above. For comparison, the axial stress σ_{ax} is (Ref. 5.15, p. 638)

$$\sigma_{ax} = PR_i^2 / (R^2 - R_i^2) . \quad (4)$$

Since $R_i^2 < R^2$, it is clear that σ_{ax} is less than half of σ . Creep strain rates are strongly dependent on stress. Ref. 5.18, Eq. 5, for example, shows an exponential dependence of strain rate on stress. The dependence in Eq. 2 above is more complex but still significant. Accordingly,

changes in the axial dimensions of the cladding will be neglected because the principal stress component in the axial direction is so much smaller than the circumferential stress. In contrast, changes in the radial dimensions of the cladding, which result from a strain in the circumferential direction, will be considered.

The interior of a fuel rod may be divided into two separate lengths: the active length, which is essentially filled with fuel pellets, and the plenum length, which is essentially filled with gas. This is an approximation. The fuel pellet dishes and chamfers will allow a small amount of gas to be present in the active length, and the expansion spring will occupy a small part of the plenum. In an irradiated fuel rod that has not been subjected to creep after discharge, the fuel-cladding gap will be negligible because the fuel pellets will expand as a result of irradiation and the cladding will have crept onto the fuel pellets during irradiation because of the reactor coolant pressure.

In view of the approximations given above, the volume of gas in an irradiated but uncrept fuel rod is $V_0 = \pi R_i^2 L_p$, where L_p is the length of the plenum. Similarly, the volume of fuel pellets is $V_f = \pi R_i^2 L_a$, where L_a is the active length.

As is discussed above, axial creep is expected to be small, so L_a and L_p may be treated as constants. In contrast, circumferential creep of the cladding will increase the radius to $r(1 + \epsilon)$ where ϵ is the principal creep strain in the circumferential direction. Because solids are essentially incompressible, the volume of the fuel pellets will be constant, but the volume of gas will increase to $V = \pi R_i^2 (1 + \epsilon)^2 (L_p + L_a) - V_f$.

To limit the amount of creep deformation after reactor discharge, it is desirable that the internal gas pressure should decrease quickly as the cladding creeps. For this to happen, what is needed is a large value of $d(V/V_0) / d\epsilon$. Conversely, a small value of $d(V/V_0) / d\epsilon$ corresponds to a fuel rod that loses pressure slowly as it creeps. The value of $d(V/V_0) / d\epsilon$ can be obtained from the equations given above:

$$\frac{d(V/V_0)}{d\epsilon} = \frac{1}{V_0} \frac{dV}{d\epsilon} = \frac{1}{V_0} \pi R_i^2 (L_p + L_a) (2 + 2\epsilon) . \quad (5)$$

For small creep strains ($\epsilon \ll 1$),

$$\frac{d(V/V_0)}{d\epsilon} \approx \frac{1}{V_0} 2\pi R_i^2 (L_p + L_a) = 2\pi R_i^2 (L_p + L_a) / \pi R_i^2 L_p = 2 + \frac{2L_a}{L_p} . \quad (6)$$

It is clear that the smallest values of L_a/L_p correspond to the smallest values of $d(V/V_0) / d\epsilon$, that is, to the weakest dependence of gas pressure on the circumferential strain and thus the greatest tendency for creep to continue.

The active length and plenum length are tabulated for many types of fuel assemblies in Table 4.1.2-1. The assembly types with the smallest values of L_a/L_p are given in Tables 7.4.2.3-1 and 7.4.2.3-2. Type B1515B has been omitted from Table 7.4.2.3-1 because there are no remaining

assemblies of this type (see Table 4.1.1-1). Pressurized water reactor assemblies and boiling water reactor assemblies are considered separately. The threshold for inclusion of an assembly type in these tables is arbitrary. The tables also include data for assembly types W1717WL and G4608GP, which are the most common spent fuel assembly types for pressurized water reactors and boiling water reactors, respectively. These data are given in shaded cells.

There are assembly types for which the active length and plenum length are not both available, so there may be assembly types with ratios of active length to plenum length that are smaller than those listed above. However, as is discussed below, the coverage of fuel types is fairly inclusive, and the effect of assembly types for which data are not available is expected to be small.

Table 7.4.2.3-1. Pressurized water reactor assembly types with the smallest ratio of active length to plenum length.

EIA Assembly Code	Active length, in.	Plenum length, in.	Length ratio L_a/L_p	Number discharged	Uranium per assembly, kg	Total uranium, metric tons
B1515B4	141.8	11.720	12.1	4134	464.5	1920
W1717WL	144.00	6.300	22.9	9525	460.2	4383

Table 7.4.2.3-2. Boiling water reactor assembly types with the smallest ratio of active length to plenum length.

EIA Assembly Code	Active length, in.	Plenum length, in.	Length ratio L_a/L_p	Number discharged	Uranium per assembly, kg	Total uranium, metric tons
G4607G2	144	16	9.0	1142	194.7	222
G4607G3A	144	16	9.0	3752	187.4	703
G4608G4A	144.0	16	9.0	1785	184.0	328
G4607G3B	146.0	14	10.4	1184	189.9	225
G4608G4B	146	14	10.4	1787	186.7	334
G2307G2A	144	11.25	12.8	1672	194.9	326
G2307G2B	144.0	11.24	12.8	5047	192.8	973
G2308G4	144.0	11.24	12.8	3876	184.1	714
G4608GP	150.0	9.48	15.8	11625	183.2	2130

In Tables 7.4.2.3-1 and 7.4.2.3-2, the active length, plenum length, and amount of uranium per assembly are as reported in Table 4.1.2-1. (For the pressurized water reactor assemblies, the active length was given as a range, and the minimum was used because this value gives the smallest value of L_a/L_p .) Numbers of assemblies discharged are as given in Table 4.1.1-1.

Table 4.1.2-1 provides plenum lengths for the assembly types B1515B and B1515B4 but not for other Babcock & Wilcox fuels. However, the general similarity of assemblies in this assembly class suggests that $L_a/L_p \geq 12.1$ is appropriate for all of them.

Since active lengths and plenum lengths are not available for all assembly types, additional justification of the design-basis values of L_a/L_p is appropriate. The justification here is based on comparisons of similar assembly types. The seven types of assemblies with the smallest values of L_a/L_p fall into two assembly classes: B&W 15 x 15 and GE BWR/4-6. For assembly class B&W 15 x 15, it has already been argued that a single value of L_a/L_p is appropriate for the entire class. For assembly class GE BWR/4-6, active and plenum lengths are both available for six assembly types besides the five listed in Table 7.4.2.3-2: G4608A, G4608GB, G4608G5, G4608GP, G4608W, and G4609A. For all six, $L_a/L_p > 14.9$. It is significant that the five types with small values of L_a/L_p are old types, with initial use years from 1972 to 1976, whereas the others are more recent, with initial use years from 1976 to 1985. For types G4608W and G4609A, no initial use year is given.

Active and plenum lengths are available for at least one assembly type in each assembly class except Indian Point 1, Palisades, San Onofre 1, and South Texas. For types XIP14W, XPA15A, XPA15C, XSO14W, a lower bound on L_a/L_p can be obtained by taking L_p to be the rod length minus the active length. For each of these assembly types, the resulting L_a/L_p is greater than 17. The value L_a/L_p for XIP14B is irrelevant because, as is reported in Table 4.1.1-1, no assemblies of this type remain.

A value of L_a/L_p could not be estimated for WST17W assemblies because neither the active length nor the plenum length are reported in Table 4.1.2-1. However, L_a/L_p can be obtained for several assembly types in classes WE 14 × 14, WE 15 × 15, and WE 17 × 17. Of these, the types with the smallest values of L_a/L_p are W1515WL and W1515W, for which the active length is reported to be at least 142 in. and the plenum length is reported to be 8.2 in., so $L_a/L_p > 17.3$. Since the South Texas reactors and fuel are also produced by Westinghouse, particularly small values of L_a/L_p would not be expected.

Tables 7.4.2.3-1 and 7.4.2.3-2 list the fuel types with the smallest ratio of active length to plenum length. The geometry of these types gives the slowest decrease in gas pressure as the cladding creeps. For a given initial cladding stress, therefore, these fuel types have the greatest tendency for prolonged creep. However, the gas pressure in a fuel rod, and thus the stress in the cladding, will depend on details of the fuel design that are not readily available and on the irradiation history of the rod.

7.5 Dry cladding oxidation

As long as at least one of the containment barriers of a waste package is unbreached, the internal environment will be inert and oxidation of the fuel and cladding cannot occur. Breaching of both barriers will allow air to enter the waste package and begin oxidizing the waste forms.

7.5.1 Degradation model

Einzig (Ref. 5.19, Eq. 11) gives the following equation for oxygen uptake by Zircaloy in air:

$$r_{ox}(T) = 276 \exp[(-27000 \text{ cal/mol})/\mathcal{R}T] \text{ mol/cm}^2\text{-day}, \quad (7)$$

where \mathcal{R} is the gas constant and T is the temperature of the cladding. Since one mole of oxygen (O_2) combines with one mole of zirconium (Zr) to form one mole of ZrO_2 , the rate of change for the thickness of the metallic cladding is $-r_{ox}m/\rho$ where m and ρ are the molar mass and density of zirconium, respectively. The molar mass of zirconium is 91.224 g/mol (Section 4.1.5) and the density of zirconium is 6490 kg/m³ (Section 4.1.5). By using these data, it is found that the rate of change for the thickness of the metallic cladding is $-38.8 \exp[(-27000 \text{ cal/mol})/\mathcal{R}T]$ m/day. It is noted in passing that the molar mass of oxygen (O) is 15.9994 g/mol (Section 4.1.5), and the density of ZrO_2 (baddeleyite) is 5890 kg/m³ (Section 4.1.5), so a 1 μm layer of zirconium will yield $[(91.224 + 15.9994 + 15.9994) / 91.224] (6490/5890) \mu\text{m} = 1.49 \mu\text{m}$ of oxide. In the discussion above, the molar mass and density of pure zirconium are used, even though the cladding is a zirconium alloy. This is a good approximation because cladding alloys contain

only small concentrations of alloying elements (Ref. 5.22, Table 2). ZrO_2 can form as either baddeleyite or zirconia. The denser of these (baddeleyite) is used in the discussion above. This choice is conservative because, if metal loss is calculated from oxide thickness, a given thickness of the denser oxide will give a larger metal loss.

7.5.2 Application of model

The time necessary to consume the cladding will depend on both the temperature history and the cladding thickness. Fuel rods in cooler locations will require more time for oxidation, as will rods with thicker cladding. It should be noted that the oxidation rate given by Eq. 7 does not depend on the amount of oxide present. This implies that the oxide layer does not become more protective as its thickness increases.

For dry cladding oxidation, the failure time will depend on the thickness of the cladding. Tables 7.5.2-1 and 7.5.2-2 list the assembly types with the smallest cladding thicknesses. The threshold for inclusion of an assembly type in these tables is arbitrary. As in previous tables, data for assembly types W1717WL and G4608GP are given in shaded cells. These are the most common spent fuel assembly types for pressurized water reactors and boiling water reactors, respectively.

There are assembly types for which the cladding thickness is not available, so there may be other assembly types with cladding that is thinner than those listed above. However, in each assembly class except Haddam Neck there is at least one Zircaloy-clad assembly type for which these data are available. The coverage of assembly types is therefore fairly inclusive, and the effect of assembly types for which data are not available is expected to be small.

In Tables 7.5.2-1 and 7.5.2-2, the cladding thickness is as reported in Table 4.1.2-1. That table refers to an EIA assembly code G4610S; this was taken to refer to the same fuel as that denoted by G4610C in Ref. 5.3, p. 121 because of the similarity of the descriptive names of these two assembly types. Types G4610C and G4609A9X have been omitted from Table 7.5.2-2 because there are no discharged assemblies of these types reported in Table 4.1.1-1. However, because their initial use year, 1989, is late, these assemblies may still have been in core when the data for Table 4.1.1-1 were compiled.

Table 7.5.2-1. Pressurized water reactor assembly types with the smallest cladding thicknesses.

EIA Assembly Code	Cladding thickness, in.	Number discharged	Uranium per assembly, kg	Total uranium, metric tons
WST17W	0.0225	421	542.0	228
W1414WL	0.0225	1410	399.1	563
W1414W	0.0225	622	393.8	245
W1717WL	0.0225	9525	460.2	4383
W1717WO	0.0225	2969	424.9	1262
W1717WV5	0.0225	1296	425.7	552

Table 7.5.2-2. Boiling water reactor assembly types with the smallest cladding thicknesses.

EIA Assembly Code	Cladding thickness, in.	Number discharged	Uranium per assembly, kg	Total uranium, metric tons
G4609AIX	0.025	4	176.8	1
G4608W	0.029	4	174	1
G2309A	0.030	176	167.7	30
G4609A	0.03	1108	173	192
G2307G2B	0.032	5047	192.8	973
G2308GB	0.032	1376	177.5	244
G2308G5	0.032	879	177.1	156
G2308GP	0.032	2832	177.0	501
G4607G2	0.032	1142	194.7	222
G4608GB	0.032	8575	184.7	1584
G4608G5	0.032	4380	183.0	802
G4608GP	0.032	11625	183.2	2130
XHB06G	0.032	176	76.4	13

7.6 Dry fuel oxidation

7.6.1 Degradation model

Oxidation of the uranium dioxide fuel requires not only a breach of the containment barriers but also a breach of the fuel cladding. Such a breach could occur either by a local failure of the cladding (for example, by creep rupture or external loading) or by oxidation of the full thickness of the cladding. Upon exposure to an oxidizing environment at appropriate temperatures, uranium dioxide oxidizes to U_4O_9 , and eventually to U_3O_8 (Ref. 5.19, p. 554). The spent fuel matrix contracts approximately 3% on oxidation to U_4O_9 , but it expands by about 35.8% on formation of the higher oxide (Ref. 5.23, p. 13). The initial contraction would tend to increase the free space inside the fuel cladding, but the subsequent expansion will cause the fuel to expand and press against the cladding. To represent this two-stage mechanism of fuel oxidation, Einziger has proposed two equations. The time to begin formation of U_3O_8 and thus initiate a split is (Ref. 5.19, Eq. 2)

$$t_{s_i}(T) = 9.8 \times 10^{-21} \exp[(47400 \text{ cal/mol}) / \mathcal{R}T] \text{ years} . \quad (8)$$

Once the split has been initiated, the speed of propagation of the split is (Ref. 5.19, Eq. 3)

$$v_{sp}(T) = 4.23 \times 10^3 \exp[(-18400 \text{ cal/mol}) / \mathcal{R}T] \text{ cm/min} . \quad (9)$$

For conservatism, the split can be taken to initiate at the middle of a rod. In that case, the split can cover the entire active length of the fuel rod by propagating only half of the active length in each direction.

It will be noted that Eq. 9 can be applied even if the temperature depends on time, but Eq. 8, as written, is strictly for isothermal exposure. One approach to generalizing Eq. 8 is to use the method of damage accumulation as follows. The fraction F_{s_i} of damage accumulated toward split initiation during the time interval from t_1 to t_2 is defined as

$$F_{s_i}(t_1, t_2) = \int_{t_1}^{t_2} \frac{d\tau}{t_{s_i}[T(\tau)]} , \quad (10)$$

where $T(\tau)$ is the temperature at time τ and $t_{s_i}[T(\tau)]$ is the split initiation time under isothermal conditions at the temperature $T(\tau)$; t_{s_i} is as given in Eq. 8. Eq. 10 applies only when the fuel is exposed to air since no oxidation occurs while the fuel is kept in an inert atmosphere. In this approach, a macroscopic split initiates when F_{s_i} reaches 1 for the entire period for which the cladding is exposed to air. It will be noted that, for isothermal exposure at some temperature T , Eq. 10 predicts that the elapsed time required for split initiation is $t_{s_i}(T)$, so Eq. 8 and Eq. 10 are consistent. Eq. 10 can be obtained from Eq. 3.5 of Ref. 5.33, p. 3.8. The equation in Ref. 5.33 is written as a sum over a finite number of time intervals, during each of which the material is exposed to isothermal conditions. In the limit of an infinite number of infinitesimal time intervals, the sum in the equation from Ref. 5.33 becomes the integral above.

7.6.2 Application of model

Failure of the cladding by dry oxidation of the fuel depends on the properties of the fuel itself rather than those of the cladding. Accordingly, the applicability of Eqs. 8 through 10 does not depend on the assembly type.

7.7 Aqueous corrosion

7.7.1 Degradation model

Aqueous corrosion is of interest in the nuclear power industry not only because corrosion decreases the cladding thickness but also because corrosion releases hydrogen. The process is described in Ref. 5.14, p. 3-24: "When Zircaloy cladding reacts with the water coolant to form zirconium oxide, hydrogen is liberated from the water. A fraction of this free hydrogen, which is primarily formed at the oxide/coolant interface, diffuses through the oxide layer and is absorbed by the Zircaloy." Hydrogen absorption is significant because an excessive hydrogen content can cause embrittlement of the cladding (Ref. 5.10, p. 47, Fig. 11).

There is a significant dependence of the amount of corrosion during irradiation on the composition of the cladding. For advanced cladding alloys, oxide thicknesses as little as one third of the amount expected for Zircaloy 4 have been observed, and at a burnup of 60 GWd/MTU the advanced alloys are expected to have oxide thicknesses as small as one quarter of that for Zircaloy 4 (Ref. 5.17, Section III.B).

7.7.2 Application of model

Rothman (Ref. 5.34, pp. 14-18) has reviewed the data on aqueous corrosion of Zircaloy. Data were found for a range of pH from 1 to 12 and a variety of ions including lithium, sodium, potassium, ammonium, nitrate, sulfate, chloride, and fluoride. No localized corrosion was noted at temperatures below the normal boiling point of water and without externally driven anodic potentials. Since these are the conditions that are relevant to the repository, general corrosion is apparently the most important corrosion mode.

Failure of the cladding by aqueous general corrosion requires that the full thickness of the cladding be removed. As a result, the assembly types that are most susceptible to aqueous corrosion are those with the thinnest cladding. These assembly types are tabulated in Section 7.5.2.

Corrosion rates may differ from one material to another, so it is appropriate to examine what materials are used in the cladding. Comparison of information on reactor type and cladding material from Table 4.1.1-1 and on cladding material from Table 4.1.2-1 shows that, with only one exception, all zirconium alloy cladding for boiling water reactor fuel is Zircaloy-2. The exception is that type XDR08G has Zircaloy-4 cladding. However, there is only one assembly of this type, so it can have but little effect on total system performance. Similarly, with two

exceptions, all zirconium alloy cladding for pressurized water reactor fuel is Zircaloy-4. The exceptions are W1717WV+ and W1717WVJ, which have Zirlo cladding. The cladding thickness for these types is not known. However, because of continued economic pressure for superior fuel performance, advanced cladding alloys are expected to provide better corrosion performance than traditional alloys, and thus these fuel types should not be among those that are most susceptible to corrosion. Direct evidence for improved corrosion performance by advanced cladding alloys is discussed in the last paragraph of Section 7.7.1.

7.8 External mechanical loading

7.8.1 Degradation model

If the containment barriers are badly degraded, the waste package may allow the fuel assemblies to be exposed to external mechanical loads. Sources of mechanical loads include the products of corrosion of the containment barriers and rubble from the crown of the drift. The conceptualization proposed here is that the fuel rods will be loaded as horizontal beams, supported intermittently by the spacer grids. External loading is expected to be much more severe for pressurized water reactor fuel than for boiling water reactor fuel because boiling water reactor fuel rods are normally enclosed in and protected by flow channels. The flow channels are typically of Zircaloy but have walls that are much thicker than the cladding, so they will have very long corrosion lifetimes.

The following sequence of events is considered. The ground support for the emplacement drifts is designed to last only until the repository is closed, so the emplacement drifts will collapse and be filled with rubble blocks. Some of these will lie on the waste containers. When the containers become sufficiently weak, the blocks will crush the container and impact the fuel assemblies inside. In this sequence of events, the fuel assemblies are exposed to both static and dynamic loads. Dynamic loads occur when the disposal container collapses; static loads occur after rubble has settled onto the fuel. The following paragraphs describe models for static and dynamic external loading of fuel cladding.

The rubble will lie on or impact on the top of the assembly and directly load only the top layer of fuel rods. That fact is supported by the data in Attachment VII. The smallest rubble block of nonzero size for which information is tabulated (second line of file `esfblock.txt`) has a volume of 0.000114999... m³. A cube with the same volume would have an edge length of more than 48 mm. Therefore, the rubble is large enough that even the smallest class of particles cannot sift into the spaces between fuel rods.

The loaded fuel rods are supported by the spacer grids. Since the diameter of the cladding is small in comparison to the distance between spacer grids, the cladding may be approximated as a simple, thin-walled, tubular beam. For simplicity, the entire load on a given span of fuel rod is taken to be applied at the middle of the span (i.e., midway between spacer grids), and the largest grid-to-grid distance is used. Placing all the load at the middle of the span is appropriate if all of the load is due to a single block and is somewhat conservative if the load is due to several blocks.

Near the middle of the assembly, the cladding supports may be approximated as fixed (clamped) ends. This approximation is appropriate if there are similar loads on each span. The bending moment for a beam with fixed ends has been discussed by Roark (Ref. 5.15, p. 101, case 1d).

Although the uranium dioxide fuel will have negligible flexural strength by itself, it will nevertheless contribute to the stiffness of the fuel rod. Since irradiated fuel will be in the form of small, tightly packed fragments, the fuel resists compression but can be readily extended. As a result, the neutral axis will move toward the compressive surface of the fuel rod. Note that the neutral axis will be on the bottom side of the fuel rod near the support and on the top side near the load.

The failure behavior of the cladding will depend on the stress-strain properties of the cladding. Two types of fuel, with different mechanical properties, were considered. The properties were chosen to simulate typical and high-burnup fuel assemblies. The data used in this analysis are listed in Section 4.1.6. Mechanical failure of fuel rods will occur only long after emplacement, when temperatures in the repository will be low. Accordingly, room-temperature mechanical properties were used. The elastic-plastic behavior is described by a piecewise linear stress-strain curve, as documented in Attachments I and II. The tensile portion of the stress-strain curve is taken to be composed of two line segments; these connect the origin, the tensile yield stress and strain, and the ultimate tensile stress and uniform tensile elongation (elastic plus plastic), respectively. The stress-strain curve is determined by properties for typical fuel. To simplify the treatment, the curve for high-burnup fuel is taken to coincide with that for typical fuel, but it is truncated at a smaller strain.

In the model of static loading, an individual fuel rod is considered. The maximum load on the rod is assumed to be that of a rectangular slab of tuff with thickness equal to the rod pitch and width equal to the grid-to-grid distance. The slab represents the portion of the overlying rubble that should be allocated to one span of a fuel rod. The weight of the slab is the product of its volume, the bulk density of tuff at in situ saturation, and the standard acceleration due to gravity. The failure load for the fuel rod is used to calculate the height of the slab. Relevant parameter values are given in Section 4.1.5.

In the model of dynamic loading, entire fuel assemblies are considered. A distribution of block sizes for the repository rock has been developed from information on joint spacings and angles for the geologic unit, TSw2, that would contain the repository (Section 4.1.8). The block size distribution has been applied in the following way. Blocks are taken to fall so that they cover the area of the fuel assemblies exactly once. The shape of the blocks is taken to be a right circular cylinder, and the height and diameter are taken to be equal. The axes of the blocks are taken to be vertical and the blocks to fall freely onto the fuel assemblies.

It was mentioned previously that the ground support is designed only for the preclosure period, so the emplacement drifts will collapse long before the containment barriers fail. In calculating dynamic loads, therefore, what is of interest is not blocks that fall from the crown of the drift but blocks that fall out of the rubble pack and into the space that becomes available when the

containment barriers lose their mechanical integrity. This degradation sequence limits the height from which blocks can fall. A conservative treatment was used to determine the drop height. In a 21-PWR disposal container, a component called a waste package basket side guide assembly supports the bottom of the fuel basket. An identical side guide is present above the basket. If the basket and side guides degrade before the containment barriers fail mechanically, the bottom layer of fuel assemblies can settle, and the overlying assemblies can also settle into the space previously occupied by assemblies below them. Accordingly, the drop height was taken to be the inside diameter of the inner containment barrier minus the distance between the top and bottom side guides. From the inside diameter of the inner containment barrier and the width of the basket side guide (Section 4.1.9), the drop height is calculated to be 203.2 mm. A 21-PWR disposal container, rather than a 12-PWR disposal container, is considered here because the drop height is greater for the former type.

In the preceding discussion, the assemblies were taken to be stacked in horizontal layers, rather than in layers that are at some arbitrary angle to the horizontal. This arrangement provides for the greatest drop height and the most effective settling of assemblies, so this choice will be conservative for calculations of the amount of damage to the assemblies.

In a 21-PWR disposal container, the assemblies are arranged in a 5×5 array with the four corner assemblies removed. The model approximates this arrangement with uniform stacks of assemblies in which each stack contains 21/5 assemblies. This stack height is chosen because it duplicates the exposure of assemblies to rock fall: for each 21 assemblies, five are exposed to falling blocks (Section 4.1.9). Edge effects and end effects are neglected. This is appropriate because blocks that fall near the edge of a waste package are expected to strike rubble as well as fuel.

If the bottom surface of a falling block had a flat surface, the energy of the block would be spread over as many rods as are exposed to the impact; this is the diameter of the block divided by the rod pitch. Since the blocks will be irregular, however, this description is not realistic. To provide greater realism, two geometries were considered that are intended to simulate the effects of irregular block surfaces. In both geometries, the bottom surface of the block is taken to have a rigid, massless protrusion called a punch. The entire energy of the falling block is concentrated onto the rods that lie under the punch. The punch is taken to be sufficiently long that only the punch contacts the fuel; the rods that lie under the remainder of the area of the block are not loaded. For the purposes of calculating the fraction of fuel exposed, the cladding is taken to be completely removed from the portion of a broken fuel rod that lies under the punch, but the remainder of the fuel is taken to be completely intact.

Two types of punches are considered. The first is a circular punch. The ratio of the diameter of the punch to the diameter of the block is called the focusing parameter. To provide maximum energy transfer, the punch may be considered to be coaxial with the block. The second type is a linear punch. Two parallel chords of equal length and the two arcs that connect them define the outline of a linear punch. A linear punch is defined by two variables: the focusing parameter and the angle. The focusing parameter is the ratio of the distance between the two chords to the

block diameter. The angle is simply the angle between a chord and the fuel rods. For both types of punch, a focusing parameter of 1.0 corresponds to a flat-bottomed block. Focusing parameters near zero describe a block with either a slender pin (circular punch) or a blade (linear punch) on the bottom. For a linear punch that is perpendicular to the fuel rods, the number of rods broken is independent of the focusing parameter. However, the fraction of fuel exposed will decrease as the focusing parameter decreases because the broken length decreases. The circular and linear punches are intended to simulate blocks that fall on their vertices and their edges, respectively.

When a block strikes the fuel, the number of breaks can vary from zero (if there is not enough energy to begin breaking rods) to the number of rods under the punch. The number of breaks is determined as a weighted arithmetic mean over the number of assemblies of each type and the distribution of block sizes.

The number of breaks is calculated by considering the energy of the falling block. The block will accumulate kinetic energy as it falls freely toward the fuel rods. It will release additional potential energy as it deforms the fuel rods, but at the same time the deformation of the rods will consume energy. If the block has sufficient energy, it will break fuel rods. After the first layer of rods is broken, the energy consumed for each additional layer is the same as that for the layer above. Again, there will be additional release of potential energy as the block continues to fall.

Two measures of the number of breaks were calculated. The first, the number of breaks per rod, is simply the ratio of the number of breaks to the number of rods. The second measure is the fraction of rods broken. Since a single rod can be broken more than once, the fraction of rods broken is less than or equal to the number of breaks per rod. The following approach is used to calculate the number of rods broken: For each block size, the depth of penetration is calculated. For each layer that is penetrated by the block, the probability that a rod will be broken by a block of a given size is calculated. This probability is calculated from the number of rods broken in one layer by one block, the total number of rods per layer, and the number of blocks of a given size. One minus the probability of being broken is the probability that a rod will be left intact. For a rod to remain intact, however, it must not be broken by any size rock, so the probability that a rod remains intact is the product of the probabilities of remaining intact for each block size. The process above is repeated for each layer of each assembly type, and the total number of broken rods is determined. Finally, that number is divided by the total number of rods. Details of the calculation are documented in Attachments V and VI.

As a falling block imparts its energy to the fuel, the rods deform and pack into an array that is denser than that of the undisturbed assembly. Because of the complexity of the packing process and uncertainties about the details of the impact geometry, the forces from an impacting rock are calculated in a one-dimensional continuum approximation, that is, (1) the actual array of rods in an assembly is replaced by a continuum that has the force-displacement behavior that would result if the rods were smeared over space, and (2) the continuum responds to the impact by being displaced only in the direction of rock motion. The details of the calculation are documented in Attachment IV. The theoretical maximum density for rod packing would be achieved if the rods were packed into a tight hexagonal array. In the calculation it is assumed that the

actual density of the packed rod array is 0.9 times this value (Section 4.3.2). The continuum calculation uses an approximate force-displacement equation for a single fuel rod; that equation was obtained from previous calculations as documented in Attachments II and III. The force-displacement equation is

$$D(F) = F \frac{D_y}{F_y} \quad \text{if } 0 \leq F < F_y$$

$$D(F) = F \frac{D_y}{F_y} + \left(D_u - D_y \frac{F_u}{F_y} \right) \left(\frac{F - F_y}{F_u - F_y} \right)^{3.468} \quad \text{if } F_y \leq F \leq F_u \quad (11)$$

In Eq. 11, F and D are the current force and displacement, respectively. F_y and D_y are the force and displacement at the onset of yielding, that is, when the maximum fiber stress reaches the yield stress, and F_u and D_u are the force and displacement when the maximum fiber strain reaches the uniform elongation (elastic plus plastic) for typical fuel. Note that positive forces and displacements are downward. For a given assembly design, F_y , D_y , F_u , and D_u are constants. They are calculated with the equations

$$F_y = 2.94053 \cdot 10^{10} \frac{tR^2}{l} \quad (12)$$

$$D_y = 1.63570 \cdot 10^{-4} \frac{l^2}{R} \quad (13)$$

$$F_u = 4.37425 \cdot 10^{10} \frac{tR^2}{l} \quad (14)$$

$$D_u = 4.01626 \cdot 10^{-4} \frac{l^2}{R} \quad (15)$$

The constants in Eqs. 12 through 15 may contain digits that are not significant; they are expressed to high precision here for consistency with Attachments III and IV. Here t , l , and R are the cladding wall thickness, the grid-to-grid spacing, and the cladding midwall radius, respectively. Eqs. 12 through 15 apply if t , l , R , D_y , and D_u are all expressed in meters, and F_y and F_u are expressed in newtons.

High-burnup fuel is less ductile than typical fuel. Eq. 11 still applies, but, to reflect the change in ductility, the force-displacement curve is truncated at smaller forces and displacements. For high-burnup fuel, the force and displacement at failure, F_{uh} and D_{uh} , respectively, are

$$F_{uh} = 3.26214 \cdot 10^{10} \frac{tR^2}{l} \quad (16)$$

$$D_{wh} = 1.82937 \cdot 10^{-4} \frac{l^2}{R} \quad (17)$$

F_{wh} and D_{wh} are the force and displacement when the maximum fiber strain reaches the uniform elongation (elastic plus plastic) for high-burnup fuel. The discussion of precision and units following Eq. 15 applies to Eqs. 16 and 17 as well. Eq. 11 agrees with the beam-theory calculation to within 0.22% of D_w for all applicable values of F .

Several integrals are required in the beam-theory calculations. These are evaluated with Mathcad's integrator, the trapezoidal rule, or Simpson's rule (Ref. 5.31, p. 14), as appropriate.

For the models described above, the following information about fuel assembly design was taken from Sections 4.1.1, 4.1.2, and 4.1.7: grid-to-grid distance, cladding thickness, fuel rod diameter, rod pitch, number of rods along one side of a fuel assembly, number of assemblies discharged, and overall rod length. In Table 7.8.1-1, these data are documented. Each line of the table contains these seven quantities, in the order listed, followed by the corresponding EIA assembly code. Values for grid-to-grid distance, cladding thickness, fuel rod diameter, rod pitch, and rod length are given in inches, following the practice of the original data sources. If the original data source included both a minimum and a maximum rod length, the arithmetic mean of these is given below. If the data source contained a distance expressed as a fraction of an inch, Table 7.8.1-1 contains enough decimal places to represent the fraction exactly, even if not all decimal places are significant. The numeric data are used as input for the Mathcad worksheets `elpl_rod.mcd` and `rodpack.mcd` (Attachments I and IV). Since Mathcad does not accept nonnumeric data, the EIA assembly codes must be removed with a text editor before the file is read.

Table 7.8.1-1. Fuel assembly data for Mathcad worksheets. See text above for explanation.

21.125	0.0265	0.43	0.568	15	4134	153.68	B1515B4
22	0.024	0.379	0.502	17	4	152.688	B1717B
18.859	0.031	0.44	0.58	14	761	146.484	C1414A
18.859375	0.028	0.44	0.58	14	3368	147	C1414C
14.8125	0.025	0.382	0.506	16	2340	161	C1616CSD
22	0.03	0.424	0.556	14	806	149.1	W1414A
26.19	0.0295	0.417	0.556	14	288	152	W1414ATR
26.19	0.0225	0.422	0.556	14	622	150.475	W1414W
26.19	0.0243	0.4	0.556	14	965	150.23	W1414WO
26.19	0.03	0.424	0.563	15	884	152.065	W1515A
26.19	0.0242	0.422	0.563	15	1580	150.235	W1515W
26.19	0.0242	0.422	0.563	15	1533	151.85	W1515WO
24.43	0.025	0.36	0.496	17	332	152	W1717A
24.43	0.0225	0.374	0.496	17	9525	151.5975	W1717WL
24.89	0.0225	0.36	0.496	17	2969	151.5975	W1717WO
22.1	0.0225	0.374	0.496	17	421	176.642	WST17W
16.8125	0.028	0.44	0.58	14	378	137	XFC14C
15.5	0.03	0.417	0.55	15	520	139.423	XPA15A
15.5	0.026	0.418	0.55	15	273	140	XPA15C
18.3	0.024	0.365	0.472	16	228	95.34	XYR16A

7.8.2 Application of model

The static loading and dynamic loading models described in Section 7.8.1 have been applied to two types of fuel: typical and high-burnup. For each type of fuel, the failure criterion is that the maximum fiber strain reaches the uniform elongation (elastic plus plastic). Since the high-burnup fuel has a smaller uniform elongation, rods of this type are easier to break. The mechanical properties of high-burnup fuel are taken to be characteristic of the most highly burned 5% of discharged fuel. This fraction was derived as follows. The uniform elongation for high-burnup fuel was obtained from a sample with a local burnup of 59.0 GWd/MTU (Section 4.1.6). From the date of the data source, it is known that the fuel was discharged no later than 1986. There were 19968 PWR fuel assemblies discharged through 1986; of these, only 200 (about 1%) had average burnups of 40 GWd/MTU or more (Section 4.1.10). It is therefore expected that it is conservative to treat 5% of the fuel as having such a high burnup. What constitutes high burnup depends on when the fuel was irradiated because there is a long-term trend toward higher burnups as experience with reactor operations increases. However, the continued demand by utilities for good fuel performance should assure that the strength and ductility of "typical" fuel assemblies will be maintained even though "typical" burnups are increasing.

The results of the calculation for static loading are shown in Table 7.8.2-1. The effective rod pitch was calculated with Mathcad worksheet `rodpack.mcd` (Attachment IV); the remaining results were calculated with Mathcad worksheet `elpl_rod.mcd` (Attachment I). Worksheet `elpl_rod.mcd` reads the numeric data from Table 7.8.1-1, which were stored in a file named `assembly.dat`. Columns with the heading "Typical" are for typical fuel; columns with the heading "High-Burnup" are for high-burnup fuel. Displacements and effective rod pitches are

given to the nearest tenth of a millimeter; loads are given to the nearest newton; energies are given to the nearest joule; slab heights are given to the nearest tenth of a meter. Some digits may not be significant. As in previous tables, data for assembly type W1717WL are given in Table 7.8.2-1 in shaded cells. This is the most common spent fuel assembly type for pressurized water reactors.

The most significant results in Table 7.8.2-1 are the slab heights. As is discussed in Section 7.8.1, this is the height of a slab of solid TSw2 tuff that would be required to load the fuel rods to the failure point. Because of bulking, a rubble pack would have to be taller than this. For some assembly types (such as W1717WO), the slab height is small enough that failures might be expected under static loads. However, for these same assembly types there will be load sharing between the top layer of rods and the underlying layers. As is discussed below, the effective rod pitch is the distance that one layer of rods must be displaced to contact the layer below. As an example, for high-burnup fuel of type W1717WO, the displacement at failure (17.1 mm) is more than twice the effective rod pitch (6.2 mm), so the load will be shared by three layers of rods. The slab heights are therefore substantial underestimates. Since the slab heights are quite large, it is concluded that static loading will not be a significant source of cladding failures.

The required data for the mechanical failure calculations were available for 20 fuel types. From the data in Table 7.8.1-1, it can be seen that these types account for 31931 assemblies, or more than 71% of the 44598 PWR fuel assemblies (Table 4.1.1-1) discharged through 1994. In the discussion below, these assemblies are taken to be characteristic of the entire population of spent PWR fuel assemblies. Accordingly, it should be determined whether there are other assembly types with failure loads, displacements, or energies that are smaller than those listed above. It is concluded here that remaining assembly types will not be significantly more subject to mechanical failure than the types considered here. The available data provide results for at least one assembly type in most of the pressurized water reactor assembly classes. Within an assembly class, the fuel geometries are generally similar, so the failure conditions for many other assembly types can be estimated from the values given in the tables. The only pressurized water reactor fuel assembly classes for which the maximum distance between spacer grids could not be determined are CE 16 × 16 System 80, Haddam Neck, and St. Lucie 2. (Fuel of the Indian Point 1 assembly class has stainless steel cladding.) Fuel of the Haddam Neck assembly class expected to be of little importance because there are only 161 zirconium alloy clad assemblies of this type (Section 4.1.3). Although complete data are not available for fuel of the CE 16 × 16 System 80 and St. Lucie 2 assembly classes, such data are available for assembly types in other assembly classes for Combustion Engineering reactors (CE 14 × 14, CE 16 × 16, Fort Calhoun, and Palisades). These assembly types are similar in that they all have large slab heights. Because of the consistency of the results among fuels for Combustion Engineering reactors, similar results are expected for the remaining assembly types.

Table 7.8.2-1. Static and dynamic mechanical loadings required to fail pressurized water reactor fuel assembly types. See text above for explanation.

EIA Assembly Code	Displacement, mm		Eff. Rod Pitch, mm	Load, N		Slab Height, m	
	Typical	High-Burnup		Typical	High-Burnup	Typical	High-Burnup
B1515B4	22.6	10.3	6.5	1441	1075	8.4	6.2
B1717B	27.9	12.7	5.8	970	723	6.1	4.6
C1414A	17.8	8.1	6.6	1941	1447	12.4	9.2
C1414C	17.6	8.0	6.6	1779	1326	11.3	8.4
C1616CSD	12.6	5.7	5.8	1518	1132	14.1	10.5
W1414A	25.1	11.4	6.2	1494	1114	8.5	6.3
W1414ATR	36.2	16.5	6.5	1194	890	5.7	4.3
W1414W	35.1	16.0	6.3	968	721	4.6	3.4
W1414WO	37.3	17.0	7.1	924	689	4.4	3.3
W1515A	35.6	16.2	6.5	1255	936	5.9	4.4
W1515W	35.2	16.0	6.6	1032	769	4.9	3.6
W1515WO	35.2	16.0	6.6	1032	769	4.9	3.6
W1717A	36.4	16.6	6.2	811	604	4.7	3.5
W1717WL	34.7	15.8	5.7	803	599	4.6	3.4
W1717WO	37.5	17.1	6.2	727	542	4.1	3.1
WST17W	28.4	12.9	5.7	888	662	5.6	4.2
XFC14C	14.0	6.4	6.6	1995	1487	14.2	10.6
XPA15A	12.7	5.8	6.2	2046	1525	16.7	12.5
XPA15C	12.5	5.7	6.2	1819	1356	14.9	11.1
XYR16A	20.0	9.1	5.1	1076	802	8.7	6.5

Eff. = Effective

Dynamic loads were treated by calculating the kinetic energy of falling blocks of rock and the dissipation of this energy as the block penetrates the rods. The Mathcad worksheet `rodpack.mcd` (Attachment IV) was used in preparation for treatment of dynamic loads. Since the details of loading for individual rods are not known, forces from an impacting block were calculated in a one-dimensional continuum approximation as described in Section 7.8.1. Since the compacted rods accumulate ahead of the block, the interface between the compacted and uncompacted regions moves faster than the block. The "effective rod pitch" is defined as the distance that the block must move to advance the interface between the compacted and uncompacted regions by one rod pitch.

As the block penetrates the fuel assemblies, the deformed but unbroken fuel rods will exert a retarding force on the rock. At first, the force on the block increases as additional rods take up more of the load. At larger penetrations, however, the force becomes constant as rods begin to break and new rods take the place of the broken rods. The one-dimensional continuum model is used to calculate the energy absorbed before rods begin to break and the additional energy per rod to break rods.

In developing the one-dimensional continuum approximation, the rock block is approximated as a rigid body. Because the rods are light, their mass is neglected. Although not all fuel rod positions are fueled, the number of fuel rod positions is taken to be equal to the square of the number of fuel rods per side.

The worksheet `rodpack.mcd` uses Eqs. 11 through 17 to calculate the displacements to start breaking rods. It then uses these same equations, in a one-dimensional continuum approximation, to calculate the energy to begin breaking rods and the energy per rod to break additional rods. These results are saved in a file `rod_engy.txt`, which is listed in Table 7.8.2-2.

(White space in this file has been modified in the table to improve readability.) Each line of the file contains the following information, in the order listed: rod pitch, number of rods along one side of an assembly, energy to start failing rods (typical fuel), energy to fail one additional rod (typical fuel), displacement to start failing rods (typical fuel), energy to start failing rods (high-burnup fuel), energy to fail one additional rod (high-burnup fuel), displacement to start failing rods (high-burnup fuel), effective rod pitch, number of assemblies discharged, rod length, and assembly type number. Rod pitches, displacements, and rod lengths are given in meters; energies are given in joules. The precision of the numbers is set by the Mathcad defaults: four significant digits with trailing zeroes suppressed. The assembly type is simply a serial number; the order of assembly types is the same in Tables 7.8.1-1, 7.8.2-1, and 7.8.2-2.

Table 7.8.2-2. Energy data for breakage of fuel rods. See text above for explanation.

0.01443	15	28.23	21.73	0.02257	2.948	5.566	0.01028	0.006471	4134	3.903	0
0.01275	17	32.46	18.03	0.02782	3.389	4.619	0.01267	0.005757	4	3.878	1
0.01473	14	23.13	23	0.01774	2.415	5.892	0.008081	0.006574	761	3.721	2
0.01473	14	20.89	20.92	0.01761	2.181	5.361	0.008023	0.006574	3368	3.734	3
0.01285	16	10.24	12.71	0.01254	1.069	3.257	0.005712	0.005804	2340	4.089	4
0.01412	14	37.56	25.01	0.02506	3.921	6.407	0.01142	0.00622	806	3.787	5
0.01412	14	59.82	28.79	0.03611	6.246	7.377	0.01645	0.006478	288	3.861	6
0.01412	14	46.96	22.64	0.03503	4.903	5.801	0.01596	0.006294	622	3.822	7
0.01412	14	45.03	23	0.03725	4.702	5.892	0.01697	0.007089	965	3.816	8
0.0143	15	60.67	29.77	0.03552	6.334	7.628	0.01618	0.006496	884	3.862	9
0.0143	15	48.4	24.25	0.03518	5.053	6.212	0.01602	0.006569	1580	3.816	10
0.0143	15	48.4	24.25	0.03518	5.053	6.212	0.01602	0.006569	1533	3.857	11
0.0126	17	42.91	19.68	0.03635	4.48	5.041	0.01656	0.006212	332	3.861	12
0.0126	17	42.04	18.58	0.03464	4.39	4.761	0.01578	0.005706	9525	3.851	13
0.0126	17	40.84	18.18	0.03745	4.264	4.657	0.01706	0.006212	2969	3.822	14
0.0126	17	31.13	16.81	0.02835	3.25	4.307	0.01291	0.005706	421	4.487	15
0.01473	14	14.8	18.65	0.014	1.545	4.779	0.006376	0.006574	378	3.48	16
0.01397	15	13.09	17.31	0.01267	1.366	4.434	0.005769	0.006243	520	3.541	17
0.01397	15	11.41	15.19	0.0125	1.191	3.893	0.005696	0.006206	273	3.556	18
0.01199	16	21.13	14.4	0.02004	2.206	3.69	0.009127	0.00509	228	2.422	19

The number of breaks per rod, the fraction of fuel rods broken, and the fraction of fuel exposed were calculated for both circular and linear punches with several values of the focusing parameter ranging from 1.0 to 0.1. The calculations were performed with Mathcad worksheets `cylsmash_circ2.mcd` (Attachment VI) and `cylsmash_lin2.mcd` (Attachment V). The results are documented in Attachment VIII. Some of the digits reported in Attachment VIII may not be significant. Values from Attachment VIII that are quoted in this section may also contain digits that are not significant. For the number of breaks per rod, fraction of rods broken, and fraction of fuel exposed, the results of most interest are those in columns labeled "95% typ. + 5% hi-burn", which contain arithmetic weighted means for a repository that contains 95% typical fuel and 5% high-burnup fuel. Except for the punch aspect ratios, the results in Attachment VIII are arithmetic weighted means that properly account for the block size distribution and the number of assemblies of each type.

Results for blocks with a circular punch are shown on page VIII-1. The number of breaks per rod and the fraction of fuel rods broken increase as the focusing parameter decreases. A smaller punch apparently makes the block more effective in breaking rods. The largest reported values of the number of breaks per rod and the fraction of rods broken are 0.2845 and 0.2341, respectively. Both of these values are reached at a focusing parameter of 0.1. In contrast to these results, the amount of fuel exposed is nearly independent of the focusing parameter over the range 1.0 to 0.4, then decreases at smaller values of the focusing parameter. The maximum fraction of fuel exposed is 0.0114 at a focusing parameter of 0.6.

Another result of interest for calculations with a circular punch is the punch aspect ratio. This is the ratio of the depth of penetration of the punch to the width of the punch. Here "depth of penetration" is defined as the number of layers of rods broken times the effective rod pitch. Different combinations of block size and assembly type will yield different punch aspect ratios.

The values reported in Attachment VIII are arithmetic means for blocks that break rods. (For blocks that do not break rods, the punch aspect ratio is zero.) Since it is improbable that a block will have a very long, slender protrusion on its bottom surface, large punch aspect ratios indicate an unrealistic focusing of energy onto a few rods. It is seen from Attachment VIII that the punch aspect ratio increases as the focusing parameter decreases. Since the punch aspect ratios are fairly large for focusing parameter of 0.1, it is expected that the actual number of breaks per rod and fraction of rods broken will be smaller than the values reported above.

For a linear punch, the results depend on the angle between the punch and the rods. For the rubble in a drift, it is expected that the rubble blocks will be randomly oriented. As a discrete approximation of this, the fraction of rods broken and the fraction of fuel exposed were calculated for eight orientations (0° , 22.5° , ... 157.5°), and the arithmetic mean was taken. Some pairs of orientations are equivalent, such as angles of 45° and 135° ; in these cases, symmetry was used to reduce the amount of calculation. The results for this composite orientation are shown on page VIII-3. As with a circular punch, the number of breaks per rod and the fraction of rods broken both increase as the focusing parameter decreases from 1 to 0.1. The largest reported values are 0.1507 and 0.1052, respectively. However, the dependence on the focusing parameter is much weaker than with a circular punch. The fraction of fuel exposed has a more complicated dependence on the focusing parameter, with a maximum at 1, a minimum near 0.2, and a second maximum at 0.1. The maximum fraction of fuel exposed is 0.0110 at focusing parameters of 0.9 and 1.0.

The two models provide substantially different results for the fraction of rods broken. With a linear punch, the largest reported value is 0.1052 for a focusing parameter of 0.1; with a circular punch, the largest reported value is 0.2341, again for a focusing parameter of 0.1. The two models agree more closely at larger focusing parameters. However, it may be that the circular punch simply represents a more severe loading configuration as regards the number of rods broken.

As regards the amount of fuel exposed, the agreement between results for a circular punch and a linear punch is much closer. With a linear punch, the maximum fraction of fuel exposed is 0.0114; with a circular punch, 0.0110 is exposed. These values are reached at fairly large values of the focusing parameter, 0.6 and 0.9 to 1.0, respectively. These results indicate that only a small fraction of fuel will be exposed by mechanical failure.

Energies for breaking fuel rods of boiling water reactor assemblies have not been calculated. For most of these, the fuel rods will be protected from both impacts and static loads by the flow channels. It would be conservative to assume that the number of breaks per rod and the fraction of fuel exposed is the same for PWR and boiling water reactor fuel. The maximum fraction of fuel exposed by mechanical loading can therefore be taken to be 0.0114, which is the largest value found in these calculations.

The model of dynamic loading contains the following conservatisms: (1) The block fall height is essentially an upper limit. There is no accounting for possible deformation of the containment

barriers before complete collapse. (2) Blocks are assumed to fall freely; there is no accounting for blocks that encounter friction or are partially supported by other rubble blocks. (3) There is no accounting for energy absorbed in deforming the remnants of the containment barriers. (4) There is no reduction of block size to account for breakage when the blocks fall onto the intact disposal container or other rubble. (5) There is no accounting for energy absorption by crushing of the spacer grids. That process would also increase the flexibility of the rods and thus increase the energy they could absorb before breaking. (6) Falling blocks are assumed to cover the entire exposed area of the assemblies; there is no accounting for bridging by rubble blocks. (7) Rod breakage is likely to cause only a few guillotine breaks in the cladding, but the amount of fuel exposed is assumed to be that in the entire length of the rod under the punch. (8) The neutral axis is taken to be at the surface of the rod. This location minimizes energy absorption. (9) No credit is taken for the protection of boiling water reactor fuel rods by their flow channels. Because of these conservatisms, the reported values of the number of breaks per rod and the fraction of fuel exposed are believed to be conservative.

8. CONCLUSIONS

All design inputs which are identified in this analysis are for the preliminary stage of the design process; some or all of these design inputs will require subsequent confirmation (or superseding inputs) as the waste package design proceeds. Consequently, the use of any data from this analysis for input into documents supporting construction, fabrication, or procurement is required to be controlled and tracked as TBV or TBD in accordance with NLP-3-15, *To Be Verified (TBV) and To Be Determined (TBD) Monitoring System*, or other appropriate procedures.

The classification analysis for the MGDS repository (which includes the waste package) carries TBV-228 because of the preliminary status of the basis for the MGDS design. Further evolution of the MGDS design is required before TBV-228 may be removed from the classification analysis. This design analysis conservatively assumes that the resolution of TBV-228 will find the waste package to be quality-affecting. With this approach, the design analysis is appropriate regardless of whether the waste package is quality-affecting or not. Consequently, outputs of this analysis do not need to carry TBV-228.

One source of design input (Ref. 5.28) contains TBV-231. However, this TBV item does not apply to the inputs taken from that document, so TBV-231 is likewise not carried to this document.

The spent fuel with stainless steel cladding contains 723 metric tons of uranium. Because of the difference in composition between stainless steel and zirconium alloys, different treatment of these two types of fuel is required. Degradation of stainless steel clad fuel was not analyzed, so no conclusions can be drawn on that subject. The remaining conclusions are applicable only to zirconium alloy clad fuel.

Fuel assembly designs were analyzed to determine which are most susceptible to various cladding degradation mechanisms. The results given below will be used in developing models of cladding degradation for total system performance assessments.

The fuel assembly types with the largest stress multiplication factors for internal gas pressure are W1414WL, W1414W, W1515W, W1515WL, and W1515WO for pressurized water reactor fuel and XHB06G, G2307G2B, G4607G2, XBR07G, G4609AIX, XBR08G, XDR06G3F, XDR06G5, G2307G2A, and XDR06G3B for boiling water reactor fuel. These are the assembly types that are most susceptible to internal gas pressure as a driving force for creep.

The fuel assembly types with the smallest ratio of active length to plenum length are B1515B4 for pressurized water reactor fuel and G4607G2, G4607G3A, G4608G4A, G4607G3B, G4608G4B, G2307G2A, G2307G2B, and G2308G4 for boiling water reactor fuel. These are the assembly types for which internal gas pressure decreases most slowly as the cladding creeps. However, the gas pressure in a fuel rod, and thus the stress in the cladding, will depend on details of the fuel design that are not readily available and on the irradiation history of the rod.

The fuel assembly types with the smallest cladding thicknesses are WST17W, W1414WL, W1414W, W1717WL, W1717WO, and W1717WV5 for pressurized water reactor fuel and G4609AIX, G4608W, G2309A, G4609A, G2307G2B, G2308GB, G2308G5, G2308GP, G4607G2, G4608GB, G4608G5, G4608GP, and XHB06G for boiling water reactor fuel. These are the assembly types that are most susceptible to cladding penetration by corrosion or oxidation. Two additional boiling water reactor fuel types, G4610C and G4609A9X would also be listed, but available data do not indicate any discharges of these types to date.

For external mechanical loading, all fuel assembly types possess adequate strength to sustain reasonable static rock or rubble loading.

Under the load of rubble fallen from the crown of the drift, the waste package containment barriers may eventually thin to the point of mechanical collapse. The dynamic loads resulting from rubble blocks that would then fall onto the fuel assemblies has been analyzed. Under the worst case considered, the fraction of fuel exposed is calculated to be 0.0114. This value is believed to be conservative.

9. ATTACHMENTS

Eight attachments are provided. Their contents are as follows:

Attachment I (1/16/98 14:38 elpl_rod.mcd): This is a Mathcad worksheet that is used in calculating the forces and displacements at failure for a single externally loaded fuel rod.

Results from this worksheet are tabulated in Table 7.8.2-1.

- | Attachment II (1/16/98 14:38 elpl_mdl.mcd): This is a Mathcad worksheet that is used in calculating various points on the force-displacement curve for a fuel rod. Results from this worksheet are tabulated in the attached file forcedsp.xls.
- | Attachment III (1/19/98 14:12 forcedsp.xls): This is an Excel spreadsheet that tabulates results from file elpl_mdl.mcd and provides a comparison between those results and the results of a simplified model for the force-displacement curve of a single externally loaded fuel rod. Attachment III documents its own results.
- | Attachment IV (1/16/98 14:40 rodpack.mcd): This is a Mathcad worksheet that is used in calculating the energy needed to begin breaking rods in an exposed fuel assembly. Results from this worksheet are tabulated in Table 7.8.2-2.
- | Attachment V (1/16/98 14:47 cylsmash_lin2.mcd): This is a Mathcad worksheet that is used in calculating the number of fuel rod breaks, number of broken fuel rods, and amount of exposed fuel for a falling block with a linear punch. Results from this worksheet are tabulated in Attachment VIII.
- | Attachment VI (1/16/98 14:44 cylsmash_circ2.mcd): This is a Mathcad worksheet that is used in calculating the number of fuel rod breaks, number of broken fuel rods, and amount of exposed fuel for a falling block with a circular punch. Results from this worksheet are tabulated in Attachment VIII.
- | Attachment VII (1/13/98 09:08 esfblock.txt): This is a listing of a data file used by Mathcad worksheet cylsmash_lin2.txt and cylsmash_circ2.txt. Each line of the file contains two numbers: a cumulative frequency of occurrence (expressed as a number from 0 to 1) and a block volume in cubic meters, respectively. See Section 4.1.8 for a discussion of the source of the data.
- | Attachment VIII (1/16/98 14:04 rodbreak.xls): This is an Excel spreadsheet that tabulates results on numbers of broken fuel rods from files cylsmash_lin2.mcd and cylsmash_circ2.mcd. It also calculates weighted averages of the results. Attachment VIII documents its own results.

Fuel rod with point load and incompressible fuel

Consider one fuel rod. Treat it as an elastic-plastic beam with a point load at midspan and fixed (clamped) ends. The load simulates a rubble block impacting or resting on the assembly. Fixed ends provide the stiffest configuration and are equivalent to having a continuous beam with many spans and a similar load on each span.

The fuel will affect the deformation of the fuel rod. Since irradiated fuel is broken into fragments, the mechanical stiffness of the fuel will be negligible. However, since the fragments are tightly packed, the fuel will resist compression. As a result, the neutral axis will move toward the compressive surface of the fuel rod. Note that the neutral axis will be on the bottom side of the fuel rod near the support and on the top side near the load. The treatment here takes the fuel as being readily extendible but completely incompressible. Since the cladding is approximated as a thin-walled tube, the neutral axis is at the surface of the fuel rod. This choice gives the stiffest configuration.

Geometric and mechanical data are entered here.

$l := 0..6$ $j := 0..19$ $msmt_{j,i} := READ(assembly\ dat)$

$msmt_{j,0}$ = maximum distance between spacer grids for assembly type j (in inches)
 $msmt_{j,1}$ = cladding thickness for assembly type j (in inches)
 $msmt_{j,2}$ = outside diameter of cladding for assembly type j (in inches)
 $msmt_{j,3}$ = rod pitch for assembly type j (in inches)
 $msmt_{j,4}$ = number of rods along one side of assembly for assembly type j
 $msmt_{j,5}$ = number of assemblies discharged (not used here)
 $msmt_{j,6}$ = length of fuel rods (not used here)

$type := 19$ type sets the type of assembly to consider. To calculate the loads and displacements in Table 7.8.2-1, set type to 0, 1, ... 19.

$l = msmt_{type,0} \cdot in$ $t = msmt_{type,1} \cdot in$ $R := \frac{1}{2} \cdot (msmt_{type,2} \cdot in - t)$ $h = msmt_{type,3} \cdot in$

$nrod = msmt_{type,4}$

$l = 0.465 \cdot m$	Distance between spacer grids
$t = 6.096 \cdot 10^{-4} \cdot m$	Cladding wall thickness
$R = 4.331 \cdot 10^{-3} \cdot m$	Cladding midwall radius
$h = 0.012 \cdot m$	Rod pitch

$E := 99.284 \cdot 10^9 \cdot Pa$ Elastic modulus from Section 4.1.6.

$\sigma_y := 780 \cdot 10^6 \cdot Pa$ $\epsilon_y := \frac{\sigma_y}{E}$ Tensile data from Section 4.1.6.

$\sigma_u := 925 \cdot 10^6 \cdot Pa$ $\epsilon_u := 0.035 + \epsilon_y$ $E2 := \frac{\sigma_u - \sigma_y}{\epsilon_u - \epsilon_y}$

$\sigma_u =$ ultimate tensile stress
 $\epsilon_u =$ uniform elongation
 $\sigma_y =$ yield stress
 $\epsilon_y =$ yield strain

$\sigma(\epsilon) := \begin{cases} \epsilon E & \text{if } |\epsilon| \leq \epsilon_y \\ \sigma_y + E2 \cdot (\epsilon - \epsilon_y) & \text{if } \epsilon > \epsilon_y \\ -\sigma_y + E2 \cdot (\epsilon + \epsilon_y) & \text{otherwise} \end{cases}$ Piecewise linear stress-strain curve

Load to bend rod to a specified strain in the extreme fiber.

$\delta = 1$ Specify offset of neutral axis from axis of cladding. To put the neutral axis on the axis of the cladding (to ignore the structural effects of the fuel), set $\delta = 0$. To put the neutral axis on the compressive side of the cladding (to make the fuel extendible but not compressible), set $\delta = 1$. To put the neutral axis on the tensile side of the cladding (to make the fuel compressible but not extendible), set $\delta = -1$. (Negative values of δ are nonphysical.)

Specify desired maximum strain (ϵ_{max}); calculate required force (W) to produce that strain. Normally, ϵ_{max} is set to the uniform strain from an axial tensile test. A strain of ϵ_{max} will be attained at the support on the upper surface of the cladding. The curvature $curv$ is d^2y/dx^2 (defined below), or the reciprocal of the radius of curvature of the neutral axis.

The relationship between the curvature and the maximum strain is obtained as follows. Suppose that a length of rod is bent with a radius of curvature ρ to form an arc of angle ϕ . The length of the neutral axis remains invariant at $\rho\phi$. The tensile side of the cladding has a larger radius of curvature, $\rho + (1+\delta)R$, so it is extended to a length $[\rho + (1+\delta)R]\phi$. The resulting strain is $(1+\delta)R/\rho$.

The equation for the bending moment below is obtained by integrating the stress times the distance from the neutral axis over the area of the beam. The integration uses a parameter θ , which is an angular coordinate of a point on the tube. The distance of a given point from the neutral axis is $R(\sin \theta + \delta)$. For a given curvature $curv$, the strain is $curv \cdot R(\sin \theta + \delta)$ and the stress is $\sigma(curv \cdot R(\sin \theta + \delta))$, where the function σ is the stress-strain curve defined above. The element of area of the tube is $tRd\theta$. The integrand is the product of the stress, the distance from the neutral axis, and the element of area. Since the left and right sides of the tube are symmetric, the integral extends only over the interval from $-\pi/2$ to $\pi/2$ and the result is doubled.

The load is obtained as follows. Because of the symmetry of the beam, it may be divided into four cantilever sections, each of the same length. Midway between the load and a support, the bending moment is zero. Consider the two cantilever sections that protrude from the supports toward the load. Each of these supports a load of $W/2$ and has a length of $L/4$. (Note that "L" is a letter, not the digit "1".) The bending moment at the fixed end of the cantilever beam is the product of the load and the length, which is $WL/8$. The equation below follows immediately.

$W(\epsilon_{max}) := \left\{ \begin{array}{l} \text{curv} \leftarrow \frac{\epsilon_{max}}{(1 + \delta) \cdot R} \\ M_{max} \leftarrow 2 \cdot \int_{-\frac{\pi}{2}}^{\frac{\pi}{2}} \sigma [\text{curv} \cdot R \cdot (\sin(\theta) + \delta)] \cdot t \cdot R^2 \cdot (\sin(\theta) + \delta) \, d\theta \\ 8 \cdot \frac{M_{max}}{l} \end{array} \right.$	<p>Curvature to produce strain of ϵ_{max}</p> <p>Bending moment for that curvature</p> <p>Load to produce that bending moment at support (or load)</p>
---	--

Determine bending moment as a function of different variables.

$$Mx(W, x) := \frac{-W \cdot l}{8} + \frac{W \cdot x}{2}$$

Bending moment (Mx) as a function of load (W) and position (x). See Roark (Ref. 5.15, p. 101, case 1d). For loading at midspan, moment at left end is $-Wl/8$; moment at midspan is $Wl/8$. Moment varies linearly between these points because there is no other load in that interval.

$Mo(\text{curv}) := 2 \cdot \int_{-\frac{\pi}{2}}^{\frac{\pi}{2}} \sigma [\text{curv} \cdot R \cdot (\sin(\theta) + \delta)] \cdot t \cdot R^2 \cdot (\sin(\theta) + \delta) \, d\theta$	<p>Bending moment for specified curvature (curv)</p>
--	--

Integrate curvature to find displacement as a function of position. x is distance from a spacer grid, y is vertical displacement of rod. $D2$, $D1$, and $D0$ are d^2y/dx^2 , dy/dx , and y , respectively. n is number of points for integration. Integration is by trapezoidal rule. To save processing time, actual integration goes only halfway from support to loading point. The small-slope approximation is used, that is, the curvature is equal to d^2y/dx^2 .

Typical fuel

$n = 20$ Number of points for integration of displacement

$i := n..0$ $x_i := \frac{l \cdot i}{4 \cdot n}$ Points for integration

$\text{curv} = 0 \cdot m^{-1}$ $W\epsilon := W(\epsilon_{su})$ Calculate load when extreme fiber reaches failure strain.

$$D2_i := \text{root}(Mx(W\epsilon, x_i) - M\sigma(\text{curv}), \text{curv})$$

$$D1_0 := 0$$

$$D0_0 := 0 \cdot m$$

Boundary conditions for fixed ends

$$i := 1..n$$

Integration by trapezoidal rule

$$D1_i := D1_{i-1} + (D2_{i-1} + D2_i) \cdot \frac{l}{8 \cdot n}$$

$$D0_i := D0_{i-1} + (D1_{i-1} + D1_i) \cdot \frac{l}{8 \cdot n}$$

$$F_0 := W\epsilon$$

$$F_0 = 1076 \cdot \text{newton}$$

Force to bend rod to failure strain

$$\text{Disp}_0 := 2 \cdot |D0_n|$$

$$\text{Disp}_0 = 20.1 \cdot \text{mm}$$

Displacement at failure

Repeat calculation above for high-burnup fuel. Plastic failure strain (0.0015) is from Section 4.1.6.

$$i := n..0$$

$$\text{curv} := 0 \cdot m^{-1}$$

$$W\epsilon := W(\epsilon_f + 0.0015)$$

$$D2_i := \text{root}(Mx(W\epsilon, x_i) - M\sigma(\text{curv}), \text{curv})$$

$$D1_0 = 0$$

$$D0_0 := 0 \cdot m$$

$$i := 1..n$$

$$D1_i := D1_{i-1} + (D2_{i-1} + D2_i) \cdot \frac{l}{8 \cdot n}$$

$$D0_i := D0_{i-1} + (D1_{i-1} + D1_i) \cdot \frac{l}{8 \cdot n}$$

$$F_1 := W\epsilon$$

$$F_1 = 802.414 \cdot \text{newton}$$

Force to bend rod to failure strain

$$\text{Disp}_1 := 2 \cdot |D0_n|$$

$$\text{Disp}_1 = 9.1270 \cdot \text{mm}$$

Displacement at failure

Calculate rock load.

$$\rho := 2270 \cdot \frac{\text{kg}}{\text{m}^3}$$

Bulk density of tuff at in situ saturation (Section 4.1.5)

$$Ht := \frac{F}{l \cdot h \cdot g \cdot \rho}$$

Height of tuff layer to impose maximum load

Save results to file.

$$\mathit{block}_0 := \mathit{mrod}$$

$$\mathit{block}_1 := \frac{\mathit{Disp}_0}{\mathit{mm}}$$

$$\mathit{block}_2 := \frac{\mathit{Disp}_1}{\mathit{mm}}$$

$$\mathit{block}_3 := \frac{\mathit{F}_0}{\mathit{newton}}$$

$$\mathit{block}_4 := \frac{\mathit{F}_1}{\mathit{newton}}$$

$$\mathit{block}_5 := \frac{\mathit{Ht}_0}{\mathit{m}}$$

$$\mathit{block}_6 := \frac{\mathit{Ht}_1}{\mathit{m}}$$

$$\mathit{block}_7 := \mathit{type}$$

$$\mathit{APPENDPRN}(\mathit{staticld \ txt}) := \mathit{block}^T$$

Force-displacement curve for fuel rod with point load and incompressible fuel

Consider one fuel rod with a point load and incompressible fuel. Calculate the force-displacement curve, following the treatment described previously in file elpl_rod.mcd. The primary differences between the treatment here and that in elpl_rod.mcd are that (1) the geometry of the beam is specified directly rather than being read from a file and (2) the user may specify several values for the maximum fiber strain.

The force-displacement data are copied to file forcedsp.xls, and a curve is fitted to them. The resulting fit is documented in file rodpack.mcd.

It is recognized that the values of l , t , and R used here are not appropriate for a simple beam-theory calculation in which the beam is a thin-walled tube. Specifically, since $l = R$, the beam is too fat for simple beam theory to be applicable, and since $t = R$, the tube is not thin-walled. However, the analysis is still valid if the resulting formulas are used with appropriate values. The analysis here does not show how the force and displacement depend on l , t , and R ; that dependence can be readily deduced by varying these parameters below.

Some of the digits in the force and displacement results may not be significant; they are carried here only to minimize propagation of errors.

Geometric and mechanical data are entered here.

$TOL := 0.00001$

Choose close tolerance for integration.

$l := 1 \cdot m$

Distance between spacer grids

$t := 1 \cdot m$

Cladding wall thickness

$R := 1 \cdot m$

Cladding radius

$E := 99.284 \cdot 10^9 \cdot Pa$

Elastic modulus from Section 4.1.6.

$\sigma_y := 780 \cdot 10^6 \cdot Pa$

$\epsilon_y := \frac{\sigma_y}{E}$

Tensile data from Section 4.1.6.

$\sigma_u := 925 \cdot 10^6 \cdot Pa$

$\epsilon_u := 0.035 + \epsilon_y$

$E2 := \frac{\sigma_u - \sigma_y}{\epsilon_u - \epsilon_y}$

σ_u = ultimate tensile stress

ϵ_u = uniform elongation

σ_y = yield stress

ϵ_y = yield strain

$$\sigma(\epsilon) := \begin{cases} \epsilon E & \text{if } |\epsilon| \leq \epsilon_y \\ \sigma_y + E2 \cdot (\epsilon - \epsilon_y) & \text{if } \epsilon > \epsilon_y \\ -\sigma_y + E2 \cdot (\epsilon + \epsilon_y) & \text{otherwise} \end{cases}$$

Piecewise linear stress-strain curve

Load to bend rod to a specified strain in the extreme fiber.

Specify offset of neutral axis from axis of cladding. To put the neutral axis on the axis of the cladding (to ignore the structural effects of the fuel), set $\delta = 0$. To put the neutral axis on the compressive side of the cladding (to make the fuel extendible but not compressible), set $\delta = 1$. To put the neutral axis on the tensile side of the cladding (to make the fuel compressible but not extendible), set $\delta = -1$. (Negative values of δ are nonphysical.)

Specify desired maximum strain (ϵ_{max}); calculate required force (W) to produce that strain. Normally, ϵ_{max} is set to the uniform strain from an axial tensile test. A strain of ϵ_{max} will be attained at the support on the upper surface of the cladding. See Attachment I for a discussion of how these equations are obtained.

$$W(\epsilon_{max}) = \left. \begin{array}{l} \text{curv} \leftarrow \frac{\epsilon_{max}}{(1 + \delta) \cdot R} \\ M_{max} \leftarrow 2 \cdot \int_{-\frac{\pi}{2}}^{\frac{\pi}{2}} \sigma [\text{curv} \cdot R \cdot (\sin(\theta) + \delta)] \cdot r \cdot R^2 \cdot (\sin(\theta) + \delta) \, d\theta \\ \frac{M_{max}}{8 \cdot \frac{l}{l}} \end{array} \right\} \begin{array}{l} \text{Curvature to produce} \\ \text{strain of } \epsilon_{max} \\ \\ \text{Bending moment for that} \\ \text{curvature} \\ \\ \text{Load to produce that} \\ \text{bending moment at} \\ \text{support (or load)} \end{array}$$

Determine bending moment as a function of different variables.

$Mx(W, x) := \frac{-W \cdot l}{8} + \frac{W \cdot x}{2}$ Bending moment (Mx) as a function of load (W) and position (x). See Roark (Ref. 5.15, p. 101, case 1d). For loading at midspan, moment at left end is $-\frac{Wl}{8}$; moment at midspan is $\frac{Wl}{8}$. Moment varies linearly between these points because there is no other load in that interval.

$$M\sigma(\text{curv}) = 2 \cdot \int_{-\frac{\pi}{2}}^{\frac{\pi}{2}} \sigma [\text{curv} \cdot R \cdot (\sin(\theta) + \delta)] \cdot r \cdot R^2 \cdot (\sin(\theta) + \delta) \, d\theta \quad \text{Bending moment for specified curvature (curv)}$$

Integrate curvature to find displacement as a function of position. x is distance from a spacer grid, y is vertical displacement of rod. $D2$, $D1$, and $D0$ are d^2y/dx^2 , dy/dx , and y , respectively. n is number of points for integration. Integration is by trapezoidal rule. To save processing time, actual integration goes only halfway from support to loading point. The small-slope approximation is used, that is, the curvature is equal to d^2y/dx^2 .

$n := 20$ Number of points for integration of displacement

$i := n..0$ $x_i := \frac{l \cdot i}{4 \cdot n}$

$$curv = 0 \cdot m^{-1}$$

$$W_{\epsilon} := W(\epsilon_y)$$

Calculate load when extreme fiber reaches yield strain.

$$D2_i := \text{root}(Mx(W_{\epsilon}, x_i) - M\sigma(curv), curv)$$

$$Dl_0 = 0$$

$$D0_0 := 0 \cdot m$$

Boundary conditions for fixed ends

$$i := 1..n$$

$$Dl_i := Dl_{i-1} + (D2_{i-1} + D2_i) \cdot \frac{l}{8 \cdot n}$$

$$D0_i := D0_{i-1} + (Dl_{i-1} + Dl_i) \cdot \frac{l}{8 \cdot n}$$

$$F_1 := W_{\epsilon}$$

$$F_1 = 2.94053 \cdot 10^{10} \cdot \text{newton}$$

Force to bend rod to yield point

$$Disp_1 := 2 \cdot |D0_n|$$

$$Disp_1 = 1.6357 \cdot 10^{-4} \cdot m$$

Displacement at yield

Repeat calculation above for four more strains. Two of these are arbitrarily chosen strains (ϵ_m , which is set twice), one is the failure strain (ϵ_u) for typical fuel, and one is the failure strain ($\epsilon_y + 0.0015$) for high-burnup fuel. Note that strain is only a parameter that is used to calculate points on the force-displacement curve. To build the table of forces and displacements in file forcedsp.xls, ϵ_m must be set to each of values of strain specified symbolically in the file forcedsp.xls.

First intermediate strain

$$i := n..0$$

$$curv := 0 \cdot m^{-1}$$

$$\epsilon_m = \frac{8 \cdot \epsilon_y + \epsilon_u}{9}$$

$$W_{\epsilon} := W(\epsilon_m)$$

$$D2_i := \text{root}(Mx(W_{\epsilon}, x_i) - M\sigma(curv), curv)$$

$$Dl_0 := 0$$

$$D0_0 := 0 \cdot m$$

$$i := 1..n$$

$$Dl_i := Dl_{i-1} + (D2_{i-1} + D2_i) \cdot \frac{l}{8 \cdot n}$$

$$D0_i := D0_{i-1} + (Dl_{i-1} + Dl_i) \cdot \frac{l}{8 \cdot n}$$

$$F_2 := W_{\epsilon}$$

$$F_2 = 3.51899 \cdot 10^{10} \cdot \text{newton}$$

$$Disp_2 := 2 \cdot |D0_n|$$

$$Disp_2 = 2.03325 \cdot 10^{-4} \cdot m$$

Second intermediate strain

$$i := n..0 \quad \text{curv} := 0 \cdot \text{m}^{-1} \quad \epsilon m := \frac{3 \cdot \epsilon y + 2 \cdot \epsilon u}{5} \quad W \epsilon := W(\epsilon m)$$

$$D2_i := \text{root}(Mx(W \epsilon, x_i) - Mo(\text{curv}), \text{curv})$$

$$D1_0 := 0 \quad D0_0 := 0 \cdot \text{m}$$

$$i := 1..n$$

$$D1_i := D1_{i-1} + (D2_{i-1} + D2_i) \cdot \frac{l}{8 \cdot n} \quad D0_i := D0_{i-1} + (D1_{i-1} + D1_i) \cdot \frac{l}{8 \cdot n}$$

$$F_3 := W \epsilon \quad F_3 = 3.94844 \cdot 10^{10} \cdot \text{newton}$$

$$Disp_3 := 2 \cdot |D0_n| \quad Disp_3 = 2.65416 \cdot 10^{-4} \cdot \text{m}$$

Failure strain (typical fuel)

$$i := n..0 \quad \text{curv} := 0 \cdot \text{m}^{-1} \quad W \epsilon := W(\epsilon u)$$

$$D2_i := \text{root}(Mx(W \epsilon, x_i) - Mo(\text{curv}), \text{curv})$$

$$D1_0 := 0 \quad D0_0 := 0 \cdot \text{m}$$

$$i := 1..n$$

$$D1_i := D1_{i-1} + (D2_{i-1} + D2_i) \cdot \frac{l}{8 \cdot n} \quad D0_i := D0_{i-1} + (D1_{i-1} + D1_i) \cdot \frac{l}{8 \cdot n}$$

$$F_4 := W \epsilon \quad F_4 = 4.37425 \cdot 10^{10} \cdot \text{newton} \quad \text{Force to bend rod to failure strain}$$

$$Disp_4 := 2 \cdot |D0_n| \quad Disp_4 = 4.01626 \cdot 10^{-4} \cdot \text{m} \quad \text{Displacement at failure strain}$$

Failure strain (high-burnup fuel)

$i := n..0$ $curv := 0 \cdot m^{-1}$ $W\epsilon = W(\epsilon_y + 0.0015)$ Plastic strain (0.0015) is from Section 4.1.6.

$$D2_i = \text{root}(Mx(W\epsilon, x_i) - M\sigma(curv), curv)$$

$$Dl_0 := 0 \quad D0_0 := 0 \cdot m$$

$i := 1..n$

$$Dl_i := Dl_{i-1} + (D2_{i-1} + D2_i) \cdot \frac{l}{8 \cdot n}$$

$$D0_i := D0_{i-1} + (Dl_{i-1} + Dl_i) \cdot \frac{l}{8 \cdot n}$$

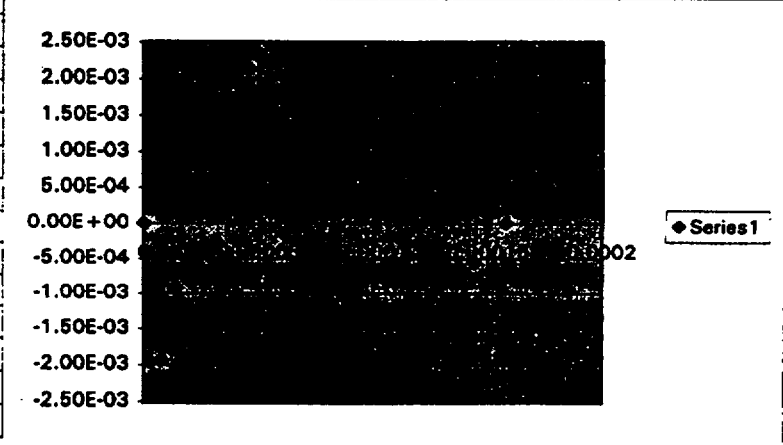
$$F_s := W\epsilon \quad F_s = 3.26214 \cdot 10^{10} \cdot \text{newton} \quad \text{Force to bend rod to failure strain}$$

$$Disp_s := 2 \cdot |D0_n| \quad Disp_s = 1.82937 \cdot 10^{-4} \cdot m \quad \text{Displacement at failure strain}$$

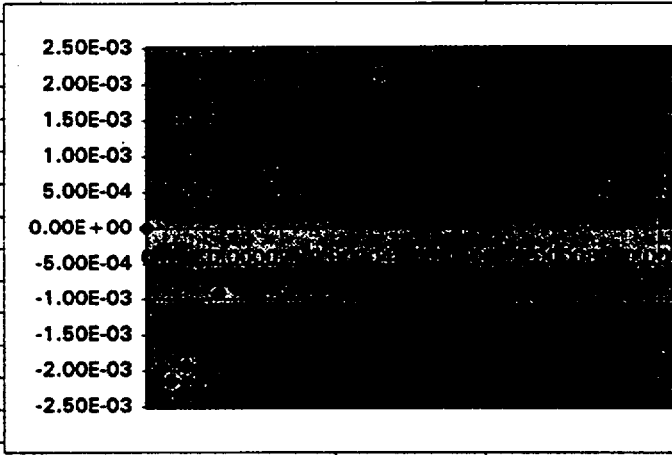
Results E and $Disp$ (arrays) are tabulated in file forcedsp.xls.

Sheet "Model" documents the model force-displacement curve.
Column E lists inputs. These are arbitrarily selected maximum fiber strains, represented symbolically. ϵ_y and ϵ_u are the tensile yield strain and uniform elongation for typical fuel, respectively, from Section 4.1.6.
Columns A and B list the the force and displacement, respectively, if the maximum fiber strains listed in column E are imposed on a "beam" with $L = 1$ m, $t = 1$ m, $B = 1$ m. These were calculated with Mathcad worksheet file eipl.mcd. See that file for definitions of L , t , and B . Note that cells A6, B6, A18, and B18 in sheet "Model" (shaded cells) are the force and displacement at the onset of yielding and at uniform elongation for typical fuel. Cells A20, and B20 in sheet "Model" are the force and displacement uniform elongation for high-burnup fuel. These values appear in the equations for F_y , D_y , F_u , and D_u , respectively, in file rodpack.mcd.
Columns C and D list the plastic parts of the force and displacement, respectively. The plastic part of the displacement is the total displacement minus the extrapolated displacement that would occur if the beam remained plastic. The plastic part of the force is the total force minus the force at the onset of plasticity.
Column F lists the predicted amounts of plastic displacement as calculated with an equation. See the formulas in this column.
Column G lists the relative error in the predicted plastic displacement. This is the predicted displacement minus the actual displacement, all divided by the displacement at failure.
The graph is solely for the purposes of illustration. It shows the relative error in displacement as a function of actual displacement.

	A	B	C	D	E	F	G
1						Predicted	Relative
2			Plastic	Plastic	Maximum	Plastic	Error in
3	Force	Displ.	Displ.	Force	Strain	Displ.	Plastic
4	(N)	(m)	(m)	(N)		(m)	Displ.
5	0.00E+00	0.00E+00			0		
6	2.94E+10	1.64E-04	0	0.00E+00	σ_y	0	0.00E+00
7	3.35E+10	1.89E-04	2.91E-06	4.14E+09	$(15\sigma_y + \epsilon)/16$	2.12E-06	-1.97E-03
8	3.43E+10	1.96E-04	4.76E-06	4.93E+09	$(11\sigma_y + \epsilon)/12$	3.90E-06	-2.14E-03
9	3.52E+10	2.03E-04	7.58E-06	5.78E+09	$(8\sigma_y + \epsilon)/9$	6.80E-06	-1.94E-03
10	3.65E+10	2.17E-04	1.4E-05	7.07E+09	$(5\sigma_y + \epsilon)/6$	1.36E-05	-9.26E-04
11	3.78E+10	2.35E-04	2.47E-05	8.42E+09	$(3\sigma_y + \epsilon)/4$	2.50E-05	7.67E-04
12	3.88E+10	2.52E-04	3.61E-05	9.42E+09	$(2\sigma_y + \epsilon)/3$	3.68E-05	1.78E-03
13	3.95E+10	2.65E-04	4.58E-05	1.01E+10	$(3\sigma_y + 2\epsilon)/5$	4.66E-05	2.14E-03
14	4.03E+10	2.86E-04	6.12E-05	1.09E+10	$(\sigma_y + \epsilon)/2$	6.20E-05	1.89E-03
15	4.16E+10	3.21E-04	8.98E-05	1.22E+10	$(\sigma_y + 2\epsilon)/3$	9.00E-05	5.49E-04
16	4.25E+10	3.52E-04	0.000115	1.31E+10	$(\sigma_y + 4\epsilon)/5$	1.15E-04	-4.54E-04
17	4.34E+10	3.85E-04	0.000144	1.40E+10	$(\sigma_y + 15\epsilon)/16$	1.44E-04	-5.52E-04
18	4.37E+10	4.02E-04	0.000158	1.43E+10	ϵ	1.58E-04	0.00E+00
19							
20	3.26E+10	1.83E-04	1.48E-06	3.22E+09	ϵ_{uhb}	8.88E-07	-1.47E-03
21							
22	Displ. = displacement						
23							
24							
25	fitting						
26	exponent						
27	3.468						
28							
29							
30							
31							
32							
33							
34							
35							
36							
37							
38							



	A	B	C	D	E
1					
2			Plastic	Plastic	Maximum
3	Force	Displ.	Displ.	Force	Strain
4	(N)	(m)	(m)	(N)	
5	0	0			0
6	29405300000	0.00016357	=B6-A6*(B\$6/A\$6)	=A6-A\$6	ϵ_y
7	33541300000	0.000189491	=B7-A7*(B\$6/A\$6)	=A7-A\$6	$(15\epsilon_y + \epsilon_u)/16$
8	34333600000	0.000195746	=B8-A8*(B\$6/A\$6)	=A8-A\$6	$(11\epsilon_y + \epsilon_u)/12$
9	35189900000	0.000203325	=B9-A9*(B\$6/A\$6)	=A9-A\$6	$(8\epsilon_y + \epsilon_u)/9$
10	36474600000	0.000216896	=B10-A10*(B\$6/A\$6)	=A10-A\$6	$(5\epsilon_y + \epsilon_u)/6$
11	37822500000	0.00023505	=B11-A11*(B\$6/A\$6)	=A11-A\$6	$(3\epsilon_y + \epsilon_u)/4$
12	38821300000	0.000252064	=B12-A12*(B\$6/A\$6)	=A12-A\$6	$(2\epsilon_y + \epsilon_u)/3$
13	39484400000	0.000265416	=B13-A13*(B\$6/A\$6)	=A13-A\$6	$(3\epsilon_y + 2\epsilon_u)/5$
14	40346700000	0.000285672	=B14-A14*(B\$6/A\$6)	=A14-A\$6	$(\epsilon_y + \epsilon_u)/2$
15	41587200000	0.00032109	=B15-A15*(B\$6/A\$6)	=A15-A\$6	$(\epsilon_y + 2\epsilon_u)/3$
16	42483100000	0.000351583	=B16-A16*(B\$6/A\$6)	=A16-A\$6	$(\epsilon_y + 4\epsilon_u)/5$
17	43356800000	0.000385417	=B17-A17*(B\$6/A\$6)	=A17-A\$6	$(\epsilon_y + 15\epsilon_u)/16$
18	43742500000	0.000401626	=B18-A18*(B\$6/A\$6)	=A18-A\$6	ϵ_u
19					
20	32621400000	0.000182937	=B20-A20*(B\$6/A\$6)	=A20-A\$6	ϵ_{uhb}
21					
22	Displ. = displacement				
23					
24					
25	fitting				
26	exponent				
27	3.468				
28					
29					
30					
31					
32					
33					
34					
35					
36					
37					
38					



	F	G
1	Predicted	Relative
2	Plastic	Error in
3	Displ.	Plastic
4	(m)	Displ.
5		
6	0	= (F6-C6)/B\$18
7	=C\$18*(D7/D\$18)^\$A\$27	= (F7-C7)/B\$18
8	=C\$18*(D8/D\$18)^\$A\$27	= (F8-C8)/B\$18
9	=C\$18*(D9/D\$18)^\$A\$27	= (F9-C9)/B\$18
10	=C\$18*(D10/D\$18)^\$A\$27	= (F10-C10)/B\$18
11	=C\$18*(D11/D\$18)^\$A\$27	= (F11-C11)/B\$18
12	=C\$18*(D12/D\$18)^\$A\$27	= (F12-C12)/B\$18
13	=C\$18*(D13/D\$18)^\$A\$27	= (F13-C13)/B\$18
14	=C\$18*(D14/D\$18)^\$A\$27	= (F14-C14)/B\$18
15	=C\$18*(D15/D\$18)^\$A\$27	= (F15-C15)/B\$18
16	=C\$18*(D16/D\$18)^\$A\$27	= (F16-C16)/B\$18
17	=C\$18*(D17/D\$18)^\$A\$27	= (F17-C17)/B\$18
18	=C\$18*(D18/D\$18)^\$A\$27	= (F18-C18)/B\$18
19		
20	=C\$18*(D20/D\$18)^\$A\$27	= (F20-C20)/B\$18
21		
22		
23		
24		
25		
26		
27		
28		
29		
30		
31		
32		
33		
34		
35		
36		
37		
38		

$$ndisch = 4.134 \cdot 10^3$$

Number of assemblies discharged

$$rodln = 3.903 \cdot m$$

Nominal rod length

$$pack := 0.9$$

Effectiveness of rods in achieving dense (hexagonal) packing, from Section 4.3.3.

$$\rho_f := pack \cdot \frac{\sqrt{3}}{6 \cdot \left(R + \frac{t}{2}\right)^2}$$

Final density of rods. If $pack = 1$, the density is that of rods that are hexagonally packed, surface to surface. Outside radius of cladding is midwall radius plus $t/2$. For hexagonally packed rods, the spacing of rods along one row is $2(R+t/2)$ and the spacing of rows is $(\sqrt{3}/2)[2(R+t/2)]$. The cross sectional area per rod is the product of the two spacings, and the areal density is the reciprocal of the cross sectional area. The actual density will be somewhat smaller (as indicated by the packing factor $pack$) because of irregularities in the initial array, as is discussed in Section 4.3.3.

$$\frac{\rho_f}{\rho_o} = 1.813$$

$$rP_{eff} := rP \cdot \left(1 - \frac{\rho_o}{\rho_f}\right)$$

Since the compressed rods still take up some space, the lower surface of the pack of compressed rods moves faster than the block that causes the compression. An additional penetration of the block into the assembly by a distance rD_{eff} will move the front of the pack forward by a distance rP , that is, through another layer of rods. In the block's frame of reference, rD_{eff} is the effective rod pitch.

Force-displacement curve and model, with proper dependence on rod geometry.

$$F_y := 2.94053 \cdot 10^{10} \cdot Pa \cdot t \cdot \frac{R^2}{l}$$

$$D_y := 1.63570 \cdot 10^{-4} \cdot \frac{l^2}{R}$$

F = force
y = yield

D = displacement
u = ultimate

$$F_u := 4.37425 \cdot 10^{10} \cdot Pa \cdot t \cdot \frac{R^2}{l}$$

$$D_u := 4.01626 \cdot 10^{-4} \cdot \frac{l^2}{R}$$

These constants in these equations were developed with file elpl_mdl.mcd and are documented in file forcedsp.xls.

$$D(F) = \begin{cases} \left(\frac{F \cdot D_y}{F_y} \right) & \text{if } F < F_y \\ \left[\frac{F \cdot D_y}{F_y} + \left(D_u - D_y \frac{F_u}{F_y} \right) \cdot \left(\frac{F - F_y}{F_u - F_y} \right)^{3.468} \right] & \text{otherwise} \end{cases}$$

The form of this equation is documented in file forcedsp.xls. The first case is for elastic deformation; the second is for elastic + plastic deformation.

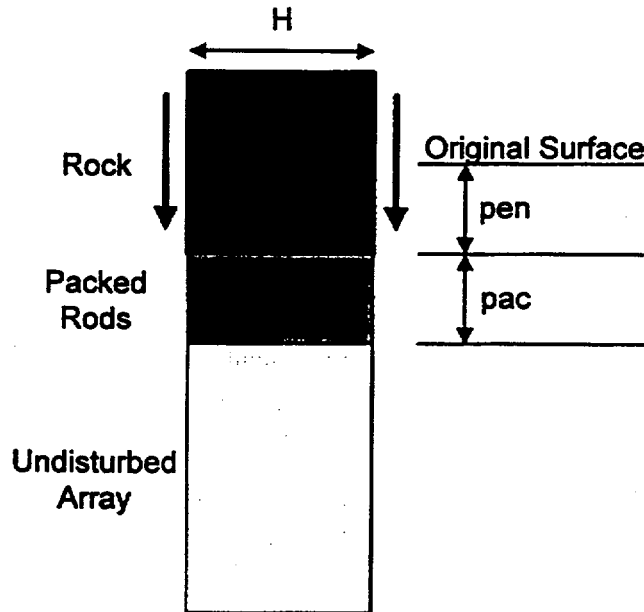
$$F_{uhb} := F_u \cdot \frac{3.26214 \cdot 10^{10}}{4.37425 \cdot 10^{10}}$$

$$D_{uhb} := D_u \cdot \frac{1.82937 \cdot 10^{-4}}{4.01626 \cdot 10^{-4}}$$

Reduce ultimate force and displacement for high-burnup fuel per file forcedsp.xls.

Consider a block that impacts an array of rods with density ρ_o and compresses them to a density ρ_f . Let H be the width over which the rod impacts the pack of rods. (This is measured in the direction normal to the axis of the rods.) In penetrating a distance pen into the array, a densified pack of thickness pac develops ahead of the block. The following equation expresses conservation of matter in forming the pack; it is derived from $\rho_o(pen+pac) = \rho_f pac$. Note that positions are measured downward from the top of the array of rods and that measurements are made relative to the undisturbed rods, not relative to the block.

$$pac(pen) = \frac{\rho_o \cdot pen}{\rho_f - \rho_o}$$



The displacement of a rod originally at a distance y from the top of the array will be 0 if $y = pen + pac$ and will be pen if $y = 0$. Between these points, the displacement will vary linearly with y .

$$disp(pen, y) = pen \cdot \left(1 - \frac{y}{pen + pac(pen)} \right)$$

A rod that is displaced by the block will exert a force to retard the block. For a rod that is displaced by a distance $Drod$, the following equation gives the force.

$f = Fy$ Arbitrary initial guess for root-finder

$force(Drod) := root(D(f) - Drod, f)$

If no rods have broken, the force on the block is given by the following equation.

$$F(pen) = \rho_p \int_0^{pen + pac(pen)} force(disp(pen, y)) \cdot \rho_o \, dy$$

$F(0 \cdot m) = 0 \cdot \text{newton}$ No displacement; no load.

Calculate block mass and energy to start breaking rods. Let failure begin when the first rods reach the displacement that corresponds to the uniform plastic strain, \underline{Du} . The calculation here is for typical fuel.

$n := 10$ $i := 0..n$ n must be even for integration by Simpson's rule below.

$$xx_i := Du \cdot \frac{i}{n} \qquad FF_i := F(xx_i)$$

Integrate energy by Simpson's rule (Ref. 5.31, p. 14).

$$Eu := \left[\sum_{i=1}^{\frac{n}{2}-1} 2 \cdot FF_{2i} + \sum_{i=1}^{\frac{n}{2}} 4 \cdot FF_{2i-1} + FF_0 + FF_n \right] \cdot \frac{xx_1}{3}$$

$$Eu = 28.23 \cdot \text{joule}$$

To break additional rods, the energy is the (now constant) force $F(Du)$ times the distance moved to encounter one rod. Equivalently, it is the energy to bend one rod until it reaches the breaking point. The latter quantity is obtained here with integration by parts. The two results are consistent.

$$Eaddu := F(Du) \cdot rp \text{ eff} \qquad Eaddu = 21.72 \cdot \text{joule}$$

$$Eaddu := Fu \cdot Du - \int_0^{Fu} D(\phi) \cdot a \phi \qquad Eaddu = 21.73 \cdot \text{joule}$$

Repeat the energy calculations above for high-burnup fuel.

$$xx_i := Du_{hb} \cdot \frac{i}{n} \qquad FF_i := F(xx_i)$$

Integrate energy by Simpson's rule (Ref. 5.31 p. 14).

$$Eu_{hb} := \left[\sum_{i=1}^{\frac{n}{2}-1} 2 \cdot FF_{2i} + \sum_{i=1}^{\frac{n}{2}} 4 \cdot FF_{2i-1} + FF_0 + FF_n \right] \cdot \frac{xx_1}{3}$$

$$E_{uhb} = 2.948 \cdot \text{joule}$$

$$E_{adduhb} := F(D_{uhb}) \cdot r_{p \text{ eff}}$$

$$E_{adduhb} = 5.57 \cdot \text{joule}$$

$$E_{adduhb} := F_{uhb} \cdot D_{uhb} - \int_0^{F_{uhb}} D(\phi) \cdot a \phi \quad E_{adduhb} = 5.57 \cdot \text{joule}$$

Save results to file.

$$\text{block}_0 := \frac{r_p}{m} \quad \text{Rod pitch}$$

$$\text{block}_1 := n_{rod} \quad \text{Number of rods per side}$$

$$\text{block}_2 := \frac{E_u}{\text{joule}} \quad \text{Energy to start failing rods, typical fuel}$$

$$\text{block}_3 := \frac{E_{addu}}{\text{joule}} \quad \text{Energy to fail one additional rod, typical fuel}$$

$$\text{block}_4 := \frac{D_u}{m} \quad \text{Displacement to start failing rods, typical fuel}$$

$$\text{block}_5 := \frac{E_{uhb}}{\text{joule}} \quad \text{Energy to start failing rods, high-burnup fuel}$$

$$\text{block}_6 := \frac{E_{adduhb}}{\text{joule}} \quad \text{Energy to fail one additional rod, high-burnup fuel}$$

$$\text{block}_7 := \frac{D_{uhb}}{m} \quad \text{Displacement to start failing rods, high-burnup fuel}$$

$$\text{block}_8 := \frac{r_{p \text{ eff}}}{m} \quad \text{Effective rod pitch}$$

$$\text{block}_9 := n_{disch} \quad \text{Number of assemblies discharged}$$

$$\text{block}_{10} := \frac{rod_{ln}}{m} \quad \text{Rod length}$$

$$\text{block}_{11} := \text{type} \quad \text{Assembly type}$$

$$APPENDPRN(\text{rod_engy.txt}) := \text{block}^T$$

Rod breakage from rock block with linear punch

Results from previous calculations are used here to determine the fraction of fuel rods that fail because of falling blocks of rock. Available data for assembly characteristics are combined with data on the block size distribution. Blocks are taken to be right circular cylinders with vertical axes that fall freely and rectilinearly. The cylinders are taken to cover the entire exposed upper surface of the assemblies exactly once. The height of each cylinder is taken to be equal to its diameter. Since the rods are light and flexible in comparison to rock, the mass of the rods is neglected and the block is taken to be a rigid body. To account for the effect of surface irregularities on the bottom face of the block, the energy of the block is assumed to be focused on a strip rather than being distributed over the entire area of the block. Conceptually, there is a protruding ridge, referred to as a "punch", on the bottom of the block. Relative to the circular bottom of the block, the outline of the punch is defined by two parallel chords of equal length and the two arcs that connect them. (See sketch on page V-3.) The width of the punch is given by the focusing parameter, which is the ratio of the distance between the two chords to the diameter of the block. The orientation of the punch is given by the angle between the chords and the fuel rods.

The phrase "column of rods" means a vertical slice, taken parallel to the fuel rods, through a full stack of assemblies, with width equal to the rod pitch and length equal to the rod length.

Parameters that describe the falling blocks and exposure of assemblies

Density of rock blocks	Fall height	Number of assemblies in one stack	Focusing param. $0 < \text{focus} \leq 1$
$\text{density} := 2270 \cdot \frac{\text{kg}}{\text{m}^3}$	$\text{fallht} := 0.2032 \cdot \text{m}$	$\text{nstack} := \frac{21}{5}$	$\text{focus} := 1$
Angle between punch blade and rods. $0 \leq \text{angle} \leq 90$ degrees		Set hb to 0 for typical fuel, 1 for high-burnup fuel. 0 and 1 are the only valid values.	
$\text{angle} := 90 \cdot \text{deg}$		$\text{hb} := 0$	

Read data from previous calculation and divide into vectors.

$\text{rodpack} := \text{READPRN}(\text{rod_engy.txt})$	Read data.
$\text{rp} := \text{rodpack}^{\langle 0 \rangle} \cdot \text{m}$	Rod pitch
$\text{nrod} := \text{rodpack}^{\langle 1 \rangle}$	Number of rods per side
$\text{Estart} := \text{rodpack}^{\langle 2 + 3 \cdot \text{hb} \rangle} \cdot \text{joule}$	Energy to start breaking rods (for one column of rods)
$\text{Eaddl} := \text{rodpack}^{\langle 3 + 3 \cdot \text{hb} \rangle} \cdot \text{joule}$	Energy to break one additional rod
$\text{zstart} := \text{rodpack}^{\langle 4 + 3 \cdot \text{hb} \rangle} \cdot \text{m}$	Displacement to start breaking rods
$\text{rp}_{\text{eff}} := \text{rodpack}^{\langle 8 \rangle} \cdot \text{m}$	Effective rod pitch (block displacement to break one additional rod in a column of rods)
$\text{ndisch} := \text{rodpack}^{\langle 9 \rangle}$	Number of assemblies discharged
$\text{rodlen} := \text{rodpack}^{\langle 10 \rangle} \cdot \text{m}$	Length of fuel rods

$type := rodpack^{<11>}$ Assembly type
 $ntypes := length(type)$ Number of types of assemblies
 $trodtype := \overrightarrow{(ndisch \cdot nrod^2)}$
 $totalrods := \sum trodtype$ $totalrods = 8.834 \cdot 10^6$ Total number of rods
 $totalllen := \sum \overrightarrow{(ndisch \cdot rodlen \cdot nrod^2)}$ $totalllen = 3.405 \cdot 10^7 \cdot m$ Total length of all rods

Read information on block size distribution and divide into vectors.

$blocks := READPRN(esfblock.txt)$ Read data
 $cumprobmx := blocks^{<0>}$ Cumulative probability for block of given volume ...
 $blkvolmx := blocks^{<1>} \cdot m^3$... and the corresponding block volume. "mx" indicates that these quantities are the maxima for the corresponding size interval.
 $nsizes := length(blkvolmx) - 1$ Number of block size intervals

Calculate properties of typical block for each size interval

$isz := 0 .. nsizes - 1$

$blkvol_{isz} := \frac{blkvolmx_{isz} + blkvolmx_{isz+1}}{2}$ Mean block volume for each size interval

$prob_{isz} := cumprobmx_{isz+1} - cumprobmx_{isz}$ Probability that a block is in a given size interval

Block mass, diameter, and area of one end, according to the cylindrical geometry, for each size interval

$blkmass := blkvol \cdot density$
 $blkdiam := 2 \cdot \overrightarrow{\left(\frac{blkvol}{2 \cdot \pi} \right)^{\frac{1}{3}}}$
 $blkarea := \pi \cdot \overrightarrow{\frac{blkdiam^2}{4}}$

$meanblkarea := blkarea \cdot prob$ Mean area of one block end

$meanblkarea = 0.244 \cdot m^2$

Calculate additional properties of different types of assemblies and impacts.

$$\text{rodspercol} = \text{nrod} \cdot \text{nstack}$$

Number of rods in one column

$$\text{nblocks} = \frac{(\text{ndisch} \cdot \text{rp} \cdot \text{rodlen} \cdot \text{nrod})}{\text{meanblkarea} \cdot \text{nstack}}$$

Total number of blocks that fall on assemblies of a given type. Value is the total exposed area of all assemblies of that type divided by the mean block area.

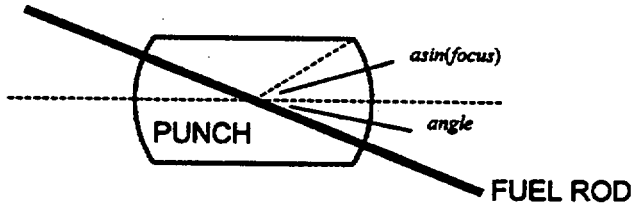
$$\text{focuswid} := \begin{cases} 1 & \text{if } \text{angle} + \text{asin}(\text{focus}) \geq 90 \cdot \text{deg} \\ (\sin(\text{angle} - \text{asin}(\text{focus}))) & \text{otherwise} \end{cases}$$

focuswid is the effective width of the punch, that is, the distance spanned by it in a direction perpendicular to the fuel rods, expressed as a fraction of the block diameter. See sketch below.

$$\text{itype} = 0 \dots \text{ntypes} - 1$$

$$\text{cols}_{\text{isz}, \text{itype}} = \frac{\text{blkdiam}_{\text{isz}}}{\text{rp}_{\text{itype}}} \cdot \text{focuswid}$$

cols_{isz, itype} is the number of fuel rod columns struck by the punch.



The sketch above explains the variable focuswid. The outline of the punch, as seen from below, is shown in solid lines. The long dashed line is the axis of the punch, and the short dashed line is a radius that extends to the point where the arc meets the chord. The angle between the two dashed lines is asin(focus). The heavy line is a fuel rod. Recall that angle is the angle between the axis of the punch and the fuel rod, and $0 \text{ degrees} \leq \text{angle} \leq 90 \text{ degrees}$. If angle + asin(focus) is greater than or equal to 90 degrees, the punch is effectively as wide as the block, that is, it will break as many rods in each layer as if there were no focusing of energy. If angle + asin(focus) is less than 90 degrees, the focusing effect of the punch will reduce the number of fuel rods broken per layer (but the number of layers penetrated will increase).

For each size interval, calculate the number of breaks caused by blocks of that size. brknum_{isz, itype} is the number of breaks that would be caused in assemblies of type itype by one block in size interval isz. Eavail is the energy available when rods start to break. g is gravity. The number of broken rods is calculated from the energy balance. Energy accumulated as the block continues to fall is included. The number of broken rods is limited by the number of rods loaded by the block. The case brkraw < 0 arises if the block is so massive that its kinetic energy increases as it penetrates the assemblies.

Note that, for blocks with end areas smaller than the mean block area, the effect is to have incomplete coverage of the assemblies. Similarly, for blocks with end areas larger than the mean block area, the effect is to have overlapping blocks. In calculating the total number of breaks, however, perfect coverage is assured by multiplying brknum_{isz, itype} by prob_{isz}, the probability that a given block is in the size interval isz.

$$\begin{aligned}
 brknum_{isz, itype} &= \begin{cases} Eavail \leftarrow blkmass_{isz} \cdot g \cdot (fallht - zstart_{itype}) - cols_{isz, itype} \cdot Estart_{itype} \\ Eavail \leftarrow 0 \text{ if } Eavail < 0 \\ brkraw \leftarrow \frac{Eavail}{Eaddl_{itype} \cdot cols_{isz, itype} - rp_{eff_{itype}} \cdot blkmass_{isz} \cdot g} \cdot cols_{isz, itype} \\ brk \leftarrow brkraw \\ brk \leftarrow cols_{isz, itype} \cdot rodspercol_{itype} \text{ if } brkraw < 0 \\ brk \leftarrow cols_{isz, itype} \cdot rodspercol_{itype} \text{ if } brkraw > cols_{isz, itype} \cdot rodspercol_{itype} \\ brk \end{cases}
 \end{aligned}$$

$totalbreaks = prob \cdot (brknum \cdot nblocks)$ Total number of breaks, summed over block size intervals

$$totalbreaks = 2.956 \cdot 10^5$$

$$\frac{totalbreaks}{totalrods} = 3.346 \cdot 10^{-2}$$

Ratio of number of breaks to the number of rods. In the limit of few breaks, this ratio approaches the fraction of rods broken.

The mean length of the broken part of a rod is the area of the punch divided by $(focuswid \cdot blkdiam_{isz})$. The total length of the broken parts is then the mean length times the number of breaks as calculated below. The area of a punch is $blkdiam^2$ times the numerator of the ratio in the right pair of square brackets below. (This is derived from equations in Ref. 5.31, p. 12.) The matrix multiplication and dot product in the left pair of square brackets below takes into account the number of blocks of each size.

$$totalbreaklen := \left[\frac{blkdiam \cdot prob}{(blkdiam \cdot prob)} \cdot (brknum \cdot nblocks) \right] \cdot \left[\frac{\frac{\pi}{4} - \frac{1}{2} \cdot (\cos(focus) - focus \cdot \sqrt{1 - focus^2})}{focuswid} \right]$$

$totalbreaklen = 2.114 \cdot 10^5 \cdot m$ Total length of broken parts, summed over block size intervals

$\frac{totalbreaklen}{totallen} = 6.21 \cdot 10^{-3}$ Fraction of total rod length broken

Calculate the fraction of rods that are broken.

$$brkdep_{isz, itype} = \frac{brknum_{isz, itype}}{cols_{isz, itype}}$$

Depth of penetration of a block, measured in rod layers. Note that the definition of $brknum$ keeps $brkdep$ from being larger than $rodspercol$.

$$rodsperlayer_{itype} = \frac{trodtype_{itype}}{rodspercol_{itype}}$$

Number of rods per layer for assemblies of type $itype$. Note that this quantity is proportional to the number of assemblies discharged.

Find the fraction of rods broken in a given layer for assemblies of type itype if that layer were to be penetrated by a block of size isz. Note that $nblocks_{itype} \cdot prob_{isz}$ is the number of blocks of size isz that strike assemblies of type itype. That is multiplied by $cols_{isz,itype}$ to find the number of rods in the layer that would be broken by such blocks. Finally, that number of rods is divided by the number of rods per layer ($rodsperlayer_{itype}$) to find the fraction of rods broken in a given layer. The ratio of number of breaks to number of rods is approximately the fraction of rods broken because $prob_{isz}$ keeps the ratio small; for large ratios the effect of multiple breaks per rod would have to be considered.

$$fbrkst_{isz,itype} = \frac{cols_{isz,itype} \cdot nblocks_{itype} \cdot prob_{isz}}{rodsperlayer_{itype}}$$

$$nbrk(il, is, it) = \begin{cases} 0 & \text{if } brkdep_{is, it} \leq il \\ 1 & \text{if } brkdep_{is, it} > il + 1 \\ brkdep_{is, it} - il & \text{otherwise} \end{cases}$$

Fraction of layer il penetrated by a block of size is that impacts on assemblies of type it. The top layer is layer 0.

$$ilr = 0 .. \max(\text{floor}(\text{rodspercol}))$$

Range variable ilr indexes the layers of rods.

$$fbrklt_{ilr,itype} = 1 - \prod_{isz} (1 - nbrk(ilr, isz, itype) \cdot fbrkst_{isz,itype})$$

The quantity in parentheses gives the fraction of rods left intact by blocks of a given size. The continued product gives the fraction left intact by rocks of all sizes. That is subtracted from 1 to give the fraction of rods broken in layer ilr for assemblies of type itype.

$$totalbrkrod = \sum(fbrklt \cdot rodsperlayer)$$

Sum over layers and assembly types to find total number of broken rods.

$$\frac{totalbrkrod}{totalrods} = 0.015$$

Save results to file.

$$block_0 = \frac{totalbreaks}{totalrods}$$

$$block_3 = focus$$

$$block_1 = \frac{totalbreaklen}{totallen}$$

$$block_4 = \frac{angle}{deg}$$

$$block_2 = \frac{totalbrkrod}{totalrods}$$

$$block_5 = hb$$

$$APPENDPRN(\text{linpunch txt}) = block^T$$

Rod breakage from rock block with circular punch

Results from previous calculations are used here to determine the fraction of fuel rods that fail because of falling blocks of rock. Available data for assembly characteristics are combined with data on the block size distribution. Blocks are taken to be right circular cylinders with vertical axes that fall freely and rectilinearly. The cylinders are taken to cover the entire exposed upper surface of the assemblies exactly once. The height of each cylinder is taken to be equal to its diameter. Since the rods are light and flexible in comparison to rock, the mass of the rods is neglected and the block is taken to be a rigid body. To account for the effect of surface irregularities on the bottom face of the rock, the energy of the rock is assumed to be focused on a smaller circular area rather than being distributed over the entire area of the block. Conceptually, there is a protrusion, referred to as a "punch", on the bottom of the block. The punch is a right circular cylinder that is coaxial with the block. The size of the punch is given by the focusing parameter, which is the ratio of the diameter of the punch to the diameter of the block.

The phrase "column of rods" means a vertical slice, taken parallel to the fuel rods, through a full stack of assemblies, with width equal to the rod pitch and length equal to the rod length.

Parameters that describe the falling blocks and exposure of assemblies

Density of rock blocks	Fall height	Number of assemblies in one stack	Focusing param. $0 < \text{focus} \leq 1$
$\text{density} = 2270 \cdot \frac{\text{kg}}{\text{m}^3}$	$\text{fallht} = 0.2032 \cdot \text{m}$	$n\text{stack} = \frac{21}{5}$	$\text{focus} = 0.6$
	Set hb to 0 for typical fuel, 1 for high-burnup fuel. 0 and 1 are the only valid values.		$hb = 0$

Read data from previous calculation and divide into vectors.

$\text{rodpack} = \text{READPRN}(\text{rod_engy.txt})$	Read data.
$rp = \text{rodpack}^{\langle 0 \rangle} \cdot \text{m}$	Rod pitch
$nrod = \text{rodpack}^{\langle 1 \rangle}$	Number of rods per side
$E\text{start} = \text{rodpack}^{\langle 2 + 3 \cdot hb \rangle} \cdot \text{joule}$	Energy to start breaking rods (for one column of rods)
$E\text{addl} = \text{rodpack}^{\langle 3 + 3 \cdot hb \rangle} \cdot \text{joule}$	Energy to break one additional rod
$z\text{start} = \text{rodpack}^{\langle 4 + 3 \cdot hb \rangle} \cdot \text{m}$	Displacement to start breaking rods
$rp\text{eff} = \text{rodpack}^{\langle 8 \rangle} \cdot \text{m}$	Effective rod pitch (block displacement to break one additional rod in a column of rods)
$n\text{disch} = \text{rodpack}^{\langle 9 \rangle}$	Number of assemblies discharged
$\text{rodlen} = \text{rodpack}^{\langle 10 \rangle} \cdot \text{m}$	Length of fuel rods
$\text{type} = \text{rodpack}^{\langle 11 \rangle}$	Assembly type

$n_{types} = \text{length}(\text{type})$ Number of types of assemblies

$$t_{rodtype} = \overline{(ndisch \cdot nrod^2)}$$

$totalrods = \sum t_{rodtype}$ $totalrods = 8.834 \cdot 10^6$ Total number of rods

$totallen = \sum \overline{(ndisch \cdot rodlen \cdot nrod^2)}$ $totallen = 3.405 \cdot 10^7 \cdot m$ Total length of all rods

Read information on block size distribution and divide into vectors.

$blocks = \text{READPRN}(esfblock_{txt})$ Read data

$cumprobmx = blocks^{<0>}$ Cumulative probability for block of given volume ...

$blkvolmx = blocks^{<1>} \cdot m^3$... and the corresponding block volume. "mx" indicates that these quantities are the maxima for the corresponding size interval.

$nsizes = \text{length}(blkvolmx) - 1$ Number of block size intervals

Calculate properties of typical block for each size interval

$isz = 0 .. nsizes - 1$

$blkvol_{isz} = \frac{blkvolmx_{isz} + blkvolmx_{isz+1}}{2}$ Mean block volume for each size interval

$prob_{isz} = cumprobmx_{isz-1} - cumprobmx_{isz}$ Probability that a block is in a given interval

Block mass, diameter, and area of one end, according to the cylindrical geometry, for each size interval

$blkmass = blkvol \cdot \text{density}$ $blkdiam = 2 \cdot \sqrt[3]{\frac{blkvol}{2 \cdot \pi}}$ $blkarea = \pi \cdot \frac{blkdiam^2}{4}$

$meanblkarea = blkarea \cdot prob$ Mean area of one block end

$meanblkarea = 0.244 \cdot m^2$

Calculate additional properties of different types of assemblies and impacts.

$rodspercol = nrod \cdot nstack$ Number of rods in one column

$nblocks = \frac{\overline{(ndisch \cdot rp \cdot rodlen \cdot nrod)}}{meanblkarea \cdot nstack}$ Number of blocks that fall on assemblies of a given type. Value is the total exposed area of all assemblies of that type divided by the mean block area.

$$itype = 0 .. ntypes - 1$$

$$cols_{isz, itype} = \frac{blkdiam_{isz}}{rp_{itype}} \cdot focus$$

$cols_{isz, itype}$ is the number of fuel rod columns struck by the punch.

For each size interval, calculate the number of breaks caused by blocks of that size. $brknum_{isz, itype}$ is the number of breaks that would be caused in assemblies of type $itype$ by one block in size interval isz . $Eavail$ is the energy available when rods start to break. g is gravity. The number of broken rods is calculated from the energy balance. Energy accumulated as block continues to fall is included. The number of broken rods is limited by the number of rods loaded by the block. The case $brkraw < 0$ arises if the block is so massive that its kinetic energy increases as it penetrates the assemblies.

Note that, for blocks with end areas smaller than the mean block area, the effect is to have incomplete coverage of the assemblies. Similarly, for blocks with end areas larger than the mean block area, the effect is to have overlapping blocks. In calculating the total number of breaks, however, perfect coverage is assured by multiplying $brknum_{isz, itype}$ by $prob_{isz}$, the probability that a given block is in the size interval isz .

$$brknum_{isz, itype} = \begin{cases} Eavail \leftarrow blkmass_{isz} \cdot g \cdot (fallht - zstart_{itype}) - cols_{isz, itype} \cdot Estart_{itype} \\ Eavail \leftarrow 0 \text{ if } Eavail < 0 \\ brkraw \leftarrow \frac{Eavail}{Eaddl_{itype} \cdot cols_{isz, itype} - rp_{eff_{itype}} \cdot blkmass_{isz} \cdot g} \cdot cols_{isz, itype} \\ brk \leftarrow brkraw \\ brk \leftarrow cols_{isz, itype} \cdot rodspercol_{itype} \text{ if } brkraw < 0 \\ brk \leftarrow cols_{isz, itype} \cdot rodspercol_{itype} \text{ if } brkraw > cols_{isz, itype} \cdot rodspercol_{itype} \\ brk \end{cases}$$

$$totalbreaks = prob \cdot (brknum \cdot nblocks)$$

Total number of breaks, summed over block size intervals and assembly types

$$totalbreaks = 6.33 \cdot 10^5$$

$$\frac{totalbreaks}{totalrods} = 7.165 \cdot 10^{-2}$$

Ratio of number of breaks to the number of rods. In the limit of few breaks, this ratio approaches the fraction of rods broken.

The mean length of the broken part of a rod is the area of the punch divided by $(focus \cdot blkdiam_{isz})$. The total length of the broken parts is then the mean length times the number of breaks as calculated below. The matrix multiplication and dot product in the left pair of square brackets below takes into account the number of blocks of each size.

$$totalbreaklen = \overrightarrow{(blkdiam \cdot prob)} \cdot (brknum \cdot nblocks) \cdot \frac{\pi}{4} \cdot focus$$

$$totalbreaklen = 2.637 \cdot 10^5 \cdot m \quad \text{Total length of broken parts, summed over block size intervals}$$

$$\frac{totalbreaklen}{totallen} = 7.744 \cdot 10^{-3} \quad \text{Fraction of total rod length that is broken}$$

Determine whether the geometry of the punch is reasonable. Calculate the ratio of the depth of penetration to the width of the punch. Extremely large ratios are unrealistic.

$$penete_{isz, itype} = zstart_{itype} \quad \text{"Elastic" penetration of block into assembly. (Actually, this is the displacement to initiate failure. Part of this displacement involves plastic deformation.)}$$

$$penetp_{isz, itype} = \frac{brknum_{isz, itype}}{cols_{isz, itype}} \cdot rp_{eff_{itype}} \quad \text{"Plastic" penetration of block into assembly. (Actually, this is the additional penetration attributable to rod breakage.)}$$

$$totalpenetp = prob \cdot (penetp \cdot nblocks) \quad \text{Total amount of "plastic" penetration for all blocks.}$$

$$sign_{isz, itype} = (brknum_{isz, itype} > 0) \quad \text{sign is 1 if rod failures occur, 0 otherwise.}$$

For each block that causes some rods to fail, calculate the width of the punch, that is, the portion of the block that causes rod failure. Add up punch widths for all combinations that cause failure.

$$totalpunchwidth = \overrightarrow{(prob \cdot blkdiam)} \cdot (sign \cdot nblocks) \cdot focus$$

$$\frac{totalpenetp}{totalpunchwidth} = 2.027 \cdot 10^{-2} \quad \text{Ratio of total punch penetration to total punch width.}$$

Calculate the fraction of rods that are broken.

$$brkdep_{isz, itype} = \frac{brknum_{isz, itype}}{cols_{isz, itype}} \quad \text{Depth of penetration of a block, measured in rod layers. Note that the definition of } brknum \text{ keeps } brkdep \text{ from being larger than } rodspercol.$$

$$rodsperlayer_{itype} = \frac{itrodtype_{itype}}{rodspercol_{itype}} \quad \text{Number of rods per layer for assemblies of type } itype. \text{ Note that this quantity is proportional to the number of assemblies discharged.}$$

Find the fraction of rods broken in a given layer for assemblies of type itype if that layer were to be penetrated by a block of size isz. Note that $nblocks_{isz,itype} \cdot prob_{isz}$ is the number of blocks of size isz that strike assemblies of type itype. That is multiplied by $\frac{cols_{isz,itype}}{rodsperlayer_{itype}}$ to find the number of rods in the layer that would be broken by such blocks. Finally, that number of rods is divided by the number of rods per layer ($rodsperlayer_{itype}$) to find the fraction of rods broken in a given layer. The ratio of number of breaks to number of rods is approximately the fraction of rods broken because $prob_{isz}$ keeps the ratio small; for large ratios the effect of multiple breaks per rod would have to be considered.

$$fbrkst_{isz,itype} = \frac{cols_{isz,itype} \cdot nblocks_{isz,itype} \cdot prob_{isz}}{rodsperlayer_{itype}}$$

$$nbrk(il, is, it) = \begin{cases} 0 & \text{if } brkdep_{is, it} \leq il \\ 1 & \text{if } brkdep_{is, it} > il + 1 \\ brkdep_{is, it} - il & \text{otherwise} \end{cases}$$

Fraction of layer il penetrated by a block of size is that impacts on assemblies of type it. The top layer is layer 0.

$$ilr := 0 .. \max(\overrightarrow{\text{floor}(rodspercol)})$$

Range variable ilr indexes the layers of rods.

$$fbrklt_{ilr,itype} = 1 - \prod_{isz} (1 - nbrk(ilr, isz, itype) \cdot fbrkst_{isz,itype})$$

The quantity in parentheses gives the fraction of rods left intact by blocks of a given size. The continued product gives the fraction left intact by rocks of all sizes. That is subtracted from 1 to give the fraction of rods broken in layer ilr for assemblies of type itype.

$$totalbrkrod = \sum(fbrklt \cdot rodsperlayer)$$

Sum over layers and assembly types to find total number of broken rods.

$$\frac{totalbrkrod}{totalrods} = 0.035$$

Save results to file.

$$block_0 = \frac{totalbreaks}{totalrods}$$

$$block_3 = \frac{totalpenetp}{totalpunchwidth}$$

$$block_1 = \frac{totalbreaklen}{totalen}$$

$$block_4 = focus$$

$$block_2 = \frac{totalbrkrod}{totalrods}$$

$$block_5 = hb$$

$$APPENDPRN(cirpunch_{txt}) = block^T$$

0 0

0.00138504155124654 0.000114999421059037
0.00277008310249307 0.000131675896136871
0.00415512465373961 0.000142309574559068
0.00554016620498615 0.000178761284919559
0.00692520775623269 0.000318803350965692
0.00831024930747922 0.000319464346704939
0.00969529085872576 0.000333333354044515
0.0110803324099723 0.000453916080030112
0.0124653739612188 0.000503120572138868
0.0138504155124654 0.000513356605792875
0.0152354570637119 0.00052145033162409
0.0166204986149584 0.000535435416050036
0.018005540166205 0.000734010809730278
0.0193905817174515 0.000762758358036664
0.0207756232686981 0.00077402735300298
0.0221606648199446 0.000799585747572491
0.0235457063711911 0.000887102242013286
0.0249307479224377 0.000950372780165557
0.0263157894736842 0.000958996813489842
0.0277008310249307 0.0010019525548505
0.0290858725761773 0.00100197809386293
0.0304709141274238 0.00100355864632541
0.0318559556786704 0.00104371843749361
0.0332409972299169 0.00108881967013501
0.0346260387811634 0.0012183722123013
0.03601108033241 0.00126855755505663
0.0373961218836565 0.00128998808923012
0.038781183434903 0.00130976605639919
0.0401662049861496 0.00136724866371401
0.0415512465373961 0.00140376190626336
0.0429362880886427 0.00140556213304528
0.0443213296398892 0.00141548981429037
0.0457063711911357 0.00158105538562106
0.0470914127423823 0.00161728062747496
0.0484764542936288 0.00162732786528373
0.0498614958448753 0.00166585378351434
0.0512465373961219 0.00166629430200277
0.0526315789473684 0.00168192116611494
0.054016620498615 0.00169696063365595
0.0554016620498615 0.00173727117484834
0.056786703601108 0.00174600425359551
0.0581717451523546 0.00182599696461532
0.0595567867036011 0.00195589847907995
0.0609418282548476 0.00202468045721514
0.0623268698060942 0.00206105508891049
0.0637119113573407 0.00206845253528645
0.0650969529085873 0.00209179427746463
0.0664819944598338 0.00211957045317393
0.0678670360110803 0.0022347995986109
0.0692520775623269 0.00228832904471846
0.0706371191135734 0.00228900356779724
0.07202216066482 0.00232653236206923
0.0734072022160665 0.00262332825525554
0.074792243767313 0.00262652201358443
0.0761772853185596 0.00262656938820112
0.0775623268698061 0.00271145903592448

0.0789473664210526 0.00273115141964354
0.0803324099722992 0.00273994830664085
0.0817174515235457 0.00280790799101263
0.0831024930747922 0.00283613389190844
0.0844875346260388 0.00292000682846573
0.0858725761772853 0.00308430216331708
0.0872576177285319 0.00333059858237589
0.0886426592797784 0.00333654180950161
0.0900277008310249 0.00337104039839142
0.0914127423822715 0.00339453769703641
0.092797783933518 0.00345497483353667
0.0941828254847645 0.00346350488877055
0.0955678670360111 0.00348420816748529
0.0969529085872576 0.00349968199822103
0.0983379501385042 0.00351533000709272
0.0997229916897507 0.00354849588563773
0.101108033240997 0.00358031152110172
0.102493074792244 0.003717654885026
0.10387811634349 0.0037817804836928
0.105263157894737 0.00388999099960405
0.106648199445983 0.00392247573388801
0.10803324099723 0.00393235772353737
0.109418282548476 0.00407195509715618
0.110803324099723 0.0041008577214262
0.11218836565097 0.00416403950388099
0.113573407202216 0.00417316486260923
0.114958448753463 0.0042140305097781
0.116343490304709 0.00434170590249797
0.117728531855956 0.00465734919039458
0.119113573407202 0.00473812725370407
0.120498614958449 0.0047393194612641
0.121883656509695 0.00474302538966539
0.123268698060942 0.00475014714134911
0.124653739612188 0.00475463711162463
0.126038781163435 0.00481831501660118
0.127423822714681 0.00482905156412655
0.128808864265928 0.00486202093044201
0.130193905817175 0.00488958110548944
0.131578947368421 0.00490255408816913
0.132963988919668 0.00496725869300948
0.134349030470914 0.0054552064378129
0.135734072022161 0.00545860759719522
0.137119113573407 0.0055407169266032
0.138504155124654 0.00557771379435766
0.1398891966759 0.00558530640489352
0.141274238227147 0.00571970338333339
0.142659279778393 0.00578820430321202
0.14404432132964 0.00591302440546754
0.145429362880886 0.00608786829745778
0.146814404432133 0.00627379439618846
0.14819944598338 0.00642500728110102
0.149584487534626 0.00650981969168216
0.150969529085873 0.00651349173288533
0.152354570637119 0.00651671061602866
0.153739612188366 0.00663378815877138
0.155124653739612 0.00669557504627578
0.156509695290859 0.00686769560079947

0.157894736842105 0.0068742741915877
0.159279778393352 0.00693906674278239
0.160664819944598 0.00696967050277418
0.162049861495845 0.0070294319641644
0.163434903047091 0.00706750098519972
0.164819944598338 0.00711792615634405
0.166204986149584 0.00715559211065109
0.167590027700831 0.00715559211065109
0.168975069252078 0.00715559211065109
0.170360110803324 0.0071801784610858
0.171745152354571 0.00739409284476395
0.173130193905817 0.00783990984779558
0.174515235457064 0.00786600279572446
0.17590027700831 0.00789153266888058
0.177285318559557 0.00789564567180414
0.178670360110803 0.00791643090861281
0.18005540166205 0.00793112161358413
0.181440443213296 0.00794062893327858
0.182825484764543 0.00794435349939586
0.184210526315789 0.00797458326053113
0.185595567867036 0.00797594877652952
0.186980609418283 0.00798718636291141
0.188365650969529 0.00800979237132532
0.189750692520776 0.00804866943574872
0.191135734072022 0.00805995675484683
0.192520775623269 0.00806826514397179
0.193905817174515 0.00807489321726801
0.195290858725762 0.00809254733405053
0.196675900277008 0.00810857645418299
0.198060941828255 0.00812852848717709
0.199445983379501 0.00813206711615024
0.200831024930748 0.00814987853601346
0.202216066481994 0.00815856519361512
0.203601108033241 0.00816512712194701
0.204986149584488 0.00821184764646968
0.206371191135734 0.00829810653912593
0.207756232686981 0.00886134686754205
0.209141274238227 0.00895754730238319
0.210526315789474 0.00906727841336053
0.21191135734072 0.00916194531377251
0.213296398891967 0.00917002082507523
0.214681440443213 0.00918889027849393
0.21606648199446 0.00923257751346726
0.217451523545706 0.00923854519397009
0.218836565096953 0.00932751222792229
0.220221606648199 0.00936518357014878
0.221606648199446 0.0093664278105157
0.222991689750693 0.00938151620367617
0.224376731301939 0.00938995856456706
0.225761772853186 0.00944747348573073
0.227146814404432 0.00947015619112863
0.228531855955679 0.00954904885848225
0.229916897506925 0.00981397832991427
0.231301939058172 0.0100558494947119
0.232686980609418 0.0101357390893545
0.234072022160665 0.0101653717718896
0.235457063711911 0.0105430313133474

0.236842105263158 0.0105562282731015
0.238227146814404 0.0105857133841917
0.239612188365651 0.0105877795893053
0.240997229916898 0.0106081623125935
0.242382271468144 0.0106282279070628
0.243767313019391 0.0107416432424394
0.245152354570637 0.0107567658510651
0.246537396121884 0.0109242161782988
0.24792243767313 0.0115538935420407
0.249307479224377 0.0115829555283719
0.250692520775623 0.0116027982464401
0.25207756232687 0.0117099581284481
0.253462603878116 0.0117491326022169
0.254847645429363 0.0119290103811436
0.256232686980609 0.0119753813256733
0.257617728531856 0.0119995030594052
0.259002770083103 0.0120840540209734
0.260387811634349 0.0121368702050861
0.261772853185596 0.0121596511465884
0.263157894736842 0.0121789176225404
0.264542936288089 0.0122302750230803
0.265927977839335 0.0122823718228009
0.267313019390582 0.0124207564008378
0.268698060941828 0.0124482561713229
0.270083102493075 0.0125737968672395
0.271468144044321 0.0125965690359041
0.272853185595568 0.0126172472312206
0.274238227146814 0.012617261295029
0.275623268698061 0.0126179121329396
0.277008310249307 0.0128346637050999
0.278393351800554 0.013038105481737
0.279778393351801 0.0138025277259329
0.281163434903047 0.0139175319058959
0.282548476454294 0.0139264358149126
0.28393351800554 0.0153211172329006
0.285318559556787 0.0154846730829868
0.286703601108033 0.0155191122896542
0.28808864265928 0.0156106683181704
0.289473684210526 0.0156272846789537
0.290858725761773 0.0156814025853009
0.292243767313019 0.0157743802479064
0.293628808864266 0.0160580808146382
0.295013850415512 0.0162145755383258
0.296398891966759 0.01634928754868
0.297783933518006 0.0165969638803019
0.299168975069252 0.0167971671734051
0.300554016620499 0.0168482002828696
0.301939058171745 0.0171772582503322
0.303324099722992 0.017327134075404
0.304709141274238 0.017385300115793
0.306094182825485 0.0175068844548297
0.307479224376731 0.0177114654513085
0.308864265927978 0.0179152737286525
0.310249307479224 0.0180543426768143
0.311634349030471 0.0184209786284855
0.313019390581717 0.0184828728196535
0.314404432132964 0.018870883813111

0.315789473684211 0.0191665602589609
0.317174515235457 0.0191678335915669
0.318559556786704 0.019177178686465
0.31994459833795 0.0193869423085704
0.321329639889197 0.0195952423986775
0.322714681440443 0.0196871255685655
0.32409972299169 0.0197557302313883
0.325484764542936 0.0198311555631473
0.326869806094183 0.0199146049192518
0.328254847645429 0.0199153178952498
0.329639889196676 0.0199371160097284
0.331024930747922 0.0200828382375316
0.332409972299169 0.0201047116696712
0.333795013850415 0.0201721271596575
0.335180055401662 0.0204833465721652
0.336565096952909 0.0209691912741569
0.337950138504155 0.0210067647561823
0.339335180055402 0.0213404296631369
0.340720221606648 0.0213435185851687
0.342105263157895 0.0214307545223669
0.343490304709141 0.0217104761809283
0.344875346260388 0.0217774830159638
0.346260387811634 0.0217893232339119
0.347645429362881 0.0217920309920532
0.349030470914127 0.0219722037047091
0.350415512465374 0.0219796954359354
0.351800554016621 0.0220313528074556
0.353185595567867 0.0221477745831036
0.354570637119114 0.0221870521549508
0.35595567867036 0.0221998948585182
0.357340720221607 0.0222806969554976
0.358725761772853 0.0225936990038979
0.3601108033241 0.0236321142028785
0.361495844875346 0.0237302822685489
0.362880886426593 0.0237970197332702
0.364265927977839 0.0237996775095101
0.365650969529086 0.0238411197064651
0.367036011080332 0.023896461032158
0.368421052631579 0.0240469197289852
0.369806094182826 0.0243194784340758
0.371191135734072 0.0250642224720026
0.372576177285319 0.0255007615797544
0.373961218836565 0.0261037496589134
0.375346260387812 0.026173488854978
0.376731301939058 0.0262673550889013
0.378116343490305 0.0264379056124973
0.379501385041551 0.0265268032294171
0.380886426592798 0.0266421260649999
0.382271468144044 0.0267149833710618
0.383656509695291 0.0267232544174444
0.385041551246537 0.0268068331690608
0.386426592797784 0.0268231204246769
0.38781163434903 0.0269715618074748
0.389196675900277 0.0270164825661651
0.390581717451524 0.0271206853728484
0.39196675900277 0.0271244263333667
0.393351800554017 0.027145031024788

0.394736842105263 0.0271482125858278
0.39612188365651 0.0275600335509055
0.397506925207756 0.0278829225236013
0.398891966759003 0.0296065957298163
0.400277008310249 0.0296663371155234
0.401662049861496 0.0298278075234597
0.403047091412742 0.0301355365634032
0.404432132963989 0.0308444391210869
0.405817174515235 0.0311763129659321
0.407202216066482 0.0312151048019536
0.408587257617729 0.0312303178410875
0.409972299168975 0.0315141137163644
0.411357340720222 0.0315775903604863
0.412742382271468 0.0319053862080925
0.414127423822715 0.032500551216919
0.415512465373961 0.0327677529659217
0.416897506925208 0.0329349100857295
0.418282548476454 0.0329594423624633
0.419667590027701 0.0331805234835024
0.421052631578947 0.0332717583256643
0.422437673130194 0.0350359512510219
0.42382271468144 0.0350667301070001
0.425207756232687 0.0351774562523797
0.426592797783933 0.0352423005747002
0.42797783933518 0.0353601630308714
0.429362880886427 0.0354148064180448
0.430747922437673 0.0354458685509262
0.43213296398892 0.0355970533645732
0.433518005540166 0.0356288016729613
0.434903047091413 0.035731090678765
0.436288088642659 0.0360467321945647
0.437673130193906 0.0365787710490582
0.439058171745152 0.036593552538733
0.440443213296399 0.0367098515290671
0.441828254847645 0.0368571052871614
0.443213296398892 0.0371176093787568
0.444598337950138 0.0374589111158615
0.445983379501385 0.0374632078063153
0.447368421052632 0.037533157426916
0.448753462603878 0.0376736834967061
0.450138504155125 0.0385722225857519
0.451523545706371 0.0386017147890897
0.452908587257618 0.0389032071764119
0.454293628808864 0.0389769268131491
0.455678670360111 0.0389913679614359
0.457063711911357 0.0390540983511519
0.458448753462604 0.0391247424044985
0.45983379501385 0.039276149272148
0.461218836565097 0.0394641051172596
0.462603878116344 0.0396433502624272
0.46398891966759 0.0396952618437833
0.465373961218837 0.0397598296293747
0.466759002770083 0.0398020430372837
0.46814404432133 0.0406856473421089
0.469529085872576 0.0407432607101458
0.470914127423823 0.0411468653102383
0.472299168975069 0.0425138344014021

0.473684210526316 0.0427630548868903
0.475069252077562 0.0427667369156194
0.476454293628809 0.0429730066714146
0.477839335180055 0.0430263204992496
0.479224376731302 0.0431248861579575
0.480609418282548 0.0432032424241309
0.481994459833795 0.0437223361941608
0.483379501385042 0.0445727052320131
0.484764542936288 0.0449053630045091
0.486149584487535 0.046382901218915
0.487534626038781 0.0467120281330468
0.488919667590028 0.0469962790995113
0.490304709141274 0.0478995125265356
0.491689750692521 0.0483186423072748
0.493074792243767 0.0488750158005835
0.494459833795014 0.0498342927369648
0.49584487534626 0.0506375525505863
0.497229916897507 0.0514815370697564
0.498614958448753 0.0532252978113975
0.5 0.0554036348860418
0.501385041551247 0.0568857763422888
0.502770083102493 0.0586695462283463
0.50415512465374 0.0623344063297702
0.505540166204986 0.0630732568919429
0.506925207756233 0.0636747396464778
0.508310249307479 0.0638436207476336
0.509695290858726 0.063916802783662
0.511080332409972 0.0641557652492768
0.512465373961219 0.064275296548991
0.513850415512465 0.0652697008873424
0.515235457063712 0.0672780048480539
0.516620498614958 0.0676150735531693
0.518005540166205 0.0682660055738122
0.519390581717452 0.0689734193097924
0.520775623288898 0.0694177049375436
0.522160664819945 0.0695606223478449
0.523545706371191 0.0696213118295224
0.524930747922438 0.0730993313466152
0.526315789473684 0.0732395319781015
0.527700831024931 0.0732710083906823
0.529085872576177 0.07341641560709
0.530470914127424 0.0738282585252923
0.53185595567867 0.0751910880123701
0.533240997229917 0.0763519551178617
0.534626038781163 0.0779232004881504
0.53601108033241 0.0785907375440735
0.537396121883656 0.0786538799573131
0.538781163434903 0.0793082243672481
0.54016620498615 0.0807432864418101
0.541551246537396 0.0811502295846153
0.542936288088643 0.0813898546478108
0.544321329639889 0.081999767850041
0.545706371191136 0.0823065197687619
0.547091412742382 0.0828509990394302
0.548476454293629 0.0835996584061801
0.549861495844875 0.0839629380169251
0.551246537396122 0.0846606201850687

0.552631578947368 0.0848541892146415
0.554016620498615 0.0849658844408878
0.555401662049862 0.0860622813500918
0.556786703601108 0.0874758014859779
0.558171745152355 0.0878957648302783
0.559556786703601 0.0902389727185094
0.560941828254848 0.0903334030486365
0.562326869806094 0.090694131650659
0.563711911357341 0.0911423758555942
0.565096952908587 0.0911931138628853
0.566481994459834 0.0929267460846997
0.56786703601108 0.0941914399114911
0.569252077562327 0.0948767210518491
0.570637119113573 0.0967184609865235
0.57202216066482 0.098050290087725
0.573407202216066 0.0992343878804646
0.574792243767313 0.099375567933841
0.57617728531856 0.0994421162987991
0.577562326869806 0.101992402014143
0.578947368421053 0.102996633994767
0.580332409972299 0.103342685157319
0.581717451523548 0.105926390965257
0.583102493074792 0.107668063558554
0.584487534626039 0.108579444372108
0.585872576177285 0.109218209835344
0.587257617728532 0.109290292104695
0.588642659279778 0.111263832478177
0.590027700831025 0.11206965352434
0.591412742382271 0.112873942164232
0.592797783933518 0.113363923690545
0.594182825484765 0.114703816401364
0.595567867036011 0.11630275727866
0.596952908587258 0.117217639529775
0.598337950138504 0.117658303204026
0.599722991689751 0.118041292776948
0.601108033240997 0.11812963850137
0.602493074792244 0.121649084617747
0.60387811634349 0.124561664619389
0.605263157894737 0.125258107722927
0.606648199445983 0.125732945831782
0.60803324099723 0.127545515152907
0.609418282548476 0.128233799672752
0.610803324099723 0.128295906508229
0.61218836565097 0.132824535535835
0.613573407202216 0.134475704937367
0.614958448753463 0.137214171720813
0.616343490304709 0.142477306601412
0.617728531855956 0.145829112764149
0.619113573407202 0.146273234156092
0.620498614958449 0.146293507022186
0.621883656509695 0.148305674565173
0.623288698060942 0.149574048466197
0.624653739612188 0.150804536234431
0.626038781163435 0.151300582136276
0.627423822714681 0.151711738443786
0.628808864265928 0.154060190258387
0.630193905817174 0.158098094719768

0.631578947368421 0.160042978892569
0.632963988919668 0.163193439996557
0.634349030470914 0.164399937752205
0.635734072022161 0.16601490612172
0.637119113573407 0.173005721955396
0.638504155124654 0.173449438304736
0.6398891966759 0.173621257065133
0.641274238227147 0.178074206987566
0.642659279778393 0.180055013697704
0.64404432132964 0.181962962962963
0.645429362880886 0.182921699718598
0.646814404432133 0.184166286421628
0.64819944598338 0.184869167822541
0.649584487534626 0.190349812897498
0.650969529085873 0.191896050085188
0.652354570637119 0.193837031225804
0.653739612188366 0.205995439033756
0.655124653739612 0.211281707044248
0.656509695290859 0.211698417719954
0.657894736842105 0.214847407700166
0.659279778393352 0.22008522648626
0.660664819944598 0.223102179628447
0.662049861495845 0.225592981463046
0.663434903047091 0.227077501415213
0.664819944598338 0.234014445163446
0.666204986149584 0.240973296215981
0.667590027700831 0.241483077422636
0.668975069252078 0.243887334475689
0.670360110803324 0.251683549396776
0.671745152354571 0.25255589824255
0.673130193905817 0.258685188443567
0.674515235457064 0.260227013560148
0.67590027700831 0.267832062788717
0.677285318559557 0.26878845441549
0.678670360110803 0.273994632665176
0.68005540166205 0.27670894844235
0.681440443213296 0.281527744403789
0.682825484764543 0.282998301852585
0.684210526315789 0.289936007532859
0.685595567867036 0.291909747431882
0.686980609418283 0.293442808200495
0.688365650969529 0.294844571506781
0.689750692520776 0.298196783112078
0.691135734072022 0.302651206986008
0.692520775623269 0.303585612100664
0.693905817174515 0.303626214186328
0.695290858725762 0.304222948533346
0.696675900277008 0.305488312737728
0.698060941828255 0.306790760269199
0.699445983379501 0.30720390392028
0.700831024930748 0.307350982463033
0.702216066481994 0.307379047574025
0.703601108033241 0.307962907616681
0.704986149584488 0.308792000000001
0.706371191135734 0.311651471348549
0.707756232686981 0.311688653480748
0.709141274238227 0.311918434042553

0.710526315789474 0.314640597040555
0.71191135734072 0.316470846132381
0.713296398891967 0.316888526523695
0.714681440443213 0.317031467620171
0.71606648199446 0.317582094420481
0.717451523545706 0.318000929102523
0.718836565096953 0.318062972770232
0.720221606648199 0.320944181502047
0.721606648199446 0.320944181502047
0.722991689750693 0.3229006
0.724376731301939 0.323242816316696
0.725761772853186 0.323816022338955
0.727146814404432 0.324473340112719
0.728531855955679 0.324524267284154
0.729916897506925 0.324731847270831
0.731301939058172 0.324990421558199
0.732686980609418 0.32512262405891
0.734072022160665 0.325444927774307
0.735457063711911 0.328398812589456
0.736842105263158 0.329534711269344
0.738227146814404 0.331800331575333
0.739612188365651 0.33292192379679
0.740997229916898 0.333639523617589
0.742382271468144 0.336295598119049
0.743767313019391 0.336837491685788
0.745152354570637 0.337812177101442
0.746537396121884 0.338000779974533
0.74792243767313 0.340250958980831
0.749307479224377 0.340431045364164
0.750692520775623 0.340872330753251
0.75207756232687 0.340971098427775
0.753462603878116 0.34289329177787
0.754847645429363 0.343835355817805
0.756232686980609 0.344529094036397
0.757617728531856 0.344719115324949
0.759002770083102 0.346198460921271
0.760387811634349 0.34671698720244
0.761772853185596 0.3471248
0.763157894736842 0.349355496122857
0.764542936288089 0.349979370212766
0.765927977839335 0.350342623977292
0.767313019390582 0.351330218959921
0.768698060941828 0.351587832838321
0.770083102493075 0.352935848888322
0.771468144044321 0.354255223737939
0.772853185595568 0.355700280149322
0.774238227146814 0.359266965674997
0.775623268698061 0.360422189413126
0.777008310249307 0.360823250096751
0.778393351800554 0.361304819512195
0.779778393351801 0.361576863199174
0.781163434903047 0.361706772889641
0.782548476454294 0.362074606300894
0.78393351800554 0.363278231539762
0.785318559556787 0.365188395200556
0.786703601108033 0.365748146846599
0.78808864265928 0.365890573545114

0.789473684210526 0.367044692384538
0.790858725761773 0.368057324557576
0.792243767313019 0.368370561694292
0.793628808864266 0.368767655364822
0.795013850415512 0.371156340132808
0.796398891966759 0.371277117244023
0.797783933518006 0.371547234042553
0.799168975069252 0.372192366568913
0.800554016620499 0.373323577856426
0.801939058171745 0.375586751244874
0.803324099722992 0.378558073321187
0.804709141274238 0.378787314232761
0.806094182825485 0.380891984956549
0.807479224376731 0.380978191892598
0.808864265927978 0.381285210574994
0.810249307479224 0.384175272690278
0.811634349030471 0.384307126436783
0.813019390581717 0.386234535915427
0.814404432132964 0.387294380000252
0.815789473684211 0.391641316403325
0.817174515235457 0.391931596347
0.818559556786704 0.392167761164968
0.81994459833795 0.395189546417568
0.821329639889197 0.396068430659313
0.822714681440443 0.397919480275504
0.82409972299169 0.398900966052185
0.825484764542936 0.399367685614048
0.826869806094183 0.40112841754158
0.828254847645429 0.402136054427097
0.829639889196676 0.403224756290254
0.831024930747922 0.405068407209685
0.832409972299169 0.405513451095548
0.833795013850416 0.405839970334274
0.835180055401662 0.406513286337492
0.836565096952909 0.407403688446559
0.837950138504155 0.40858233910074
0.839335180055402 0.409536225081503
0.840720221606648 0.411340964833639
0.842105263157895 0.411572985621112
0.843490304709141 0.411637787062756
0.844875346260388 0.411722666666667
0.846260387811634 0.412255368692831
0.847645429362881 0.413506111441058
0.849030470914127 0.413561905979298
0.850415512465374 0.415942827236355
0.85180055401662 0.416762367031905
0.853185595567867 0.417314971181317
0.854570637119114 0.420095762992708
0.85595567867036 0.420563581164885
0.857340720221607 0.420719948349829
0.858725761772853 0.421587941793371
0.8601108033241 0.421924731652874
0.861495844875346 0.423089776727187
0.862880886426593 0.423487836660642
0.864265927977839 0.428438971959166
0.865650969529086 0.429112460978148
0.867036011080332 0.432351392821662

0.868421052631579 0.433827559265546
0.869806094182826 0.435688469345884
0.871191135734072 0.436935842699383
0.872576177285319 0.438582513276254
0.873961218836565 0.439749096228347
0.875346260387812 0.442439788492981
0.876731301939058 0.448077235294117
0.878116343490305 0.449669956995063
0.879501385041551 0.449950933703768
0.880886426592798 0.450021124458309
0.882271468144044 0.454431013599825
0.883656509695291 0.455144300734962
0.885041551246537 0.457725672879802
0.886426592797784 0.457898159982818
0.88781163434903 0.459883791059343
0.889196675900277 0.461083909262006
0.890581717451524 0.465533342975991
0.89196675900277 0.469093580982587
0.893351800554017 0.469928761912549
0.894736842105263 0.473856209150326
0.89612188365651 0.480068899498091
0.897506925207756 0.483453822422671
0.898891966759003 0.495865719759476
0.900277008310249 0.5002624
0.901662049861496 0.5029728
0.903047091412742 0.505343685848887
0.904432132963989 0.511201365506468
0.905817174515235 0.51144206900018
0.907202216066482 0.511523166736915
0.908587257617729 0.511568921742288
0.909972299168975 0.517241081436461
0.911357340720222 0.517419786046159
0.912742382271468 0.517545417256444
0.914127423822715 0.52163557373176
0.915512465373961 0.523788517278688
0.916897508925208 0.5260112
0.918282548476454 0.527568512754605
0.919667590027701 0.530402981232842
0.921052631578947 0.539270679511981
0.922437673130194 0.541066731567432
0.92382271468144 0.543767168262705
0.925207756232687 0.545161920613947
0.926592797783934 0.551471221220097
0.92797783933518 0.551568127972044
0.929362880886427 0.551705373902752
0.930747922437673 0.555118675014979
0.93213296398892 0.568084264632866
0.933518005540166 0.573713187808806
0.934903047091413 0.582921095124158
0.936288088642659 0.584923474794016
0.937673130193906 0.585033538191106
0.939058171745152 0.586172722829705
0.940443213296399 0.595255794056659
0.941828254847645 0.595853148758659
0.943213296398892 0.599918794295875
0.944598337950138 0.601843478260869
0.945983379501385 0.605443918358817

0.947368421052632 0.610298963537123
0.948753462603878 0.615709452077224
0.950138504155125 0.625893405776052
0.951523545708371 0.638218405299389
0.952908587257618 0.638944865303884
0.954293628808864 0.642989866180614
0.955678670360111 0.647578941910446
0.957063711911357 0.651260284917703
0.958448753462604 0.670218945354933
0.95983379501385 0.672217758463414
0.961218838565097 0.678325386510451
0.962603878116344 0.678537184677391
0.96398891966759 0.678742795525097
0.965373961218837 0.678810000000002
0.966759002770083 0.693768727114836
0.96814404432133 0.7139253033606
0.969529085872576 0.726512777365209
0.970914127423823 0.727613934856836
0.972299168975069 0.727787893536433
0.973684210526316 0.749966120620113
0.975069252077562 0.764946623589748
0.976454293628809 0.786005568381811
0.977839335180055 0.786313846153848
0.979224376731302 0.789850036355122
0.980609418282548 0.800423467254801
0.981994459833795 0.809330162718227
0.983379501385042 0.814425448859412
0.984764542936288 0.834093333333333
0.986149584487535 0.834539531612037
0.987534626038781 0.834645043160017
0.988919667590028 0.854657265408474
0.990304709141274 0.860821416247358
0.991689750692521 0.861267171635853
0.993074792243767 0.904516584446829
0.994459833795014 1.1680615208617
0.99584487534626 1.17578974117647
0.997229916897507 1.20783235873209
0.998614958448753 1.27940950331548
1 1.27988305874478

	A	B	C	D	E	F	G	H	I	J	K	L
1	Cylindrical rocks with circular punch											
2	Number of breaks			Fraction of			Fraction of			Focus- ing param.	Punch aspect ratio	
3	per rod			rods broken			fuel exposed				typical	hi-burn
4	typical	hi-burn	95% typ. + 5% hi-burn	typical	hi-burn	95% typ. + 5% hi-burn	typical	hi-burn	95% typ. + 5% hi-burn		typical	hi-burn
5	3.25E-02	6.15E-01	0.0616	1.42E-02	1.80E-01	0.0225	6.02E-03	1.06E-01	0.0110	1	0.0062	0.0454
6	3.86E-02	6.45E-01	0.0689	1.75E-02	2.05E-01	0.0268	6.43E-03	9.97E-02	0.0111	0.9	0.0080	0.0580
7	4.63E-02	6.83E-01	0.0782	2.17E-02	2.38E-01	0.0325	6.83E-03	9.41E-02	0.0112	0.8	0.0100	0.0787
8	5.68E-02	7.34E-01	0.0906	2.73E-02	2.83E-01	0.0401	7.25E-03	8.86E-02	0.0113	0.7	0.0132	0.1084
9	7.00E-02	8.07E-01	0.1069	3.45E-02	3.48E-01	0.0501	7.59E-03	8.39E-02	0.0114	0.6	0.0199	0.1562
10	8.53E-02	9.06E-01	0.1263	4.41E-02	4.34E-01	0.0636	7.62E-03	7.85E-02	0.0112	0.5	0.0332	0.2475
11	1.03E-01	1.04E+00	0.1500	5.76E-02	5.49E-01	0.0822	7.31E-03	7.16E-02	0.0105	0.4	0.0594	0.4400
12	1.28E-01	1.14E+00	0.1771	7.84E-02	6.48E-01	0.1089	6.87E-03	5.76E-02	0.0092	0.3	0.1215	0.8682
13	1.65E-01	9.98E-01	0.2066	1.17E-01	6.28E-01	0.1429	5.78E-03	3.23E-02	0.0071	0.2	0.3292	1.766
14	2.68E-01	5.93E-01	0.2845	2.23E-01	4.47E-01	0.2341	4.84E-03	9.02E-03	0.0049	0.1	1.918	4.616

	A	B	C	D	E	F	G	H	I	J	K	L
15	Cylindrical rocks with linear punch parallel to rods											
16	Number of breaks per rod			Fraction of rods broken			Fraction of fuel exposed			Focusing param.		
17	typical	hi-burn	95% typ. + 5% hi-burn	typical	hi-burn	95% typ. + 5% hi-burn	typical	hi-burn	95% typ. + 5% hi-burn			
18	3.25E-02	6.15E-01	0.0616	1.42E-02	1.80E-01	0.0225	6.02E-03	1.06E-01	0.0110			
19	3.86E-02	6.45E-01	0.0689	1.75E-02	2.05E-01	0.0268	7.64E-03	1.18E-01	0.0132			0.9
20	4.83E-02	6.83E-01	0.0782	2.17E-02	2.38E-01	0.0325	9.56E-03	1.32E-01	0.0157			0.8
21	5.68E-02	7.34E-01	0.0906	2.73E-02	2.83E-01	0.0401	1.20E-02	1.47E-01	0.0188			0.7
22	7.00E-02	8.07E-01	0.1069	3.45E-02	3.48E-01	0.0501	1.51E-02	1.87E-01	0.0227			0.6
23	8.53E-02	9.06E-01	0.1263	4.41E-02	4.34E-01	0.0636	1.86E-02	1.91E-01	0.0272			0.5
24	1.03E-01	1.04E+00	0.1500	5.76E-02	5.49E-01	0.0822	2.26E-02	2.22E-01	0.0326			0.4
25	1.26E-01	1.14E+00	0.1771	7.84E-02	6.48E-01	0.1069	2.79E-02	2.41E-01	0.0385			0.3
26	1.65E-01	9.98E-01	0.2066	1.17E-01	6.28E-01	0.1429	3.66E-02	2.05E-01	0.0450			0.2
27	2.68E-01	5.93E-01	0.2845	2.23E-01	4.47E-01	0.2341	5.90E-02	1.15E-01	0.0618			0.1
28	Cylindrical rocks with linear punch at 22.5° to rods											
29	Number of breaks per rod			Fraction of rods broken			Fraction of fuel exposed			Focusing param.		
30	typical	hi-burn	95% typ. + 5% hi-burn	typical	hi-burn	95% typ. + 5% hi-burn	typical	hi-burn	95% typ. + 5% hi-burn			
31	3.25E-02	6.15E-01	0.0616	1.42E-02	0.1799	0.0225	6.02E-03	1.06E-01	0.0110			1
32	3.86E-02	6.45E-01	0.0689	1.75E-02	0.2050	0.0268	6.43E-03	9.97E-02	0.0111			0.9
33	4.83E-02	6.83E-01	0.0782	2.17E-02	0.2383	0.0325	6.83E-03	9.41E-02	0.0112			0.8
34	5.68E-02	7.34E-01	0.0906	2.73E-02	0.2830	0.0401	7.26E-03	8.86E-02	0.0113			0.7
35	7.00E-02	8.07E-01	0.1069	3.45E-02	0.3481	0.0501	7.59E-03	8.39E-02	0.0114			0.6
36	8.53E-02	9.06E-01	0.1263	4.41E-02	0.4343	0.0636	7.82E-03	7.85E-02	0.0112			0.5
37	1.03E-01	1.04E+00	0.1500	5.76E-02	0.5490	0.0822	7.31E-03	7.16E-02	0.0105			0.4
38	1.26E-01	1.14E+00	0.1771	7.84E-02	0.6482	0.1069	6.67E-03	5.76E-02	0.0092			0.3
39	1.65E-01	9.98E-01	0.2066	1.17E-01	0.6276	0.1429	5.78E-03	3.23E-02	0.0071			0.2
40	2.68E-01	5.93E-01	0.2845	2.23E-01	0.4467	0.2341	4.84E-03	9.02E-03	0.0049			0.1
41	Cylindrical rocks with linear punch at 45° to rods											
42	Number of breaks per rod			Fraction of rods broken			Fraction of fuel exposed			Focusing param.		
43	typical	hi-burn	95% typ. + 5% hi-burn	typical	hi-burn	95% typ. + 5% hi-burn	typical	hi-burn	95% typ. + 5% hi-burn			
44	3.25E-02	6.15E-01	0.0616	1.42E-02	1.80E-01	0.0225	6.02E-03	1.06E-01	0.0110			1
45	3.25E-02	6.15E-01	0.0616	1.42E-02	1.80E-01	0.0225	6.80E-03	1.02E-01	0.0106			0.9
46	3.25E-02	6.15E-01	0.0616	1.42E-02	1.80E-01	0.0225	5.40E-03	9.45E-02	0.0099			0.8
47	3.25E-02	6.15E-01	0.0616	1.42E-02	1.80E-01	0.0225	4.89E-03	8.56E-02	0.0089			0.7
48	3.30E-02	6.17E-01	0.0622	1.45E-02	1.82E-01	0.0229	4.42E-03	7.66E-02	0.0080			0.6
49	3.44E-02	6.24E-01	0.0639	1.52E-02	1.88E-01	0.0238	4.02E-03	6.75E-02	0.0072			0.5
50	3.66E-02	6.35E-01	0.0685	1.64E-02	1.97E-01	0.0254	3.80E-03	6.80E-02	0.0063			0.4
51	3.95E-02	6.49E-01	0.0700	1.80E-02	2.09E-01	0.0275	3.10E-03	4.73E-02	0.0053			0.3
52	4.34E-02	6.69E-01	0.0747	2.01E-02	2.26E-01	0.0304	2.43E-03	3.49E-02	0.0041			0.2
53	4.87E-02	6.95E-01	0.0810	2.30E-02	2.48E-01	0.0343	1.47E-03	1.96E-02	0.0024			0.1

	A	B	C	D	E	F	G	H	I	J	K	L
57	Cylindrical rocks with linear punch at 67.5° to rods											
58	Number of breaks			Fraction of rods broken			Fraction of fuel exposed			Focusing param.		
59	per rod											
60	typical	hi-burn	95% typ. + 5% hi-burn	typical	hi-burn	95% typ. + 5% hi-burn	typical	hi-burn	95% typ. + 5% hi-burn			
61	3.25E-02	6.15E-01	0.0616	1.42E-02	1.80E-01	0.0225	6.02E-03	1.06E-01	0.0110	1		
62	3.25E-02	6.15E-01	0.0616	1.42E-02	1.80E-01	0.0225	5.80E-03	1.02E-01	0.0106	0.9		
63	3.25E-02	6.15E-01	0.0616	1.42E-02	1.80E-01	0.0225	5.40E-03	9.45E-02	0.0099	0.8		
64	3.25E-02	6.15E-01	0.0616	1.42E-02	1.80E-01	0.0225	4.89E-03	8.56E-02	0.0089	0.7		
65	3.25E-02	6.15E-01	0.0616	1.42E-02	1.80E-01	0.0225	4.31E-03	7.54E-02	0.0079	0.6		
66	3.25E-02	6.15E-01	0.0616	1.42E-02	1.80E-01	0.0225	3.67E-03	6.42E-02	0.0067	0.5		
67	3.25E-02	6.15E-01	0.0616	1.42E-02	1.80E-01	0.0225	2.98E-03	5.23E-02	0.0054	0.4		
68	3.27E-02	6.16E-01	0.0618	1.43E-02	1.81E-01	0.0226	2.29E-03	3.99E-02	0.0042	0.3		
69	3.35E-02	6.20E-01	0.0628	1.47E-02	1.84E-01	0.0232	1.60E-03	2.74E-02	0.0029	0.2		
70	3.49E-02	6.27E-01	0.0645	1.55E-02	1.90E-01	0.0242	8.59E-04	1.43E-02	0.0015	0.1		
71	Cylindrical rocks with linear punch perpendicular to rods											
72	Number of breaks			Fraction of rods broken			Fraction of fuel exposed			Focusing param.		
73	per rod											
74	typical	hi-burn	95% typ. + 5% hi-burn	typical	hi-burn	95% typ. + 5% hi-burn	typical	hi-burn	95% typ. + 5% hi-burn			
75	3.25E-02	6.15E-01	0.0616	1.42E-02	1.80E-01	0.0225	6.02E-03	1.06E-01	0.0110	1		
76	3.25E-02	6.15E-01	0.0616	1.42E-02	1.80E-01	0.0225	5.80E-03	1.02E-01	0.0106	0.9		
77	3.25E-02	6.15E-01	0.0616	1.42E-02	1.80E-01	0.0225	5.40E-03	9.45E-02	0.0099	0.8		
78	3.25E-02	6.15E-01	0.0616	1.42E-02	1.80E-01	0.0225	4.89E-03	8.56E-02	0.0089	0.7		
79	3.25E-02	6.15E-01	0.0616	1.42E-02	1.80E-01	0.0225	4.31E-03	7.54E-02	0.0079	0.6		
80	3.25E-02	6.15E-01	0.0616	1.42E-02	1.80E-01	0.0225	3.67E-03	6.42E-02	0.0067	0.5		
81	3.25E-02	6.15E-01	0.0616	1.42E-02	1.80E-01	0.0225	2.98E-03	5.23E-02	0.0054	0.4		
82	3.25E-02	6.15E-01	0.0616	1.42E-02	1.80E-01	0.0225	2.27E-03	3.97E-02	0.0041	0.3		
83	3.25E-02	6.15E-01	0.0616	1.42E-02	1.80E-01	0.0225	1.62E-03	2.67E-02	0.0028	0.2		
84	3.25E-02	6.15E-01	0.0616	1.42E-02	1.80E-01	0.0225	7.65E-04	1.34E-02	0.0014	0.1		
85	Cylindrical rocks with composite linear punch (eight orientations)											
86	Number of breaks			Fraction of rods broken			Fraction of fuel exposed			Focusing param.		
87	per rod											
88	typical	hi-burn	95% typ. + 5% hi-burn	typical	hi-burn	95% typ. + 5% hi-burn	typical	hi-burn	95% typ. + 5% hi-burn			
89	3.25E-02	6.15E-01	0.0616	1.42E-02	1.80E-01	0.0225	6.02E-03	1.06E-01	0.0110	1		
90	3.48E-02	6.26E-01	0.0643	1.54E-02	1.89E-01	0.0241	6.18E-03	1.03E-01	0.0110	0.9		
91	3.77E-02	6.40E-01	0.0678	1.70E-02	2.02E-01	0.0262	6.27E-03	9.90E-02	0.0109	0.8		
92	4.16E-02	6.59E-01	0.0725	1.91E-02	2.19E-01	0.0291	6.37E-03	9.40E-02	0.0108	0.7		
93	4.67E-02	6.88E-01	0.0787	2.19E-02	2.44E-01	0.0329	6.50E-03	8.92E-02	0.0106	0.6		
94	6.28E-02	7.28E-01	0.0864	2.57E-02	2.77E-01	0.0382	6.61E-03	8.45E-02	0.0105	0.5		
95	6.00E-02	7.79E-01	0.0959	3.10E-02	3.22E-01	0.0456	6.68E-03	7.97E-02	0.0103	0.4		
96	6.95E-02	8.21E-01	0.1071	3.92E-02	3.63E-01	0.0554	6.78E-03	7.13E-02	0.0100	0.3		
97	8.52E-02	7.73E-01	0.1196	5.45E-02	3.60E-01	0.0698	7.21E-03	5.26E-02	0.0095	0.2		
98	1.26E-01	6.30E-01	0.1507	8.50E-02	3.00E-01	0.1052	9.21E-03	2.67E-02	0.0101	0.1		

	A	B	C	D	E
1					Cylindrical rocks with cir
2	Number of breaks			Fraction of	
3	per rod			rods broken	
4	typical	hi-burn	95% typ. + 5% hi-burn	typical	hi-burn
5	0.03246	0.6146	=0.95*A6+0.05*B5	0.01419	0.1799
6	0.03861	0.6446	=0.95*A6+0.05*B6	0.01745	0.205
7	0.04634	0.6831	=0.95*A7+0.05*B7	0.02171	0.2383
8	0.05676	0.7339	=0.95*A8+0.05*B8	0.02727	0.283
9	0.07003	0.8073	=0.95*A9+0.05*B9	0.03445	0.3481
10	0.08529	0.9058	=0.95*A10+0.05*B10	0.04407	0.4343
11	0.1032	1.039	=0.95*A11+0.05*B11	0.0576	0.549
12	0.1264	1.141	=0.95*A12+0.05*B12	0.0784	0.6482
13	0.165	0.9878	=0.95*A13+0.05*B13	0.1174	0.6278
14	0.2682	0.5934	=0.95*A14+0.05*B14	0.2229	0.4467

	A	B	C	D	E
15					Cylindrical rocks with linear punch parallel
16	Number of breaks per rod			Fraction of rods broken	
17			95% typ. + 5% hi-burn		
18	typical	hi-burn		typical	hi-burn
19	0.03248	0.6145	=0.95*A19+0.05*B19	0.01419	0.1799
20	0.03861	0.6446	=0.95*A20+0.05*B20	0.01745	0.205
21	0.04634	0.6831	=0.95*A21+0.05*B21	0.02171	0.2383
22	0.05675	0.7339	=0.95*A22+0.05*B22	0.02727	0.283
23	0.07003	0.8073	=0.95*A23+0.05*B23	0.03445	0.3481
24	0.08529	0.9058	=0.95*A24+0.05*B24	0.04407	0.4343
25	0.1032	1.039	=0.95*A25+0.05*B25	0.0576	0.549
26	0.1264	1.141	=0.95*A26+0.05*B26	0.0784	0.6482
27	0.165	0.9978	=0.95*A27+0.05*B27	0.1174	0.6276
28	0.2682	0.5934	=0.95*A28+0.05*B28	0.2229	0.4467
29					Cylindrical rocks with linear punch at 22.5°
30	Number of breaks per rod			Fraction of rods broken	
31			95% typ. + 5% hi-burn		
32	typical	hi-burn		typical	hi-burn
33	0.03248	0.6145	=0.95*A33+0.05*B33	0.01419	0.1799
34	0.03861	0.6446	=0.95*A34+0.05*B34	0.01745	0.205
35	0.04634	0.6831	=0.95*A35+0.05*B35	0.02171	0.2383
36	0.05675	0.7339	=0.95*A36+0.05*B36	0.02727	0.283
37	0.07003	0.8073	=0.95*A37+0.05*B37	0.03445	0.3481
38	0.08529	0.9058	=0.95*A38+0.05*B38	0.04407	0.4343
39	0.1032	1.039	=0.95*A39+0.05*B39	0.0576	0.549
40	0.1264	1.141	=0.95*A40+0.05*B40	0.0784	0.6482
41	0.165	0.9978	=0.95*A41+0.05*B41	0.1174	0.6276
42	0.2682	0.5934	=0.95*A42+0.05*B42	0.2229	0.4467
43					Cylindrical rocks with linear punch at 45°
44	Number of breaks per rod			Fraction of rods broken	
45			95% typ. + 5% hi-burn		
46	typical	hi-burn		typical	hi-burn
47	0.03248	0.6145	=0.95*A47+0.05*B47	0.01419	0.1799
48	0.03248	0.6145	=0.95*A48+0.05*B48	0.01419	0.1799
49	0.03248	0.6145	=0.95*A49+0.05*B49	0.01419	0.1799
50	0.03248	0.6145	=0.95*A50+0.05*B50	0.01419	0.1799
51	0.03301	0.6173	=0.95*A51+0.05*B51	0.01448	0.1822
52	0.0344	0.624	=0.95*A52+0.05*B52	0.01521	0.1877
53	0.03655	0.6346	=0.95*A53+0.05*B53	0.01635	0.1965
54	0.03953	0.6492	=0.95*A54+0.05*B54	0.01796	0.2089
55	0.04344	0.6689	=0.95*A55+0.05*B55	0.02012	0.2259
56	0.04874	0.6946	=0.95*A56+0.05*B56	0.023	0.2483

	A	B	C	D	E
67					Cylindrical rocks with linear punch at 67.5°
68	Number of breaks per rod			Fraction of rods broken	
69			95% typ. + 5% hi-burn		
60	typical	hi-burn		typical	hi-burn
61	0.03246	0.6145	=0.95*A61+0.05*B61	0.01419	0.1799
62	0.03246	0.6145	=0.95*A62+0.05*B62	0.01419	0.1799
63	0.03246	0.6145	=0.95*A63+0.05*B63	0.01419	0.1799
64	0.03246	0.6145	=0.95*A64+0.05*B64	0.01419	0.1799
65	0.03246	0.6145	=0.95*A65+0.05*B65	0.01419	0.1799
66	0.03246	0.6145	=0.95*A66+0.05*B66	0.01419	0.1799
67	0.03246	0.6145	=0.95*A67+0.05*B67	0.01419	0.1799
68	0.03267	0.6156	=0.95*A68+0.05*B68	0.0143	0.1808
69	0.03347	0.6195	=0.95*A69+0.05*B69	0.01473	0.184
70	0.0349	0.6265	=0.95*A70+0.05*B70	0.01548	0.1898
71					Cylindrical rocks with linear punch perpendicular
72	Number of breaks per rod			Fraction of rods broken	
73			95% typ. + 5% hi-burn		
74	typical	hi-burn		typical	hi-burn
75	0.03246	0.6145	=0.95*A75+0.05*B75	0.01419	0.1799
76	0.03246	0.6145	=0.95*A76+0.05*B76	0.01419	0.1799
77	0.03246	0.6145	=0.95*A77+0.05*B77	0.01419	0.1799
78	0.03246	0.6145	=0.95*A78+0.05*B78	0.01419	0.1799
79	0.03246	0.6145	=0.95*A79+0.05*B79	0.01419	0.1799
80	0.03246	0.6145	=0.95*A80+0.05*B80	0.01419	0.1799
81	0.03246	0.6145	=0.95*A81+0.05*B81	0.01419	0.1799
82	0.03246	0.6145	=0.95*A82+0.05*B82	0.01419	0.1799
83	0.03246	0.6145	=0.95*A83+0.05*B83	0.01419	0.1799
84	0.03246	0.6145	=0.95*A84+0.05*B84	0.01419	0.1799
85					Cylindrical rocks with composite linear punch (eig)
86	Number of breaks per rod			Fraction of rods broken	
87			95% typ. + 5% hi-burn		
88	typical	hi-burn		typical	hi-burn
89	=(A19+A75+2*(A33+A47+A61))/8	=(B19+B75+2*(B33+B47+B61))/8	=0.95*A89+0.05*B89	=(D19+D75+2*(D33+D47+D61))/8	=(E19+E75+2*(E33+E47+E61))/8
90	=(A20+A76+2*(A34+A48+A62))/8	=(B20+B76+2*(B34+B48+B62))/8	=0.95*A90+0.05*B90	=(D20+D76+2*(D34+D48+D62))/8	=(E20+E76+2*(E34+E48+E62))/8
91	=(A21+A77+2*(A35+A49+A63))/8	=(B21+B77+2*(B35+B49+B63))/8	=0.95*A91+0.05*B91	=(D21+D77+2*(D35+D49+D63))/8	=(E21+E77+2*(E35+E49+E63))/8
92	=(A22+A78+2*(A36+A50+A64))/8	=(B22+B78+2*(B36+B50+B64))/8	=0.95*A92+0.05*B92	=(D22+D78+2*(D36+D50+D64))/8	=(E22+E78+2*(E36+E50+E64))/8
93	=(A23+A79+2*(A37+A51+A65))/8	=(B23+B79+2*(B37+B51+B65))/8	=0.95*A93+0.05*B93	=(D23+D79+2*(D37+D51+D65))/8	=(E23+E79+2*(E37+E51+E65))/8
94	=(A24+A80+2*(A38+A52+A66))/8	=(B24+B80+2*(B38+B52+B66))/8	=0.95*A94+0.05*B94	=(D24+D80+2*(D38+D52+D66))/8	=(E24+E80+2*(E38+E52+E66))/8
95	=(A25+A81+2*(A39+A53+A67))/8	=(B25+B81+2*(B39+B53+B67))/8	=0.95*A95+0.05*B95	=(D25+D81+2*(D39+D53+D67))/8	=(E25+E81+2*(E39+E53+E67))/8
96	=(A26+A82+2*(A40+A54+A68))/8	=(B26+B82+2*(B40+B54+B68))/8	=0.95*A96+0.05*B96	=(D26+D82+2*(D40+D54+D68))/8	=(E26+E82+2*(E40+E54+E68))/8
97	=(A27+A83+2*(A41+A55+A69))/8	=(B27+B83+2*(B41+B55+B69))/8	=0.95*A97+0.05*B97	=(D27+D83+2*(D41+D55+D69))/8	=(E27+E83+2*(E41+E55+E69))/8
98	=(A28+A84+2*(A42+A56+A70))/8	=(B28+B84+2*(B42+B56+B70))/8	=0.95*A98+0.05*B98	=(D28+D84+2*(D42+D56+D70))/8	=(E28+E84+2*(E42+E56+E70))/8

	F	G	H	I	J	K	L
1	ular punch						
2	Fraction of fuel exposed						
3	95% typ. + 5% hi-burn				Focus- ing param.	Punch aspect ratio	
4		typical	hi-burn	95% typ. + 5% hi-burn		typical	hi-burn
5	=0.95*D5+0.05*E5	0.006021	0.1055	=0.95*G5+0.05*H5	1	0.006231	0.04544
6	=0.95*D6+0.05*E6	0.006428	0.09967	=0.95*G6+0.05*H6	0.9	0.007964	0.05786
7	=0.95*D7+0.05*E7	0.006826	0.09405	=0.95*G7+0.05*H7	0.8	0.01004	0.07666
8	=0.95*D8+0.05*E8	0.007254	0.08863	=0.95*G8+0.05*H8	0.7	0.01324	0.1064
9	=0.95*D9+0.05*E9	0.007687	0.0839	=0.95*G9+0.05*H9	0.6	0.01994	0.1562
10	=0.95*D10+0.05*E10	0.007822	0.07848	=0.95*G10+0.05*H10	0.5	0.03316	0.2475
11	=0.95*D11+0.05*E11	0.007313	0.07158	=0.95*G11+0.05*H11	0.4	0.0594	0.44
12	=0.95*D12+0.05*E12	0.006866	0.05769	=0.95*G12+0.05*H12	0.3	0.1215	0.8682
13	=0.95*D13+0.05*E13	0.005782	0.03234	=0.95*G13+0.05*H13	0.2	0.3292	1.766
14	=0.95*D14+0.05*E14	0.004642	0.008015	=0.95*G14+0.05*H14	0.1	1.818	4.616

	F	G	H	I	J	K	L
15	o rods						
16	Fraction of fuel exposed						Focusing param.
17	95% typ. + 5% hi-burn		typical		hi-burn		
18	95% typ. + 5% hi-burn		typical		hi-burn		95% typ. + 5% hi-burn
19	=0.95*D19+0.05*E19	0.008021	0.1055		=0.95*G19+0.05*H19		1
20	=0.95*D20+0.05*E20	0.007839	0.1184		=0.95*G20+0.05*H20		0.9
21	=0.95*D21+0.05*E21	0.009555	0.1317		=0.95*G21+0.05*H21		0.8
22	=0.95*D22+0.05*E22	0.01202	0.1468		=0.95*G22+0.05*H22		0.7
23	=0.95*D23+0.05*E23	0.01507	0.1667		=0.95*G23+0.05*H23		0.6
24	=0.95*D24+0.05*E24	0.01857	0.1912		=0.95*G24+0.05*H24		0.5
25	=0.95*D25+0.05*E25	0.02264	0.2216		=0.95*G25+0.05*H25		0.4
26	=0.95*D26+0.05*E26	0.02786	0.2407		=0.95*G26+0.05*H26		0.3
27	=0.95*D27+0.05*E27	0.03666	0.2045		=0.95*G27+0.05*H27		0.2
28	=0.95*D28+0.05*E28	0.05901	0.1146		=0.95*G28+0.05*H28		0.1
29	to rods						
30	Fraction of fuel exposed						Focusing param.
31	95% typ. + 5% hi-burn		typical		hi-burn		
32	95% typ. + 5% hi-burn		typical		hi-burn		95% typ. + 5% hi-burn
33	=0.95*D33+0.05*E33	0.006021	0.1055		=0.95*G33+0.05*H33		1
34	=0.95*D34+0.05*E34	0.006428	0.09887		=0.95*G34+0.05*H34		0.9
35	=0.95*D35+0.05*E35	0.006826	0.09405		=0.95*G35+0.05*H35		0.8
36	=0.95*D36+0.05*E36	0.007254	0.08863		=0.95*G36+0.05*H36		0.7
37	=0.95*D37+0.05*E37	0.007587	0.0839		=0.95*G37+0.05*H37		0.6
38	=0.95*D38+0.05*E38	0.007822	0.07848		=0.95*G38+0.05*H38		0.5
39	=0.95*D39+0.05*E39	0.007313	0.07158		=0.95*G39+0.05*H39		0.4
40	=0.95*D40+0.05*E40	0.006666	0.05759		=0.95*G40+0.05*H40		0.3
41	=0.95*D41+0.05*E41	0.005782	0.03234		=0.95*G41+0.05*H41		0.2
42	=0.95*D42+0.05*E42	0.004642	0.009015		=0.95*G42+0.05*H42		0.1
43	o rods						
44	Fraction of fuel exposed						Focusing param.
45	95% typ. + 5% hi-burn		typical		hi-burn		
46	95% typ. + 5% hi-burn		typical		hi-burn		95% typ. + 5% hi-burn
47	=0.95*D47+0.05*E47	0.005021	0.1055		=0.95*G47+0.05*H47		1
48	=0.95*D48+0.05*E48	0.005796	0.1015		=0.95*G48+0.05*H48		0.9
49	=0.95*D49+0.05*E49	0.005395	0.0945		=0.95*G49+0.05*H49		0.8
50	=0.95*D50+0.05*E50	0.004889	0.08564		=0.95*G50+0.05*H50		0.7
51	=0.95*D51+0.05*E51	0.004424	0.07655		=0.95*G51+0.05*H51		0.6
52	=0.95*D52+0.05*E52	0.00402	0.06754		=0.95*G52+0.05*H52		0.5
53	=0.95*D53+0.05*E53	0.003602	0.05789		=0.95*G53+0.05*H53		0.4
54	=0.95*D54+0.05*E54	0.003101	0.04732		=0.95*G54+0.05*H54		0.3
55	=0.95*D55+0.05*E55	0.00243	0.03488		=0.95*G55+0.05*H55		0.2
56	=0.95*D56+0.05*E56	0.001471	0.01963		=0.95*G56+0.05*H56		0.1

	F	G	H	I	J	K	L
57	to rods						
58							
59							
60							
61							
62							
63							
64							
65							
66							
67							
68							
69							
70							
71	to rods						
72							
73							
74							
75							
76							
77							
78							
79							
80							
81							
82							
83							
84							
85	(orientations)						
86							
87							
88							
89							
90							
91							
92							
93							
94							
95							
96							
97							
98							